Universidad
Carlos III de Madrid
www.uc3m.es

TESIS DOCTORAL

GAS MALDISTRIBUTION IN FLUIDIZED BEDS

Autor:
Javier Sánchez Prieto

Directores de Tesis:
Domingo Santana Santana
Javier Villa Briongos

DEPARTAMENTO DE INGENIERÍA TÉRMICA Y DE FLUIDOS

Leganés, Madrid, Marzo de 2015.

TESIS DOCTORAL

GAS MALDISTRIBUTION IN FLUIDIZED BEDS

Autor: Javier Sánchez Prieto

Directores de Tesis: Domingo Santana Santana

Javier Villa Briongos

Firma del Tribunal Calificador,

Firma

Presidente:

Vocal:

Secretario:

Calificación: _____

Leganés, Madrid, Marzo de 2015

Contents

List of Figures

List of Tables

Preface

This PhD Thesis has been performed in the University Carlos III of Madrid, School of Engineering, in the Department of Thermal and Fluid Engineering, under the supervision of Dr. Domingo Santana Santana and Dr. Javier Villa Briongos. The thesis was iniciated in Autumn 2010 and lasted until Spring 2015.

The author deeply appreciates the funding support by the Spanish Government (Project DPI2009-10518) and the Autonomous Community of Madrid (Project S2009 /ENE-1660), which has been of great help during the PhD.

All the results presented here have been obtained by the author unless otherwise specified.

Javier Sánchez Prieto
Department of Thermal and Fluid Engineering,
University Carlos III of Madrid.
March 2015.

Resumen

Uno de los problemas más comunes de los lechos fluidizados industriales es la mala distribución del gas en el lecho. Se deben emplear elevadas velocidades de gas para generar grandes pérdidas de carga en el distribuidor que garanticen la distribución uniforme del gas en el interior del lecho. Sin embargo, una elevada pérdida de carga en el distribuidor supone también un aumento en la potencia consumida por los elementos de impulsión del gas, que se traducen en un aumento de los costes de operación. Además, en los reactores industriales de lecho fluidizado la velocidad del gas es raramente constante. Dado que las perturbaciones en el flujo de gas generan a su vez perturbaciones en la pérdida de carga del distribuidor, es importante conseguir que esta pérdida de carga sea lo más baja posible.

La mala distribución del gas depende de la velocidad superficial del gas, del tipo de sólido empleado como material inerte y de varios aspectos del diseño del distribuidor. Si se emplean velocidades de gas demasiado bajas, el gas es más propenso a la mala distribución, y por ello varios autores recomiendan operar por encima de un valor crítico de velocidad por encima del cual todos los orificios o campanas del distribuidor se consideran activos. El tipo de sólido empleado como material inerte determina la tendencia del lecho a la aglomeración. Es importante seleccionar un material adecuado puesto que la aglomeración del lecho puede conducir a la mala distribución del gas e incluso a la defluidización. El diseño del distribuidor afecta principalmente al valor de la pérdida de carga, que a su vez depende de otros factores como son la velocidad del gas, el número de orificios y su tamaño, el espesor de la placa distribuidora, la temperatura...

Tanto la medidas de presión como el análisis visual de la superficie del lecho son técnicas de medida robustas que se utilizan comúnmente en la monitorización de reactores de lecho fluidizado. Por lo tanto, estas técnicas se han empleado en esta tésis para el estudio de la mala distribución del gas en el lecho.

El análisis visual se utilizó en un lecho fluidizado cilíndrico (3D) para la detección de la mala distribución del gas en la superficie del lecho. Para conseguir un estado de mala distribución inducida se tapó la mitad de los orificios de la placa distribuidora. Se

observó que, aunque una velocidad de gas elevada puede hacer que la mala distribución no se detecte en la superficie, el problema persiste en la zona baja del lecho. De acuerdo con este hecho, se investigó el uso de las medidas de fluctuaciones de presión en el interior del lecho como herramienta para la detección de la mala distribución del gas. Se emplearon varios métodos de monitorización basados en el análisis de las fluctuaciones de presión para establecer el umbral de grado de mala distribución que puede ser detectado. También se investigó el efecto de la localización de las sondas de presión y se concluyó que deben ser colocadas a una altura entre el 50 y el 75% de la altura total del lecho si el objetivo es detectar la mala distribución del gas. Una única sonda puede ser suficiente para la detección en un lecho de escala de laboratorio, sin embargo, se deberán emplear varias sondas en lechos industriales para poder cubrir la medida en toda la sección del lecho.

El análisis visual se utilizó también para el desarrollo de un modelo capaz de estimar el tamaño de las zonas muertas generadas por el bloqueo de una parte de los orificios del distribuidor. Se obtuvo una correlación a partir del análisis digital de imagen y la velocimetría de partículas de imágenes tomadas en un lecho fluidizado bidimensional (2D). La correlación propuesta, junto a otras correlaciones de la literatura, se utilizó para extrapolar datos a un lecho 3D. Se observó que el modelo es capaz de predecir el tamaño de las zonas muertas en un lecho 3D con un error máximo del 20%, y puede además emplearse para estimar el tamaño de la sección afectada del distribuidor.

Se estudió el efecto de la temperatura de operación en la pérdida de carga del distribuidor para dos tipos distintos de distribuidores (placa perforada y campanas) en una planta piloto de gasificación de biomasa en lecho fluidizado. Los resultados obtenidos se utilizaron en el desarrollo de una metodología para el diseño de distribuidores a alta temperatura. El modelo propuesto predice la mínima área de orificios necesaria para cumplir una relación dada de pérdida de carga entre el distribuidor y el lecho, y para una temperatura y condiciones de operación fijadas.

Abstract

Gas maldistribution is one of the most common problems in large-scale fluidized beds. High superficial gas velocities should be used to create a high pressure drop across the distributor plate to achieve an even gas distribution within the bed. However, higher pressure drop leads to higher power consumption in blowers, which means higher operational costs. In addition, the superficial gas velocity in large-scale reactors is seldom constant. As long as gas velocity perturbations lead to pressure drop variations, it is important to maintain the distributor pressure drop as low as possible.

Maldistribution depends on the superficial gas velocity, the type of solids used as bed material and the distributor plate design. Low values of superficial gas velocity are more prone to generate gas maldistribution and therefore, several authors recommend operating beyond a critical value of gas velocity, at which all distributor plate orifices or tuyeres are considered active. The type of solids used as bed material determines the tendency of the bed to agglomerate. Since agglomeration could lead to maldistribution and defluidization, it is important to select the bed material properly. The distributor design affects mainly to the pressure drop, which is also dependent of other variables such the superficial gas velocity, the number of orifices and its diameter, the distributor plate thickness, the temperature...

Pressure measurements and visual inspection of the bed surface are robust techniques commonly used in fluidized bed reactors for monitoring purposes. Therefore, these techniques were employed in this thesis to study maldistribution.

Visual inspection technique was employed in a 3D cylindrical bubbling fluidized bed to detect maldistribution in the bed surface. To create a controlled induced maldistribution, the half of the distributor plate cross-section was covered. It was found that a high superficial gas velocity could overcome maldistribution at the bed surface, even though the maldistribution problem could still prevail at the bottom of the bed. According to that, pressure fluctuations measurements were investigated as a detection method for maldistribution. Several monitoring methods based on the pressure signal analysis were studied to evaluate the boundary of maldistribution grade that can be detected. The effect of the pressure probe location was also investigated and it was

concluded that pressure probes should be located at 50-75% of the bed height for maldistribution detection purposes. A single pressure probe could be sufficient to detect maldistribution in a lab-scale fluidized bed; however, several pressure probes should be placed in a large-scale fluidized bed reactor to cover all the bed cross-section.

Visual inspection technique was also employed to develop a model for estimating the size of the stagnant zones created by covered parts of the distributor plate. A correlation was obtained using Digital Image Analysis and Particle Image Velocimetry of pictures taken in a pseudo-2D fluidized bed. The proposed correlation, coupled with correlations from the literature, was extrapolated to a 3D facility. The model was found to predict the size of the stagnant zones in a 3D fluidized bed with a maximum relative error of 20% and it could be used to estimate the size of the distributor cross-section affected by maldistribution.

The distributor plate performance under operational conditions was also investigated. The effect of temperature on the distributor pressure drop was studied for two different distributor plates (i.e. multiorifice and tuyere type) in a Biomass Bubbling Fluidized Bed Gasifier. The results were employed to develop a methodology to design gas distributor plates at elevated temperature. The model predicts accurately the minimum distributor open area needed to satisfy a distributor to bed pressure drop ratio for a given temperature and operation conditions.

Chapter 1

Introduction

Contents

1.1 A brief introduction to fluidization

Fluidization is the operation by which solid particles are transformed into a fluid-like state through suspension in a gas or liquid (Kunii and Levenspiel, 1991). When a fluid passes through a bed of particles at a low velocity it percolates through the voids between particles. This is called a fixed bed. However, at higher velocities, a point is reached where particles are suspended by the fluid flow. At this point, the pressure drop through any section of the bed equals the weight of particles and fluid in this section and the bed is considered to be at minimum fluidization conditions. The superficial velocity required to reach this state is called minimum fluidizattion velocity, U_{mf}, and it is a function of both particle and fluid properties.

The bed pressure drop, ΔP_{bed}, at minimum fluidization conditions can be expresed as follows:

$$\frac{\Delta P_{bed}}{H_{mf}} = (\rho_p - \rho_g)\, g\, (1 - \epsilon_{mf}) \tag{1.1}$$

where H_{mf} is the bed heigh at minimum fluidization conditions, ρ_p and ρ_g are the particle and fluid densities and ϵ_{mf} is the bed voidage at minimum fluidization conditions. In gas fluidization, the gas density is typically much smaller than particle density and hence terms involving gas density are often neglected.

To estimate the minimum fluidization velocity of a given type of particles in gas fluidization, the transition between fixed and fluidized bed has to be estudied. Ergun (1952) developed an expression to calculate the pressure drop across a fixed bed of particles, ΔP, when a gas passes through it (Equation 1.2).

$$\frac{\Delta P}{H} = 150 \frac{(1 - \epsilon_0)^2}{\epsilon_0^3} \frac{\mu_g U_0}{(\phi d_p)^2} + 1.75 \frac{1 - \epsilon_0}{\epsilon_0^3} \frac{\rho_g U_0^2}{\phi d_p} \tag{1.2}$$

where H is the fixed bed height, ϵ_0 is the packed bed voidage, ρ_g and μ_g are the gas density and viscosity, ϕ is the particle sphericity, defined as the relation between the surface of a sphere and the surface of a particle both of them having the same volume, d_p is the mean particle diameter and U_0 is the superficial gas velocity. Ergun's equation shows that the fixed bed pressure drop increases with U_0 until the bed reaches the minimum fluidization velocity. Equation 1.2 can be combined with equation 1.1 to obtain an expression of the minimum fluidization velocity:

$$Ar = 150 \frac{1 - \epsilon_{mf}}{\epsilon_{mf}^3} Re_{mf} + 1.75 \frac{1}{\epsilon_{mf}^3} Re_{mf}^2 \tag{1.3}$$

where Ar is the Archimedes number (Equation 1.4), also called Galileo number (Ga), and Re_{mf} is the Reynolds number at minimum fluidization conditions (Equation 1.5).

$$Ar = \frac{d_p^3 \rho_g\, (\rho_p - \rho_g)\, g}{\mu_g^2} \tag{1.4}$$

$$Re_{mf} = \frac{U_{mf} d_p \rho_g}{\mu_g} \tag{1.5}$$

Since particle and gas properties are easy to measure, even at different pressures and temperatures, the main obstacle in the estimation of U_{mf} is the minimum fluidization voidage, ϵ_{mf}, measurement.

The main advantages and drawbacks of the fluidization technology are listed below:

Advantages

- The smooth, liquid-like flow of particles allows continuous automatically controlled operations with easy handling.
- The rapid mixing of solids permits isothermal conditions.
- The fluidized bed can resist rapid temperature changes, responding slowly to abrupt changes in operating conditions, and giving a large margin of safety in avoiding temperature runaways for highly exothermic reactions.
- The circulation of solids between two fluidized beds makes possible to remove the heat produced in large reactors.
- It is suitable for large-scale operations.
- Heat and mass transfer rates between gas and particles are high when compared with other contacting methods.
- The rate of heat transfer between a fluidized bed and an immersed object is high; hence heat exchangers within fluidized beds require relatively small surface areas.

Disadvantages

- For bubbling beds of fine particles, the gas–particle contact can be ineficient, leading to low conversion rates of gaseous reactants and low selectivity.
- The rapid mixing of solids in the bed leads to nonuniform residence times of solids in the reactor. For continuous treatment of solids, this gives a nonuniform product and poorer performance, especially at higher conversion levels. For catalytic reactions, the motion of porous catalyst particles, which continually capture and release reactant gas molecules, contributes to the backmixing of gaseous reactant, thereby reducing yield and performance.
- For deep beds the presure drop is high, resulting in large power consumption.
- Solids can be pulverized and entrained by the gas bubbles and must be captured or replaced.
- Erosion of pipes and vessels due to abrasion by particles can be significant.
- For noncatalytic operations at high temperatures, the agglomeration and sintering of fine particles can require a lowering in operation temperature, thereby reducing the reaction rate considerably.

Because of the advantages of the fluidization technology, it has been employed in many industrial processes such as coal combustion and gasification, production of gasoline from other petroleum fractions, natural gas or synthesis gas, heat exchange processes, coating of particles, drying of solids, fluid catalytic cracking (FCC)... More recently, the interest on the valorization of low-grade fuels such as biomass and other wastes made the fluidization a very promising technology to carry out combustion and gasification of biomass.

1.1.1 Fluidization regimes

As long as the velocity of the gas passing through the bed increases, a smooth and progresive expansion of the bed occurs. As a consequence of this increase in velocity, different regimes of fluidization can be observed:

- If the gas velocity is low enough (i.e. below minimum fluidization velocity), the gas merely percolates through the void spaces between stationary particles. This is called a fixed bed (Figure 1.1 a)).

- When the gas velocity is increased above the minimum fluidization velocity, bubbles are observed. The bed is said to be fluidized, and the bed height is larger than the fixed bed height (Figure 1.1 b)).

- If the gas velocity continues increasing, the bubbles grow up until they became slugs. The bed expansion is higher than in the typical bubbling regime because the slugs push the particles upward. The slugging regime is typical of narrow beds and it is usually not desirable (Figure 1.1 c)).

- When the particles are fluidized beyond the terminal velocity, the bed surface dissapears and the entrainment becomes appreciable. A turbulent motion of clusters is observed instead of bubbles. This is the turbulent regime (Figure 1.1 d)). For steady state operation of this type of fluidized beds, the entrained particles have to be collected by cyclones and returned back to the bed (i.e. Circulating fluidized beds).

- A different type of fluidization regime is the spouted regime, that can be enhanced on a fluidized bed with some special design parameters. The bottom part of a fluidized bed is usually conical and the gas distribution system consists on a large orifice in which the gas velocity is very high. The spout created in the orifice punches the bed material transporting it to the top of the bed. The rest of solids

move downward slowly around the spout, generating solids circulation (Figure 1.1 e)).

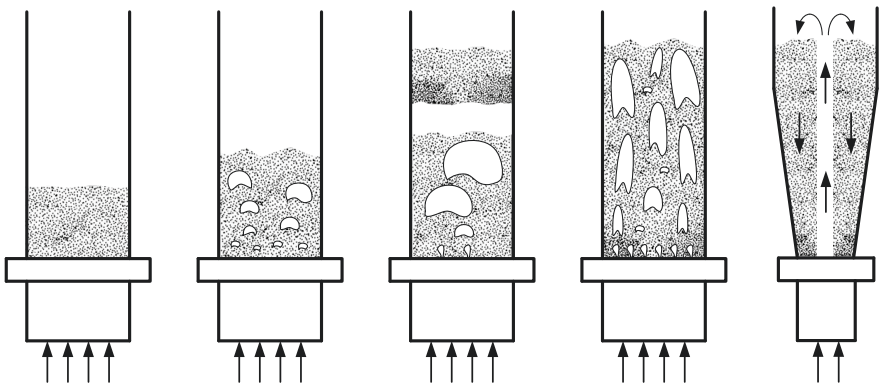

Figure 1.1: Examples of gas fluidization regimes.

1.1.2 Liquid-like behavior of fluidized beds

A dense-phase gas fluidized bed is similar to a boiling liquid and in many ways exhibits a liquid-like behavior, that can be observed carriying out some easy experiments (Figure 1.2):

- An object of lower density than the bed (for example, a rubber duck) will pop up and float on the surface, even if it was sunken at the bottom of the bed before switching on the gas flow (Figure 1.2 a)).
- When the fluidized bed is tilted, the upper surface of the bed remains horizontal (Figure 1.2 b)).
- If there is a hole at the bed wall, solids will gush in a jet out of the bed. The velocity of the jet particles will be similar to $\sqrt{2gH_b}$, where H_b is the distance between the bed surface and the hole (Figure 1.2 c)).
- When two beds of different heights are connected, a flow of particles would pass from the deeper to the shallower bed until both levels equalize (Figure 1.2 d)).
- The differential pressure between two points of the bed is equal to the static pressure of the bed between these points (hydrodynamic pressure) (Figure 1.2 e)).

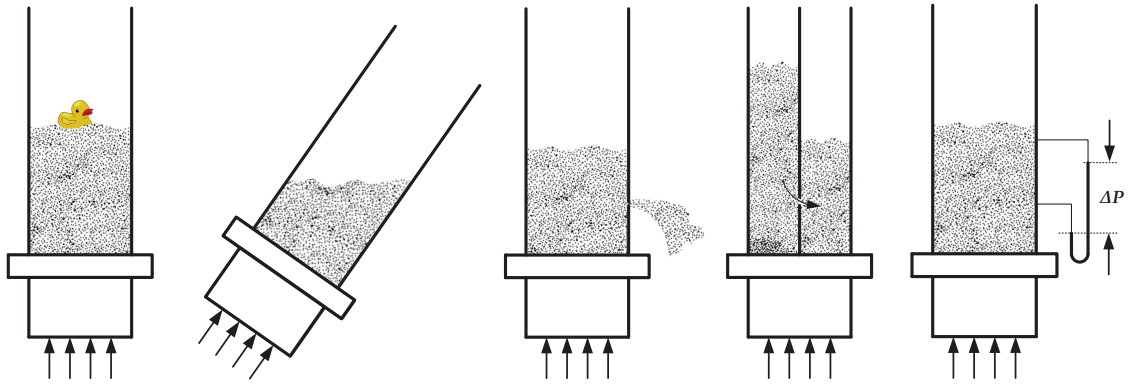

Figure 1.2: Liquid-like behavior of gas fluidized beds (Adapted from Kunii and Levenspiel (1991)).

1.1.3 The Geldart classification of particles

Geldart (1973) classified powders into four groups according to their gas-fluidization properties: the particle size and the difference in density between solid and gas. An example of a modified Geldart's classification is shown in figure 1.3.

- **Type A particles** (aeratable): this group is formed by particles of small mean particle size and/or low density. They are easily fluidized with smooth fluidization at low gas velocities, forming small bubbles at higher gas velocities.
- **Type B particles** (sand-like): this group is formed by particles of medium size and density, similar to silica sand particles commonly used in fluidization. They fluidize properly with vigorous bubbling, and these bubbles grow and coalesce as they rise through the bed.
- **Type C particles** (cohesive): this group is formed by fine powders. Fluidization is extremely difficult because inter-particle forces (i.e. van der Waals forces) are greater than drag forces resulting from the action of gas.
- **Type D particles** (spoutable): this group is formed by large and/or dense particles. They are difficult to fluidize because of its size, they need very high gas velocities. The behavior of type D particles during fluidization is erratic, large exploding bubbles or severe channels are formed, even spouting if the gas distribution is uneven.

Molerus (1982) proposed a new powder classification based on the forces that appears during fluidization: cohesive inter-particle forces (i.e. van der Waals forces), gravity forces and drag forces. Van der Waals forces are dominant in fine powders

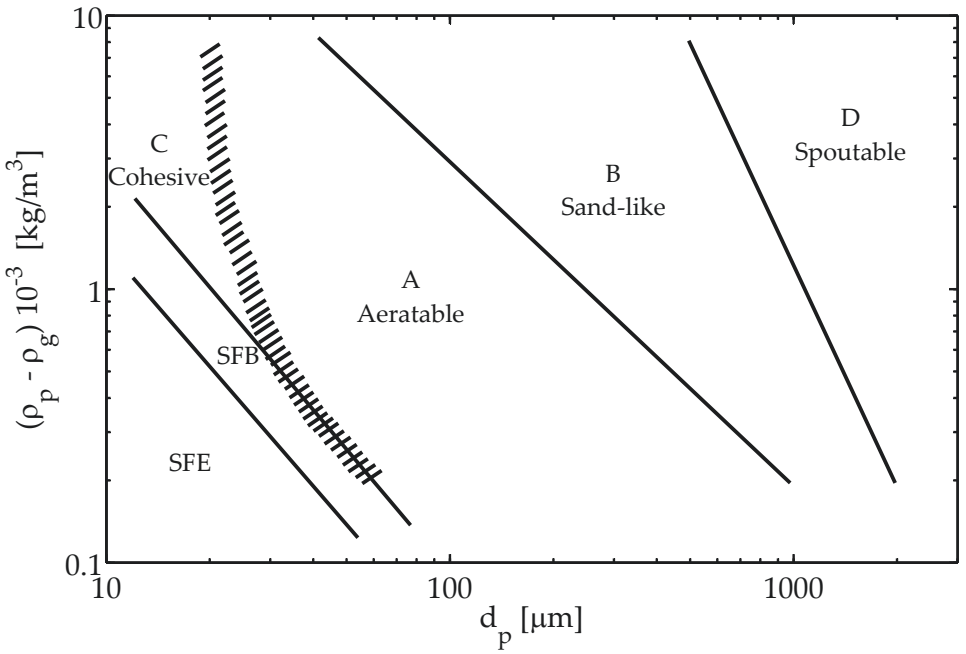

Figure 1.3: Geldart's classification of particles for fluidization with air at atmospheric pressure with modifications of Valverde and Castellanos for C group particles (Adapted from Geldart (1973) and Valverde and Castellanos (2007).

such as type C particles whereas gravity forces are dominant in large particles such type D. In the case of type B, both gravity and drag forces are of the same order, and inter-particle forces are negligible. For type A particles, the three forces are of the same order.

Valverde and Castellanos (2007) proposed a new classification for type C particles. They used empirical relations for liquid-fluidization of larger particles and modified them to take into account the agglomeration in gas fluidization of cohesive particles. The authors distinguished between two different stages of fluidization for type C powders:

- **Solid-to-fluid like to bubbling behavior** (SFB): this group is formed by micron-sized particles and nanoparticles of high density. The fluidization of this type of particles is similar to type A fluidization: bubbles are present but there is a trend to agglomerarion because of the role of inter-particle forces. This type of fluidization is called Agglomerate Bubbling Fluidization (ABF) (Wang et al., 2002).

- **Solid-to-fluid like to elutriation beahavior** (SFE): this group is formed by low density nanoparticles, usually fluidized as agglomerates of very high voidage.

The bed expansion is very high and no bubbles are present during fluidization. This type of fluidization is called Agglomerate Particulate Fluidization (APF) (Wang et al., 2002).

Taking into account the heat transfer properties of particles, Saxena and Ganzha (1984) proposed a new powder classification. The authors divided the particles into three groups: group I, group II and group III. Group I correspond to small particles with high heat transfer coefficient, h_w, and group III correspond to large particles with low heat transfer coefficient. Group II is an intermediate group, with medium sized paticles and moderate heat transfer coefficients. The boundaries between groups were established in terms of the Archimedes number, Ar, and the Reynolds number at minimum fluidization conditions, Re_{mf}.

1.2 Maldistribution in fluidized beds

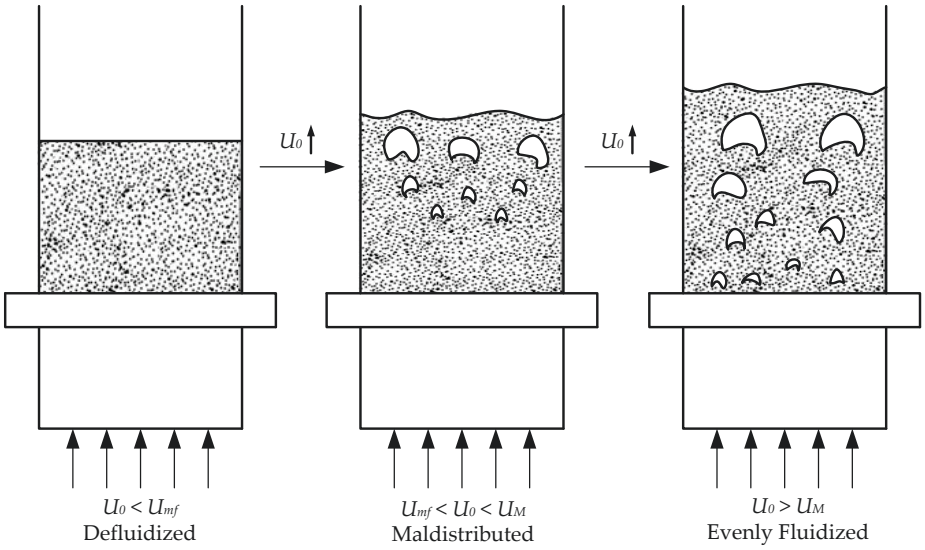

Figure 1.4: Definition of gas maldistribution (Adapted from Thorpe et al. (2002))

Gas maldistribution is one of the most common problems related to distributor design and has an important effect on the performance of fluidized beds. When the gas velocity exceeds the value required for incipient fluidization, U_{mf}, gas bubbles appear in the bed; however there are zones, tipically close to the distributor plate, called dead zones (Geldart and Baeyens, 1985), where bubbles are prevented to appear. The bubbling areas and the dead zones often move with time. Thorpe et al. (2002) defined this state as the maldistribution state (Figure 1.4). These authors reported that when the superficial gas velocity is increased above a certain value, U_M, the distribution of

bubbles through the bed became uniform and the bed is termed evenly fluidized. This value of U_M has been defined as the superficial gas velocity at which all the orifices or tuyeres of the distributor plate become operative, which usually means they are jetting (Sathiyamoorthy and Rao, 1981; Whitehead, 1971). Sathiyamoorthy and Rao (1981) reported that the stable operation (i.e. no maldistribution present) of a fluidized bed can be achieved when all the orifices or tuyeres of the distributor are operating at the same time and additionally, when there is a uniform distribution of gas and solids without any channeling in the bed. As previously reported by Whitehead (1971), the number of operating orifices or tuyeres depends on the gas flow rate, the bed aspect ratio, the bed material and the open area of the distributor.

Maldistribution is industrially undesirable: for dryers, because in the dead zones the drying rate drastically decreases; for reactors, because bypassing of reactants and uneven temperature in the bed are obtained; and in general, because it affects the heat and mass transfer capabilities and in case of sticky or aggregative solids, agglomeration problems and defluidization of the entire bed may occur (Briens et al., 1988). In most of the industrial processes carried out in fluidized beds, it is of crucial importance to prevent defluidization. If a defluidization problem is not detected and solved, major damage can be caused to bed internals, agglomeration of bed particles may occur and, as a consequence, the heat and mass transfer capabilities of the bed will be drastically reduced (van Ommen et al., 2004).

Maldistribution problems are directly related to the distributor plate design, which often determines the success of failure of a fluidized bed. Distributor plates must have sufficient strenght to resist deformation during operation and to support the weight of fixed bed. They must be capable to resist stresses induced by thermal expansion, operate for long periods without orifice blocking, prevent backflow of solids into the plenum chamber and operate at as low a pressure drop as possible to minimize the power consumption (Geldart and Baeyens, 1985). It is difficult to fulfill all these requeriments at the same time, because not all of them are compatible, and their relative importance may change with the process requirements.

Traditionally, the ratio, R, of pressure drop across the distributor, ΔP_{dist}, to that across the bed, ΔP_{bed}, has been used as a simplistic criterion to design distributor plates in fluidized beds (Qureshi and Creasy, 1979; Saxena et al., 1979; Sathiyamoorthy and Rao, 1981; Geldart and Baeyens, 1985; Sathiyamoorthy and Horio, 2003). Over the past 50 years several authors have specified that R should be greater than a certain critical value to ensure even fluidization (Zenz and Othmer, 1960; Hiby, 1967; Avery and Tracey, 1968; Perry et al., 1997; Thorpe et al., 2000; Karri and Werther, 2003). However, there is no consensus in the literature about the critical value of R, since

authors reported values in the range 0.02 to 1. A value of 0.2-0.4 (Kunii and Levenspiel, 1991; Perry et al., 1997; Karri and Werther, 2003) was generally used, as a rule of thumb. As a result, it has been concluded (Qureshi and Creasy, 1979; Thorpe et al., 2002) that there is no universality in selecting a specific value of R for distributor design.

Even though the use of R as a parameter on distributor plate design has been rejected by some authors (Thorpe et al., 2000, 2002), it is still an important variable in the performance of a fluidized bed. If a very large value is chosen for design, it will be, in many cases, wasteful in terms of the energy required to pump the fluidizing gas through the distributor plate. However, if a lower value is chosen there is a risk of maldistribution.

1.3 Objectives of the thesis

As stated above, the maldistribution phenomena is a field of great interest from the industrial perspective since maldistribution problems typically appear in fluidized beds reactors. Thus, this thesis is focused on the experimental study of several aspects related to the gas maldistribution in fluidized beds. The main objectives of the thesis are the following:

- The study of the effect of the operational temperature on the distributor to bed pressure drop ratio, R, since it is an important factor in the gas distributor plate design.
- The study of the boundary of gas maldistribution detection and the possibilities of online monitoring of maldistribution.
- The development of a model to estimate the size of dead zones generated by maldistribution in large-scale fluidized beds.

1.4 Structure of the thesis

This PhD thesis has been organized in six chapters. An overall explanation of the experimental facilities and measurement systems used in this thesis is included in **Chapter 2**. A more detailed description can be found in the experimental setup section of each chapter.

Chapter 3 presents a study of the effect of bed temperature on the distributor to bed pressure drop ratio, R. First, the effect of the temperature on the distributor

pressure drop was analyzed for two different distributor plates and, finally, a simplified model to estimate the optimal distributor open area at a given operation temperature was developed.

Chapter 4 shows a study of the onset of maldistribution in fluidized beds. The maldistribution phenomena was first investigated using Digital Image Analysis of images of the bed surface. Then, in order to establish a criteria for maldistribution detection, pressure fluctuations signals were analyzed. Finally, several monitoring tools reported in the literature were tested to prove its performance for online monitoring of maldistribution problems in fluidized beds. The effect of the rotation of the distributor plate is also investigated in this chapter as a counteracting mechanism to overcome maldistribution.

Chapter 5 presents a model to estimate the dead zones generated by maldistribution in large-sacale fluidized beds. The internal structure of an induced maldistributed pseudo-2D fluidized bed was first studied. The results were extrapolated to 3D beds by means of correlations. It was found that the proposed model can predict the volume of the dead zones with a maximum relative error of 20%.

Finally, the main conclusions of the thesis are summarized in **Chapter 6**.

1.5 Notation

d_p	Mean particle diameter [m]
g	Gravity [m/s^2]
H_b	Bed height [m]
H_{mf}	Bed height at minimum fluidization conditions [m]
ΔP_{bed}	Bed pressure drop [Pa]
ΔP_{dist}	Distributor pressure drop [Pa]
R	Pressure drop ratio [-]
Re_{mf}	Reynolds number at minimum fluidization conditions [-]
U_0	Air superficial velocity [m/s]
U_M	Superficial gas velocity at which all the orifices became operative [m/s]
U_{mf}	Minimum fluidization velocity [m/s]

Greek letters

ϵ_{mf}	Voidage at minimum fluidization conditions [-]
ϵ_0	Fixed bed voidage [-]
μ_g	Air viscosity at bed temperature [kg/ms]

ρ_g	Air density at bed temperature [kg/m^3]
ρ_p	Particle density [kg/m^3]
ϕ	Particle sphericity [-]

Abbreviattions

ABF	Agglomerate Bubbling Fluidization.
APF	Agglomerate Particulate Fluidization.
FCC	Fluid Cracking Catalyst.
SFB	Solid–to–fluid like to bubbling behavior.
SFE	Solid–to–fluid like to elutriation behavior.

Bibliography

Avery, D.A., Tracey, D.H., 1968. The application of fluidised beds of activated carbon. In: *Proceedings of the I Chem E Symposium*, Montreal, Canada; I Chem E: London. 28.

Briens, C.L., Tyagi, A.K., Bergougnou, M.A., 1988. Pressure drop through multiorifice gas distributors in fluidized bed columns. *Can. J. Chem. Eng.* 66, 740-748.

Ergun, S., 1952. Fluid flow through packed column. *Chem. Eng. Prog.* 48, 89-94.

Geldart, D.,1973. Types of gas fluidization. *Powder Technol.* 7, 285-292.

Geldart, D., Baeyens, J., 1985. The design of distributors for gas-fluidized beds. *Powder Technol.* 42, 67-78.

Hiby, J.W., 1964. Critical minimum pressure drop of gas distributor plate in fluidized bed units. *Chem. Ing. Techn.* 36, 328.

Karri, S.B.R., Werther, J., 2003. Gas distributor and plenum design in fluidized beds. In: Yang, W.C. *Handbook of fluidization and fluid-particle systems.* Marcel Dekker Inc., New York, 164-179.

Kunii, D., Levenspiel, O., 1991. *Fluidization engineering*, Butterworth-Heinemann, Stoneham, UK, 2nd ed.

Molerus, O., 1982. Interpretation of Geldart's type A, B, C and D powders by taking into account interparticle cohesion forces. *Powder Technol.* 33, 81-87.

Perry, R.H., Green, D.W., Maloney, J.O., 1997. Perry's Chemical Engineers' Handbook. McGraw-Hill: New York. 17-6.

Qureshi, A.E., Creasy, D.E., 1979. Fluidised bed distributors.*Powder Technol.* 22, 113-119.

Sathiyamoorthy, D., Sridhar Rao, C.H., 1981. The choice of distributor to bed pressure drop ratio in gas fluidised beds. *Powder Technol.* 30, 139-143.

Sathiyamoorthy, D., Horio, M., 2003. On the influence of aspect ratio and distributor in gas fluidized beds. *Chem. Eng. J.* 93, 151-161.

Saxena, S.C., Chatterjee, A., Patel, R.C., 1979. Effect of distributors on gas-solid fluidization. *Powder Technol.* 22, 191-198.

Saxena, S.C., Ganzha, V.L., 1985. Heat transfer to inmersed surfaces in gas-fluidized beds of large particles and powder characterization. *Powder Technol.* 39, 199-208.

Thorpe, R.B., Davidson, J.F., Downing, S.J., Dusad, A., Farthing, P., Ferdinando, G., Holden, A., Martin, A., Negyal, O., Saundry, J., 2000. On the minimum distributor pressure drop for uniform fluidization. In: *Proceedings of 3rd European Conference on Fluidization*, Toulouse 189.

Thorpe, R.B., Davidson, J.F., Pollitt, M., Smith, J., 2002. Maldistribution in fluidized beds. *Ind. Eng. Chem. Res.* 41 , 5878-5889.

Valverde, J.M., Castellanos, A., 2007. Types of gas fluidization of cohesive granular materials. *Phys. Rev. E* 75, 301-306.

van Ommen, J.R., de Korte, R.J., van den Bleek, C.M., 2004. Rapid detection of defluidization using the standard deviation of pressure fluctuations. *Chem. Eng. Process.* 43, 1329-1335.

Wang, Y., Gu, G., Wei, F., Wu, J., 2002. Fluidization and agglomerate structure of SiO_2 nanoparticles. *Powder Technol.* 124, 152-159.

Whitehead, A.B., 1971. In Davidson, J.F., Harrison, D. (Eds.) *Fluidization*. Academic Press, London. 781.

Zenz, F.A., Othmer, D.F., 1960. Fluidization and fluid particle systems. Rheinhold: New York. 260.

Chapter 2

Experimental Setup

Contents

2.1 Introduction

This chapter contains the description of the three fluidized beds where the experiments were carried out. Details of the different distributor plates used are also provided. Finally, a summary of the measurement systems has been included, although specific details will be described in each chapter.

2.2 Biomass bubbling fluidized bed gasifier

A Biomass Bubbling Fluidized Bed Gasifier (BBFBG) pilot-plant was used in this thesis to perform experiments at elevated temperature. It consisted of a cylindrical

vessel made of stainless steel. The column has a total height of 2.5 m divided into two sections: the bed section of 0.134 m inner diameter and the freeboard region of 0.25 m inner diameter. A schematic diagram of this facility is shown in Figure 2.1.

The facility is equipped with three electrical furnaces of 10 kW, 5 kW and 5 kW respectivelly, to heat up the bed and to compensate the heat losses during operation. The fluidizing air passes through an air preheater of 9 kW to heat up the air stream before entering the fluidized bed. A cyclone is placed in the exhaust air stream to collect entrained particles and ashes.

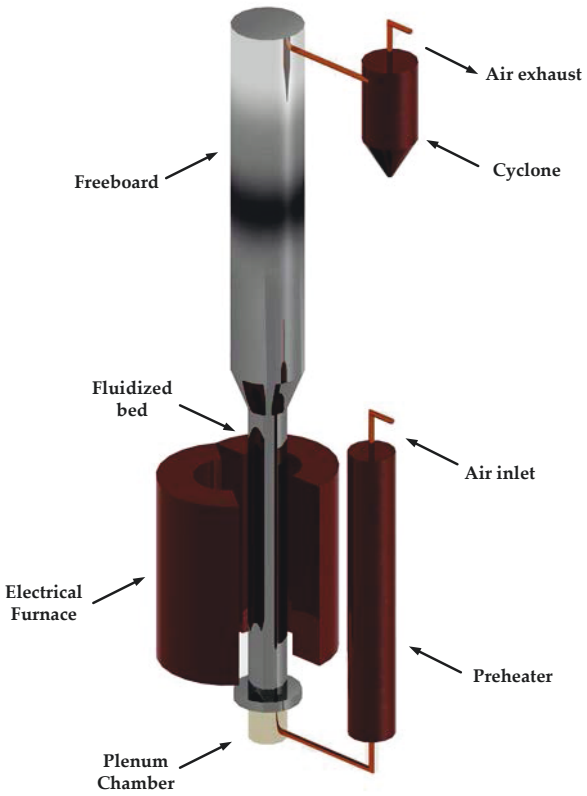

Figure 2.1: Schematic diagram of the Biomass Bubbling Fluidized Bed Gasifier.

Two different distributor plates were employed in this facility: a perforated plate (Figure 2.2a) and a tuyere type distributor (Figure 2.2b). Both distributor plates were made of stainless steel and were designed intending to minimize the dead zones between orifices (Soria-Verdugo et al., 2011). The perforated plate counts on 140 orifices of 0.001 m diameter arranged in a square configuration with 0.01 m pitch. The tuyere type distributor consists of 19 tuyeres arranged in a triangular configuration with 0.02 m pitch and screwed in a perforated plate. Each tuyere has 8 orifices of the same

diameter than the orifices of the perforated plate. Both distributors count on a similar open area.

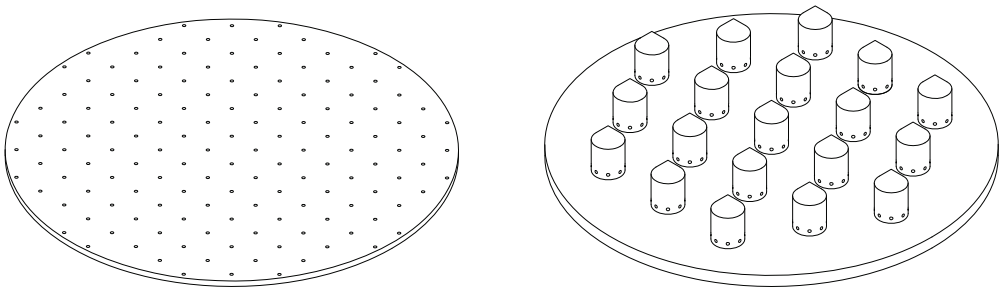

(a) (b)

Figure 2.2: Distributor plate designs: (a) Multiorifice type, (b) Tuyere type.

According to Kunii and Levenspiel (1991), the bubble generation in a perforated plate distributor is noticeable different to the bubble generation in a tuyere type distributor (Figure 2.3). The different characteristics of these distributors leads to different pressure drop curves, even thought both distributor plates have a similar open area. This issue will be discused in detail in Chapter 3.

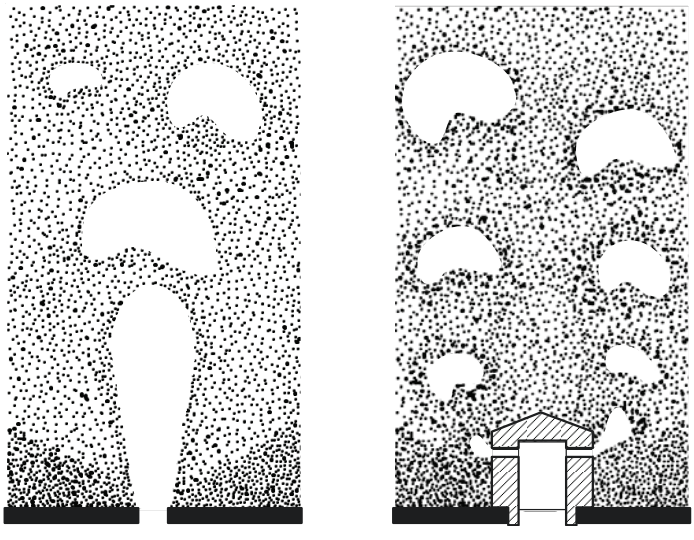

(a) (b)

Figure 2.3: Bubble generation patterns: (a) Multiorifice distributor and (b) Tuyere type distributor (Adapted from Kunii and Levenspiel (1991)).

2.3 3D rotating facility

This experimental setup consist on a lab-scale cylindrical BFB, equipped with an electrical motor to produce the rotation of the distributor plate in the horizontal plane. The column is a transparent tube with an inner diameter of 0.192 m and 1 m in height. A mirror was attached to the top of the bed in order to reflect the bed surface, allowing taking pictures of the bed surface with a camera located in the front part of the bed. Figure 2.4 shows a schematic diagram of the 3D facility.

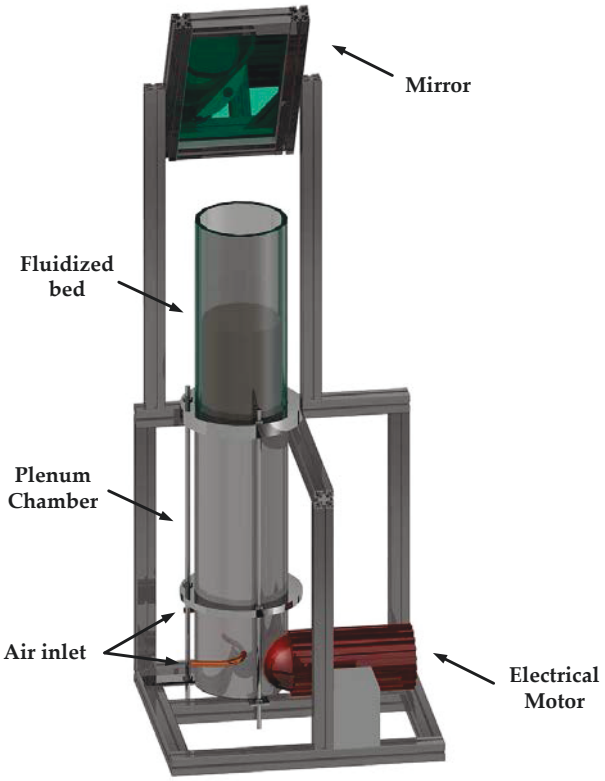

Figure 2.4: Schematic diagram of the 3D rotating facility.

The distributor plate was a perforated plate of 0.006 m thickness, counting on 264 orifices of 0.002 m diameter. The orifices were distributed in a triangular configuration with 0.011 m pitch. A mesh with 200 μm in aperture and 30 % open area was employed to avoid the falling of particles inside the plenum chamber. The distributor pressure drop is plotted in Figure 2.5 as a function of the gas velocity. The characterization has been done taking into account the mesh and because of that the results of Figure 2.5 show the combined pressure drop resulting from the sum of both the distributor plate

and mesh pressure drop contributions. The solid line represents the predictions of the model described in Chapter 3.

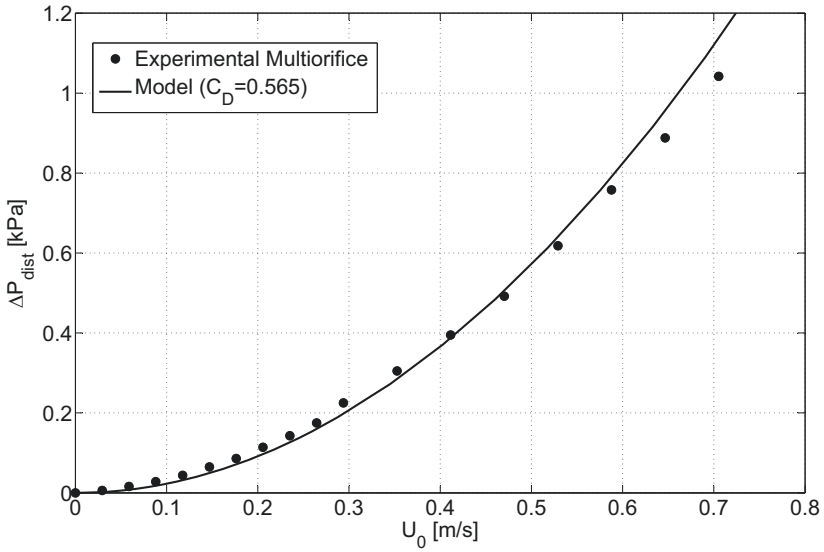

Figure 2.5: Variation of distributor pressure drop with gas superficial velocity at ambient temperature for the 3D facility multiorifice distributor plate.

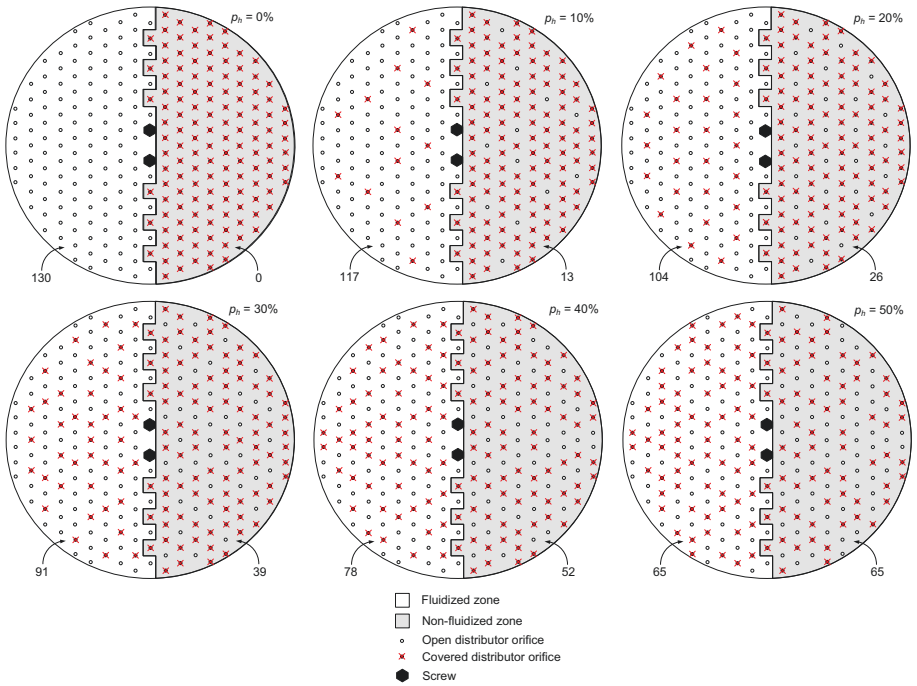

Figure 2.6: Orifice distribution patterns in the 3D rotating facility for the study of the onset of maldistribution detection.

Different orifice configurations were used for the experiments carried out in Chapter 4 (Figure 2.6). All the orifice distribution tested had the same number of orifices, exactly half of the total orifices of the distributor plate (132), and therefore they have a similar pressure drop. A more detailed explanation about the purpose of these orifice configurations can be found in Chapter 4.

2.4 2D facility

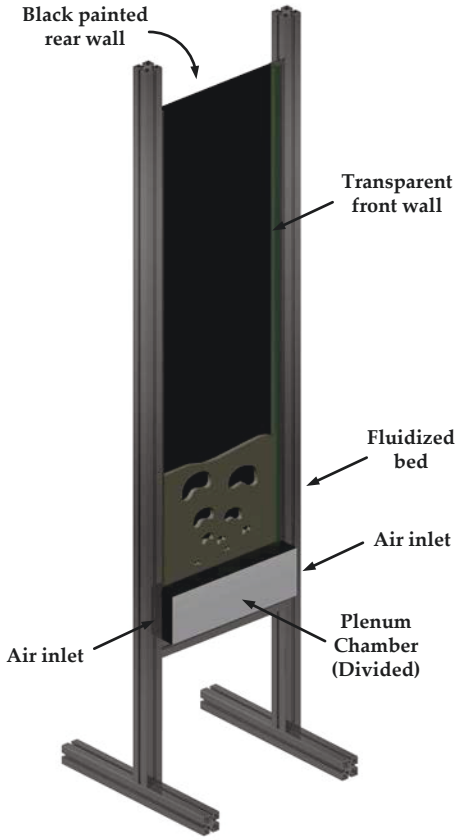

Figure 2.7: Schematic diagram of the 2D facility.

This experimental facility consists on a pseudo-2D cold fluidized bed with a width of 0.3 m, a height of 1 m, and a thickness of 0.01 m. A schematic diagram of the experimental setup is shown in Figure 2.7. The bed and the plenum chamber were made of aluminium and the front and rear walls were made of glass to allow optical access. The rear wall was painted in black to increase the contrast in the front images.

The air distributor was an aluminium perforated plate with two rows of orifices, each one consisting of 30 orifices of 0.001 m diameter arranged in a triangular configuration

with 0.01 m pitch. A mesh was also employed to avoid the falling of particles inside the plenum chamber and to ensure a proper distributor to bed pressure drop ratio, R, to avoid gas maldistribution (Karri and Werther, 2003). Figure 2.8 shows a schematic diagram of the distributor plate used in the 2D facility.

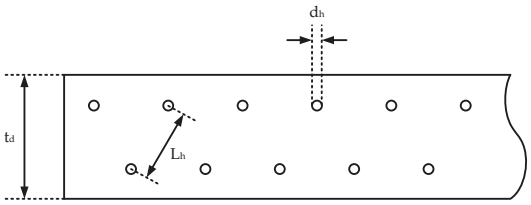

Figure 2.8: Schematic diagram of the distributor plate of the 2D facility.

The plenum chamber was divided in two separated chambers of the same size and volume to perform the experiments of Chapter 5. It allows the air to be supplied only to one half of the fluidized bed and also allows to conduct experiments where the air superficial velocity is different in the two chambers. A more detailed explanation of the experiments can be found in Chapter 5. The distributor pressure drop is shown in Figure 2.9 for the two separated plenum chambers. As can be seen, the differences in pressure drop between both chambers are negligible.

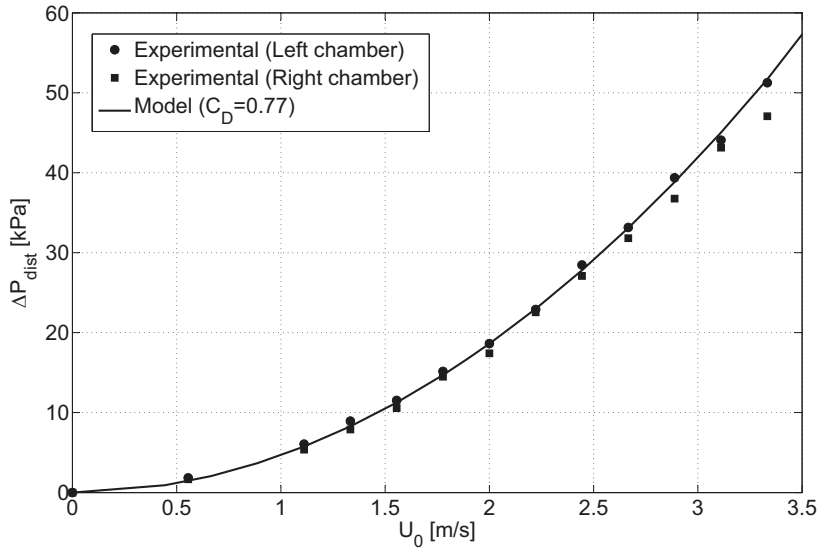

Figure 2.9: Variation of distributor pressure drop with gas superficial velocity at ambient temperature for the two different plenum chambes of the 2D facility.

2.5 Experimental techniques

Three non-intrusive experimental techniques have been used in this thesis: pressure signal analysis, Digital Image Analysis (DIA) and Particle Image Velocimetry (PIV). These techniques are well-known in the field of fluidized beds, and a brief description of them is presented below.

2.5.1 Pressure signal analysis

Pressure is often chosen to characterize the fluid dynamics of gas-solid fluidized beds. The advantage of using pressure is that it is easily measured, even under harsh, industrial conditions. In addition, a pressure measurement system, including pressure sensor and pressure tap, is robust, relatively cheap and virtually nonintrusive, thus avoiding distortion of the flow around the point of measurement (van Ommen et al., 2011). Pressure measurements are probably the most common measurement technique for verifying models as well as to determine gas-solid distributions in a fluidized bed. An example of a pressure fluctuation signal measured in the BBFBG facility is shown in Figure 2.10.

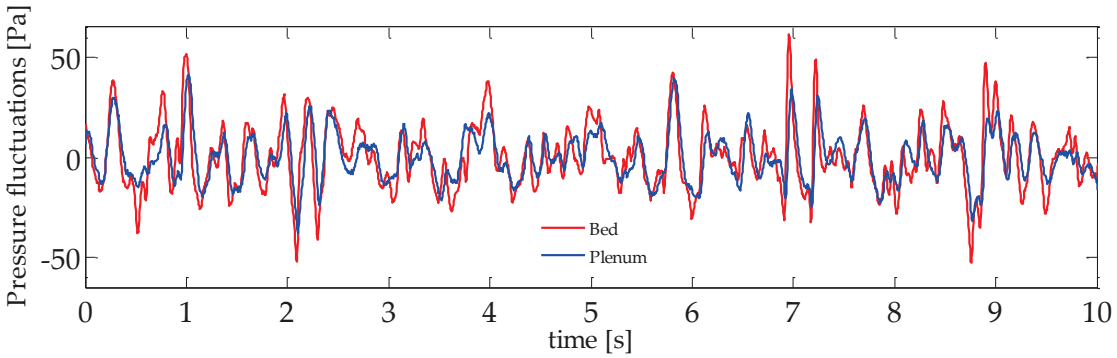

Figure 2.10: Pressure fluctuations signal measured simultaneously in the plenum chamber and inside the bed.

There is a large number of methods for the analysis of time-series of pressure signals recorded in fluidized beds that can be found in the literature (Johnsson et al., 2000; van Ommen et al., 2011). These methods can be grouped into three main categories:

- **Time domain methods**: standard deviation (Wilkinson , 1995; Puncochár et al., 1985; Sobrino et al., 2008; van Ommen et al., 2004), average cycle time (Briens and Briens , 2002), V-statistic (Briens et al., 1999), autoregressive models (Brown and Brue , 2001).

- **Frequency domain methods**: power spectrum (Kage et al., 1991; Johnsson et al., 2000), transient power spectral density (Gómez-Hernández et al., 2012), wide band energy division (Johnsson et al., 2000; Gómez-Hernández et al., 2014), wavelet analysis (de Martín et al., 2010; Villa Briongos et al., 2006, 2007).
- **State space methods**: attractor comparison (Diks et al., 1996; van Ommen et al., 2000), Kolmogorov entropy (van der Schaaf et al., 2004).

2.5.2 Digital Image Analysis (DIA)

(a) (b)

Figure 2.11: Example of DIA for image processing: a) Original picture and b) Black and white picture.

The DIA technique can be applied to images acquired with a digital camera over an optically accessible part of the bed. This optical access is usually the front part in a 2D fluidized bed and the bed surface in a 3D fluidized bed. Two main objectives are usually pursued with DIA:

- A clear identification of the two phases of the fluidized bed: the bubble phase free of particles and the dense phase free of bubbles.
- The complete characterization of the bubbles based in equivalent diameter, mass center position and bubble velocity.

The digital images can be acquired in grey scale with values ranging from 0 to 255. A threshold transformation is needed for the identification of the two phases explained above. The original image is transformed into a black and white image where the pixels with values equal to 0 represent the bubble phase and the pixels of the dense phase take a value equal to 1 (Otsu, 1979). The bubble properties are typically calculated with the black and white images. Figure 2.11 shows an example of the picture transformation

into grey scale and the global pattern in the bed surface resulting from the integration of all the pictures taken in a given measurement time.

2.5.3 Particle Image Velocimetry (PIV)

The PIV technique has been used to characterize the dense phase velocity (Raffel et al., 2007; Sveen, 1998-2008). PIV takes two consecutive frames to measure the displacement of the particles, Δx or Δy, and therefore to calculate the velocity using the time elapsed between the two frames, Δt.

$$u(x,t) = \frac{\Delta x(x,t)}{\Delta t} \tag{2.1}$$

$$v(y,t) = \frac{\Delta y(y,t)}{\Delta t} \tag{2.2}$$

Tipically, the PIV technique is applied to a single phase flow field seeded with particles small enough to follow the flow motion exactly (Raffel et al., 2007). The particles are illuminated by a light sheet generated by a laser. The domain (images of the particles in a two-dimensional plane) is divided into smaller sections called interrogation windows, whose size is fixed or can be reduced along consecutive steps. The light is generated in two pulses, and the displacement of the tracer particles between the two light pulses is determined with statistical methods, such as the cross-correlation function, for each window.

PIV can be applied to pseudo-2D fluidized beds since the transparent wall allows optical access to the interior of the bed. In this case, the bed is continuosly illuminated, and the images are recorded at high frequency. The window size is tipically between 16 to 64 pixels, with an overlap of 0.5. The velocity can be calculated by dividing the displacement by the time elapsed between the two consecutive images; therefore, the velocity vectors are obtained every 8 pixels. Since bubbles are considered regions free of particles, a mask must be applied to the images that rejects dense phase velocity inside bubbles.

According to Raffel et al. (2007), the estimation of each velocity vector can be affected by bias and subpixel errors. If the bed is uniformly illuminated, the bias errors are principally generated by velocity gradients smaller than the interrogation window lenght. The bias error can be reduced using multigrid PIV techniques with small interrogation windows at the final stages of the PIV procedure (Hernández-Jiménez et al., 2011). Provided that the concentration of particles in the dense phase is high, the background noise and the peak-locking, which are the main sources of subpixel error in PIV, are not expected to be relevant for the accuracy of the results (Raffel et al.,

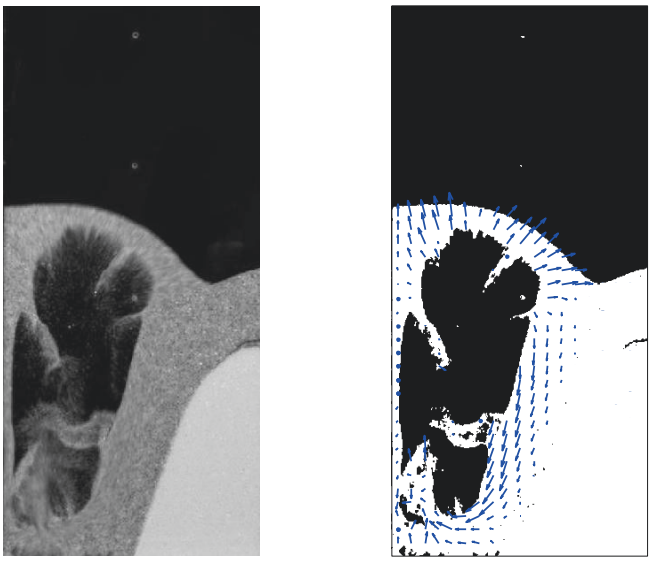

(a) (b)

Figure 2.12: PIV processing (a) Raw particle image and (b) bubble mask and PIV velocity vectors.

2007).

PIV has been widely used in fluidized beds: Almendros-Ibáñez et al. (2006, 2010); Busciglio et al. (2008); Müller et al. (2007); Laverman et al. (2008); Sánchez-Delgado et al. (2010, 2013); Santana et al. (2005); Vun et al. (2010); Hernández-Jiménez et al. (2011).

Figure 2.12 shows an example of an adquired raw image (a) as well as the threshold transformation explained in the DIA section, together with the PIV velocity vectors calculated between two consecutive frames for the solid phase (b).

2.6 Measurement systems

This section is a summary of all the measurements systems used on the experiments of this thesis.

- **Piezo-electric pressure transducers** (*Kistler type 5015*): three piezo-electric pressure transducers were used in the experiments to measure the pressure fluctuations in different positions of the bed. Each transducer is equipped with an amplifier that includes two filters: high-pass filter with a characteristic frequency of 0.16 Hz and low-pass filter at the Nyquist frequency of the system.

  These transducers have been used in the BBFBG facility and the 3D rotating

facility. The data provided by the pressure transducers was used to estimate the minimum fluidization velocity of the different solid materials employed with the method of Puncochár et al. (1985) and to obtain hydrodynamic information of the bed.

- **Gauge pressure sensors** (*Honeywell SPT Series*): two gauge sensors were used to characterize the distributor pressure drop in the three experimental facilities employed in the thesis. The range of operation of the two gauge sensors is 0 – 5 psi and 0 – 15 psi.

- **Differential pressure sensor** (*Setra*): a differential pressure sensor was used to measure the minimum fluidization voidage, ϵ_{mf}, of the different solids employed in this thesis. The range of operation of the differential sensor is 0 – 10 inH_2O.

- **Camera Casio Exilim 6.0 Mpx**: a digital camera was used to take images of the bed surface in the 3D rotating facility. The maximum frame rate of the camera is 30 fps and the spatial resolution of the picture is 480 x 640 pixels.

- **K-type thermocouples**: two thermocouples were used to measure the temperature in the BBFBG facility. One of them was placed in the plenum chamber to monitor the temperature of the preheated air before entering the fluidized bed, and the other one was located inside the bed to measure the bed temperature. The range of operation of the K-type thermocouples is -200 – 1250°C.

- **Air flow meters** (*SMC*): several air flow meters were used to measure the volumetric flow of fluidizing air before entering the fluidized bed. The ranges of operation of the air flow meters of the 3D rotating facility and the BBFBG facility are 0 – 500 l/min and 150 – 3000 l/min, and 0 – 200 l/min and 0 – 500 l/min for the 2D facility. The air flow meter used was selected taking into account the superficial gas velocity needed for the experiment, usually determined by the type and size of solids employed.

- **Camera Basler A640**: a digital camera was used to take images of the front view in the 2D facility. The maximum frame rate of the camera is 100 fps and the spatial resolution of the pictures is 300 x 600 pixels.

All the signals were transferred to a PC using a National Instruments data acquisition system type 9234 with 4 analog input channels, 24-bit resolution. The sampling frequency of pressure signals was always 2000 Hz. After the sampling process, the signals were resampled to the desired frequency for the specific analysis employed.

Bibliography

Almendros-Ibáñez, J.A., Sobrino, C., de Vega, M., Santana, D., 2006. A new model for ejected particle velocity from erupting bubbles in 2-D fluidized beds. *Chem. Eng. Sci.* 61, 5981-5990.

Almendros-Ibáñez, J.A., Pallarès, D., Johnsson, F., Santana, D., 2010. Voidage distribution around bubbles in a fluidized bed: influence of throughflow. *Powder Technol.* 197, 73-82.

Briens, L.A., Briens, C.L., 2002. Cycle detection and characterization in chemical engineering. *AIChE J.* 48, 970980.

Briens, C.L., Briens, L.A., Barthel, E., Le Blévec, J.M., Tedoldi, A., Margaritis, A., 1999. Detection of local fluidization characteristics using the V statistic. *Powder Technol.* 102, 95103

Brown, R.C., Brue, E., 2001. Resolving dynamical features of fluidized beds from pressure fluctuations. *Powder Technol.* 119, 6880.

Busciglio, A., Vella, G., Micale, G., Rizzuti, L., 2008. Analysis of the bubbling behaviour of 2D gas solid fluidized beds: Part I. Digital image analysis technique. *Chem. Eng. J.* 140, 398-413.

de Martín, L., Villa Briongos, J., Aragón, J.M., Palancar, M.C., 2010. Can low frequency accelerometry replace pressure measurements for monitoring gassolid fluidized beds?. *Chem. Eng. Sci.* 65, 40554064

Diks, C., van Zwet, W.R., Takens, F., DeGoede, J., 1996. Detecting differences between delay vector distributions. *Phys. Rev. E* 53, 2169-2176.

Gómez-Hernández, J., Soria-Verdugo, A., Briongos, J.V., Santana, D., 2012. Fluidized bed with a rotating distributor operated under defluidization conditions. *Chem. Eng. J.* 195-196, 198-207.

Gómez-Hernández, J., Sánchez-Prieto, J., Briongos, J.V., Santana, D., 2014. Wide band energy analysis of fluidized bed pressure fluctuation signals using a frequency division method. *Chem. Eng. Sci.* 105, 92-103.

Hernández-Jiménez, F., Sánchez-Delgado, S., Gómez-García, A., Acosta-Iborra, A., 2011. Comparison between two-fluid model simulations and particle image analysis & velocimetry (PIV) results for a two-dimensional gas-solid fluidized bed. *Chem. Eng. Sci.* 66, 3753-3772.

Johnsson, F., Zijerveld, R.C., Schouten, J.C., van den Bleek, C.M., Leckner, B., 2000. Characterization of fluidization regimes by time-series analysis of pressure fluctuations. *Int. J. Multiphase Flow* 26, 663-715.

Kage, H., Iwasaki, N., Yamaguchi, H., Matsuno, Y., 1991. Frequency analysis of pressure fluctuation in fluidized bed plenum. *J. Chem. Eng. Jpn.* 24, 7681.

Karri, S.B.R., Werther, J., 2003. Gas distributor and plenum design in fluidized beds. In: Yang, W.C. *Handbook of fluidization and fluid-particle systems*. Marcel Dekker Inc., New York, 164-179.

Kunii, D., Levenspiel, O., 1991. *Fluidization engineering*, Butterworth-Heinemann, Stoneham, UK, 2nd ed.

Müller, C.R., Davidson, J.F., Dennis, J.S., Hayhurst, A.N., 2007. A study of the motion and eruption of a bubble at the surface of a two-dimensional fluidized bed using particle image velocimetry (PIV). *Ind. Eng. Chem. Res.* 46, 1642-1652.

Laverman, J.A., Roghair, I., van Sint Annaland, M., Kuipers, H., 2008. Investigation into the hydrodynamics of gas-solid fluidized beds using particle image velocimetry coupled with digital image analysis. *Can. J. Chem. Eng.* 86, 523-535.

Otsu, N., 1979. A threshold selection method from gray-level histograms, *IEEE Transactions on Systems Man and Cybernetic*s 9, 62-66.

Puncochár, M., Drahos, J., Cermák, , J., Selucký, K., 1985. Evaluation of minimum fluidization velocity in gas fluidized beds from pressure fluctuations. *Chem. Eng. Commun.* 35, 81-87.

Raffel, M., Willert, C., Kompenhans, J., 2007. Particle Image Velocimetry, A Practical Guide. Springer, Berlin.

Sánchez-Delgado, S., Marugán-Cruz, C., Acosta-Iborra, A., Santana, D., 2010. Dense-phase velocity fluctuation in a 2-D fluidized bed. *Powder Technol.* 200, 37-45.

Sánchez-Delgado, S., Marugán-Cruz, C., Soria-Verdugo, A., Santana, D., 2013. Estimation and experimental validation of the circulation time in a 2D gas-solid fluidized beds. *Powder Technol.* 235, 669-676.

Santana, D., Nauri, S., Acosta, A., Garca, N., Macas-Machn, A., 2005. Initial particle velocity spatial distribution from 2-D erupting bubbles in fluidized beds. *Powder Technol.* 150, 1-8.

Sobrino, C., Sánchez-Delgado, S., García-Hernando, N., de Vega, M., 2008. Standard deviation of absolute and differential pressure fluctuations in fluidized beds of group B particles. *Chem. Eng. Res. Des.* 86, 12361242.

Soria-Verdugo, A., Garca-Hernando, N., Almendros-Ibáez, J.A., Ruiz-Rivas, U., 2011. Motion of a large object in a bubbling fluidized bed with a rotating distributor. *Chemical Engineering and Processing: Process Intensification* 50, 859-868.

Sveen, J.K., 1998-2008. MATPIV. http://www.math.uio.no/jks/matpiv/.

van der Schaaf, J., van Ommen, J.R., Takens, F., Schouten, J.C., van den Bleek, C.M., 2004. Similarity between chaos analysis and frequency analysis of pressure fluctuations in fluidized beds. *Chem. Eng. Sci.* 59, 18291840.

van Ommen, J.R., Coppens, M.C., van den Bleek, C.M., Schouten, J.C., 2000. Early warning of agglomeration in fluidized beds by attractor comparison. *AIChE J.* 46, 2183-2197.

van Ommen, J.R., de Korte, R.J., van den Bleek, C.M., 2004. Rapid detection of defluidization using the standard deviation of pressure fluctuations. *Chem. Eng. Process.* 43, 1329-1335.

van Ommen, J.R., Sasic, S., van der Schaaf, J., Gheorghiu, S., Johnsson, F., 2011. Time-series analysis of pressure fluctuations in gas-solid fluidized beds A review. *International Journal of Multiphase flow* 37, 403-428.

Villa Briongos, J., Aragón, J.M., Palancar, M.C., 2006. Phase space structure and multi-resolution analysis of gassolid fluidized bed hydrodynamics: part I the EMD approach. *Chem. Eng. Sci.* 61, 69636980.

Villa Briongos, J., Aragón, J.M., Palancar, M.C., 2007. Phase space structure and multi-resolution analysis of gassolid fluidized bed hydrodynamics: part II: dynamic analysis. *Chem. Eng. Sci.* 62, 28652879.

Vun, S., Naser, J., Witt, P.J., Yang, W., 2010. Measurements and numerical predictions of gas vortices formed by single bubble eruptions in the freeboard of a fluidised bed. *Chem. Eng. Sci.* 65, 5808-5820.

Wilkinson, D., 1995. Determination of minimum fluidization velocity by pressure fluctuation measurement. *Can. J. Chem. Eng.* 73, 562-565.

Chapter 3

The effect of temperature on the distributor design

Contents

3.1 Introduction

Bubbling gas-solid fluidized beds (BFBs) are broadly applied in industry, particularly in thermochemical energy conversion processes such as combustion and gasification. The fluidization process offers a high heat transfer rate, good gas-solid mixing and solid handling, and provides a uniform and controllable temperature. Moreover, its ability to process low grade fuels with low pollutant emission makes the use of BFBs a very promising technology for the valorization of biomass and wastes in energy conversion processes. According to that, a better understanding of the fluidization hydrodynamics during operation is needed to enhance the reactor design and scale-up processes. Many authors have reported experimental results of biomass gasification in bubbling fluidized

bed pilot-plants and lab-scale facilities (Olivares et al., 1997; Campoy et al., 2009; de Andrés et al., 2011; Lahijani and Zainal, 2011; Mayerhofer et al., 2012; Fotovat et al., 2013; Kim et al., 2013; Wilk et al., 2013). However, in these works there is a lack of information concerning technical facility details, especially about the distributor design, and it is not clear if the operating temperature has been taken into account during the design of the distributor plate. Some operational problems found in combustors and gasifiers such as dead zones, hot spots or ash sinterization might be attributed to an incorrect design of the distributor plate.

The performance of a fluidized bed reactor depends primarily on the satisfactory design of the gas distribution system. The design of the gas distributor often determines the success or failure of a fluidized bed (Geldart and Baeyens, 1985). The gas distributor plate must ensure the uniform distribution of the gas in a fluidized bed. Non-uniform distributions can lead to poor conversion rates in reactions, formation of dead zones and, in case of sticky or aggregative solids, agglomeration problems and defluidization of the entire bed (Briens et al., 1988). Several authors have studied the design and performance of different types of gas distributors for fluidized beds, and also its effects on the segregation and distribution of bed solids. Most of these studies are focused on the ratio, R, of the distributor pressure drop, ΔP_{dist}, to the bed pressure drop, ΔP_{bed}, and it is generally assumed that the value of this ratio ranges from 0.015 to 0.4 (Hiby, 1964; Zuiderweg, 1967; Whitehead, 1971; Siegel, 1976; Mori and Moriyama, 1978). Karri and Werther (2003) assumed that this ratio should be larger than 0.3 to ensure a uniform velocity distribution. If a very large value is chosen for design, it will be, in many cases, wasteful in terms of the energy required to pump the fluidized gas through the distributor plate. However, if a lower value is chosen there is a risk of maldistribution.

Sathiyamoorthy and Rao (1981) reported that the stable operation (i.e. no maldistribution present) of a fluidized bed can be achieved when all the orifices or tuyeres of the distributor are operating at the same time and additionally, when there is a uniform distribution of gas and solids without any channeling in the bed. As previously reported by Whitehead (1971), the number of operating orifices or tuyeres depends on the gas flow rate, the bed aspect ratio, the bed material and the open area of the distributor. The authors (Sathiyamoorthy and Rao, 1981) showed that there is a superficial gas velocity, U_M , at which all the orifices of the distributor became operative, related to a critical value of R that defines the boundary between stable and unstable operation, and proposed a correlation to estimate it. However, Thorpe et al. (2000) have cast doubt on the use of R to predict maldistribution and, therefore, the utility for distributor design. The authors also found that the correlation of Sathiyamoorthy

and Rao (1981) is too conservative in the predictions of R. Accordingly, a more recent work of Thorpe et al. (2002) rejects the use of R as a parameter for distributor design.

Besides, novel measurement techniques reported in recent studies, such as magnetic resonance imaging (Köhl et al., 2013; Rees et al., 2006; Pore et al., 2010), gamma ray tomography (Patel et al., 2008; Mandal et al., 2012) and electrical capacitance tomography (Chandrasekera et al., 2012; Rautenbach et al., 2013), have shown to be very useful in the characterization of the hydrodynamics of fluidized beds and the study of the bottom zone region close to the distributor plate.

The knowledge of the effect of temperature on the distributor performance is of particular interest in industrial applications such as fluidized bed combustors and gasifiers, since industrial and pilot-scale plants operate at high temperature and the distributor plate design directly affects the bed hydrodynamic.

In this chapter, two different gas distributor plates, multiorifice and tuyere, operating at high temperature are compared using experimental pressure drop measurements. The effect of the temperature on the distributor pressure drop is established. Moreover, the variation of the distributor open area with temperature to satisfy a given value of R is studied, and a methodology to obtain the distributor open area as a function of the bed temperature for different bed aspect ratios is provided.

3.2 Experimental setup

Experiments were carried out in a biomass bubbling fluidized bed gasifier (BFBG), sketched in Figure 3.1. The column was made of stainless steel and it has a total height of 2.5 m divided into two sections, the bed section of 0.134 m inner diameter (D) and the freeboard region of 0.25 m inner diameter. The air flow was measured with a set of two mass flow meters, with ranges of $0-500$ l/min and $150-3000$ l/min and with an accuracy of 1% of full-scale span (FSS). The fluidizing air passes through an air preheater to heat up the air stream before entering the fluidized bed.

Two different solids were used as bed material, silica sand particles with 2645 kg/m^3 density and 725 μm mean diameter and sepiolite (clay) particles (SG36) with 1551 kg/m^3 density and 450 μm mean diameter. Both bed materials are type B according to Geldart's classification (Geldart, 1973). The main physical properties of the two solids are summarized in Table 3.1, including experimental values of minimum fluidization voidage, ϵ_{mf}, and minimum fluidization velocity, U_{mf}, at ambient temperature, which were determined using pressure measurements. Taking into account the experimental values of minimum fluidization velocity and minimum fluidization voidage, the particle sphericity, ϕ, was calculated by means of the Carman-Kozeny equation for each type

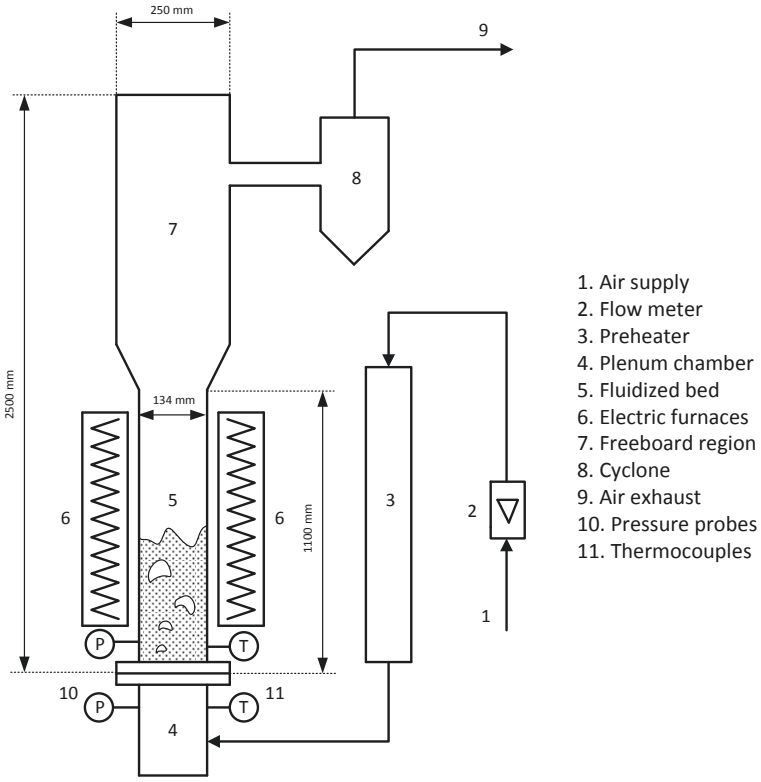

Figure 3.1: Schematic diagram of the experimental setup.

of particle studied in this work.

Table 3.1: Physical properties of solid particles.

	d_p [μm]	ρ_p [kg/m^3]	ϕ [-]	Geldart type	ϵ_{mf} [-]	U_{mf} [m/s]
Silica sand	725	2645	0.7	B	0.44	0.34
Sepiolite (SG36)	450	1551	0.43	B	0.64	0.13

Two piezo-electric pressure transducers (*Kistler type 5015*) and two absolute pressure sensors (*Honeywell SPT Series*), with an accuracy of ±0.01% of FSS, were used to measure the pressure fluctuations in the plenum chamber and at 55 mm above the distributor plate. Pressure fluctuation signals were used to obtain the minimum fluidization velocity and absolute pressure signals were used to characterize the distributor pressure drop at different temperatures. In order to analyze the repeatability of the pressure measurements, two sets of experiments were carried out obtaining relative errors under 5%. A differential pressure transducer (*Setra*) was used to measure the minimum fluidization voidage, ϵ_{mf}, at different temperatures. The two sampling ports were placed at 55 and 115 mm above the distributor plate respectively. The signals were transferred to a PC using a National Instruments data acquisition system type

9234 with 4 analog input channels, 24-bit resolution, working at a sampling frequency of 2000 Hz. K-type thermocouples were used to measure the temperature in the plenum chamber and inside the bed.

Two different distributor plates were compared in this study: a perforated plate and a tuyere type distributor. The perforated plate counts on 140 orifices of 1 mm diameter arranged in a square configuration with 10 mm pitch. The tuyere type distributor consists of 19 tuyeres arranged in a triangular configuration with 20 mm pitch and screwed in a perforated plate. Each tuyere has 8 orifices of the same diameter than the orifices of the perforated plate. Both distributors count on a similar open area. The main design parameters of the distributor plates are summarized in table 3.2.

Table 3.2: Distributor plate design parameters.

	Multiorifice distributor	Tuyere type distributor
D_t [m]	0.134	0.134
t_d [m]	0.002	0.004
Number of orifices	140	152
Number of tuyeres	-	19
Orifices per tuyere	-	8
L_h [m]	0.01	0.025
d_{tuy} [m]	-	0.01
d_h [m]	0.001	0.001
Open area [%]	0.78	0.85

3.3 Theory

The superficial gas velocity inside the bed was evaluated taking into account the air density variation with temperature considering the air as an ideal gas, according to equation 3.1.

$$\rho_g = \rho_{g,amb} \frac{T_{amb}}{T} \tag{3.1}$$

where ρ_g is the air density at temperature T and $\rho_{g,amb}$ is the air density at the reference temperature T_{amb}. The air viscosity at elevated temperature was calculated using a power-law viscosity law (Equation 3.2).

$$\mu = \mu_{amb} \left[\frac{T}{T_{amb}} \right]^n \tag{3.2}$$

where μ is the air viscosity at temperature T, μ_{amb} is the air viscosity at the reference temperature T_{amb} and n is the power-law factor. In this work the reference conditions are the following: $T_{amb} = 20°C$, $\rho_{g,amb} = 1.2$ kg/m^3, $\mu_{amb} = 1.8 \cdot 10^{-5}$ kg/m·s and $n = 2/3$.

The mass balance between the air entering the mass flow meter (Section 2 in Figure 3.1) and the heated gas entering the plenum chamber (Section 4 in Figure 3.1) (Equation 3.3) must be fulfilled. The temperature in section 2 is $T_2 = T_{amb}$ and the temperature in section 4 is T_4.

$$\dot{m} = \rho_{g,amb} U_2 A_2 = \rho_4 U_4 A_4 \tag{3.3}$$

where $\dot{m}$ is the mass flow of air. The air density in section 4 can be corrected using Equation 3.1, and Equation 3.3 can be rearranged considering the volumetric flow, Q_2 (Equation 3.4).

$$\rho_{g,amb} Q_2 = \rho_{g,amb} \frac{T_{amb}}{T_4} U_4 A_4 \tag{3.4}$$

$$U_4 = \frac{Q_2}{A_4} \frac{T_4}{T_{amb}} \tag{3.5}$$

For a given mass flow of air, the superficial gas velocity increases when the temperature increases as a result of air density changes with temperature. The distributor pressure drop can be calculated using the orifice theory (Equation 3.6).

$$\Delta P_{dist} = \frac{\rho_g}{C_D^2} \frac{U_h^2}{2} \tag{3.6}$$

where ΔP_{dist} is the distributor pressure drop, C_D is the orifice discharge coefficient and U_h is the air superficial velocity in the orifices, that can be calculated as a function of the number of orifices per unit of area of the distributor, N_h, the orifice diameter, d_h, and the superficial velocity of the air passing through the distributor plate, U_0 (Equation 3.7).

$$U_h = \left(\frac{4}{\pi}\right) \left(\frac{1}{N_h d_h^2}\right) U_0 \tag{3.7}$$

It should be noted that in the case of using the tuyere distributor, the number of orifices per unit area of the distributor is calculated as the product of orifices per tuyere and tuyeres per unit area of the distributor.

Assuming $U_0 = U_4$ in Equation 3.7, the distributor pressure drop will increase if the temperature increases and the mass flow of air is kept constant. However, for a

constant gas superficial velocity, when the temperature increases the mass flow of air has to be suitably lowered. Accordingly, it is expected that, in that case, a higher temperature should lead to a lower distributor pressure drop due to the decrease in gas density and, therefore, to a lower value of R.

3.4 Discharge coefficient

The orifice discharge coefficient, C_D, has to be estimated using correlations. Most of the authors estimate this coefficient to be 0.6, a typical value for a sharp-edge orifice (Kunii and Levenspiel, 1991). Nevertheless, distributor orifices are not usually sharp-edged and, therefore, greater values should be expected. A better evaluation of the discharge coefficient can be found in Karri and Werther (2003), where C_D is calculated as a function of the distributor plate thickness, t_d, the orifice diameter, d_h, and the distance between orifices, L_h. An equation proposed by Qureshi and Creasy (1979) can be used to estimate the discharge coefficient with similar results (Equation 3.8).

$$C_D = 0.82 \left(\frac{d_h}{t_d} \right)^{-0.13} \tag{3.8}$$

The discharge coefficient can also be estimated using the equation given by Idelchik (1994) for the entrance into a straight tube through a perforated plate with thick orifices (Equation 3.9).

$$C_D = \frac{1}{\sqrt{\left(0.5 + \tau\sqrt{1 - \frac{A_h}{A_d}}\right)\left(1 - \frac{A_h}{A_d}\right) + \left(1 - \frac{A_h}{A_d}\right)^2}} \tag{3.9}$$

where the thickness parameter, τ, is equal to 0 for thick plates ($t_d/d_h > 2$).

The discharge coefficient of the tuyere type distributor can be obtained as the sum of two different contributions: the discharge coefficient through the perforated plate and the discharge coefficient through orifices (Equation 3.10).

$$C_D = \frac{1}{\sqrt{\frac{1}{C_{D,plate}^2} + \frac{1}{C_{D,h}^2}}} \tag{3.10}$$

The discharge coefficient can be estimated with the equation of Qureshi and Creasy (1979) (Equation 3.8) using d_h for the orifice contribution and d_{tuy} for the perforated plate contribution.

The discharge coefficient through the perforated plate can also be estimated using the equation given by Idelchik (1994) for orifices or perforated plates installed in a

transition section (Equation 3.11) and the discharge coefficient through orifices can be estimated using Equation 3.9.

$$C_D = \frac{1}{\sqrt{0.5\left(1-\frac{A_h}{A_d}\right)+\left(1-\frac{A_h}{A_d}\right)^2+\tau\sqrt{\left(1-\frac{A_h}{A_d}\right)}\left(1-\frac{A_h}{A_d}\right)}} \tag{3.11}$$

The calculated discharge coefficients for both multiorifice and tuyere type distributors are summarized in Table 3.3. Experimental results of discharge coefficient were obtained fitting the measured distributor pressure drop data with the gas superficial velocity, and compared with the discharge coefficient calculated with different correlations. It was found that the discharge coefficient is always underestimated if any of the aforementioned correlations is used. For the tuyere type distributor it was found that, for all the correlations investigated, the contribution of the perforated plate to the discharge coefficient is very similar to the experimental results. Thus, any of these correlations can be fairly used to estimate the discharge coefficient for a tuyere type distributor if the contribution of the discharge coefficient through orifices is neglected. Nevertheless, as it is shown in Table 3.3, the Qureshi and Creasy correlation (Qureshi and Creasy, 1979) seems to predict the discharge coefficient in agreement with experimental data for both distributor plates. Therefore, if the discharge coefficient cannot be obtained experimentally, the Qureshi and Creasy correlation can be used to estimate it.

Table 3.3: Discharge coefficient estimation.

	Multiorifice distributor	Tuyere type distributor		
		Plate	Orifice	Total
Kunii and Levenspiel (1991)	0.6	0.6	0.6	0.42
Karri and Werther (2003)	0.79	0.70	0.83	0.54
Qureshi and Creasy (1979)	0.90	0.73	0.90	0.57
Idelchik (1994)	0.82	0.82	0.82	0.58
Experimental	0.94	-	-	0.74

3.5 Results and discussion

The distributor pressure drop was first measured at ambient temperature for both multiorifice and tuyere type distributors. Figure 3.2 shows that the pressure drop of the tuyere type distributor is higher than the multiorifice distributor, even considering that both distributors have a similar open area. This fact can be easily explained in terms

of the discharge coefficient. As it was shown in the previous section, a lower discharge coefficient of the tuyere type distributor produces a higher distributor pressure drop.

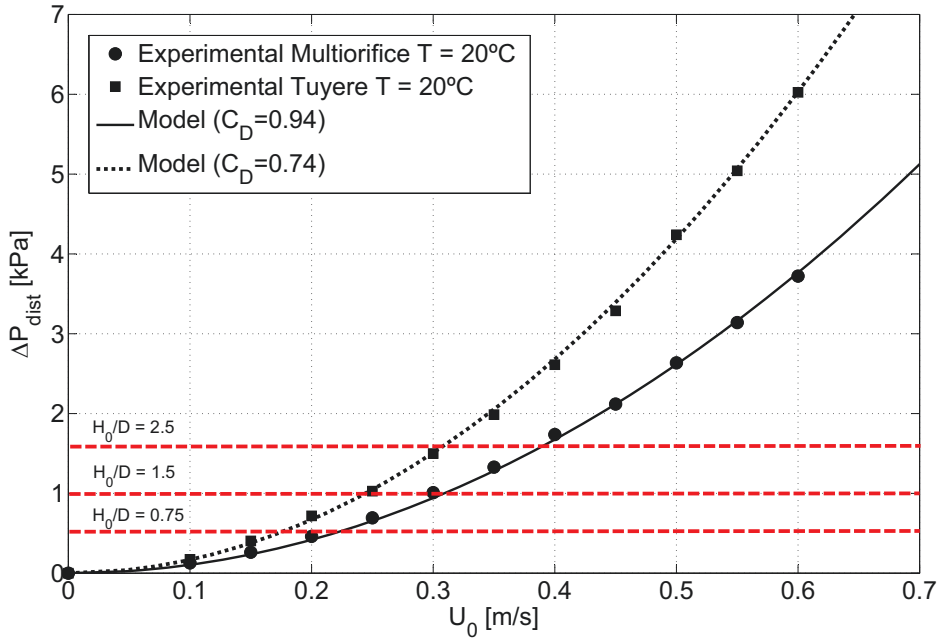

Figure 3.2: Variation of distributor pressure drop with gas superficial velocity at ambient temperature for both multiorifice type and tuyere type. Dash lines correspond to 30% of bed pressure drop for different aspect ratios (H_0/D) in a silica sand bed.

Figure 3.2 illustrates the effect of the operating superficial gas velocity on the distributor pressure drop and, consequently, its close relationship with the design value of the distributor to bed pressure drop ratio, R. Dash lines in Figure 3.2 correspond to the 30% of the bed pressure drop ($R = 0.3$ (Karri and Werther, 2003)) for three different bed aspect ratios $H_0/D = 2.5, 1.5, 0.75$. This value of $R = 0.3$ ensures that the distributor pressure drop is high enough to compensate pressure drop variations that can appear during operation, guarantying the stable and homogeneous fluidization of the bed.

It is shown that, when operating at fixed temperature, a higher velocity is needed to satisfy the pressure drop ratio criteria when the aspect ratio is increased. Thus, for the multiorifice distributor case, a gas superficial velocity of 0.2 m/s satisfies the pressure drop ratio criteria for an aspect ratio of 0.75. However, if the aspect ratio is increased to $H_0/D = 2.5$, the superficial gas velocity needed to satisfy the criteria is around 0.4 m/s. It is clear that, for the case studied, in order to keep a design value of $R = 0.3$ both the current bed aspect ratio and the range of operating gas superficial velocities has to be taken into account simultaneously to perform a proper design. Otherwise,

the pressure drop ratio criteria could not be satisfied and maldistribution effects can appear.

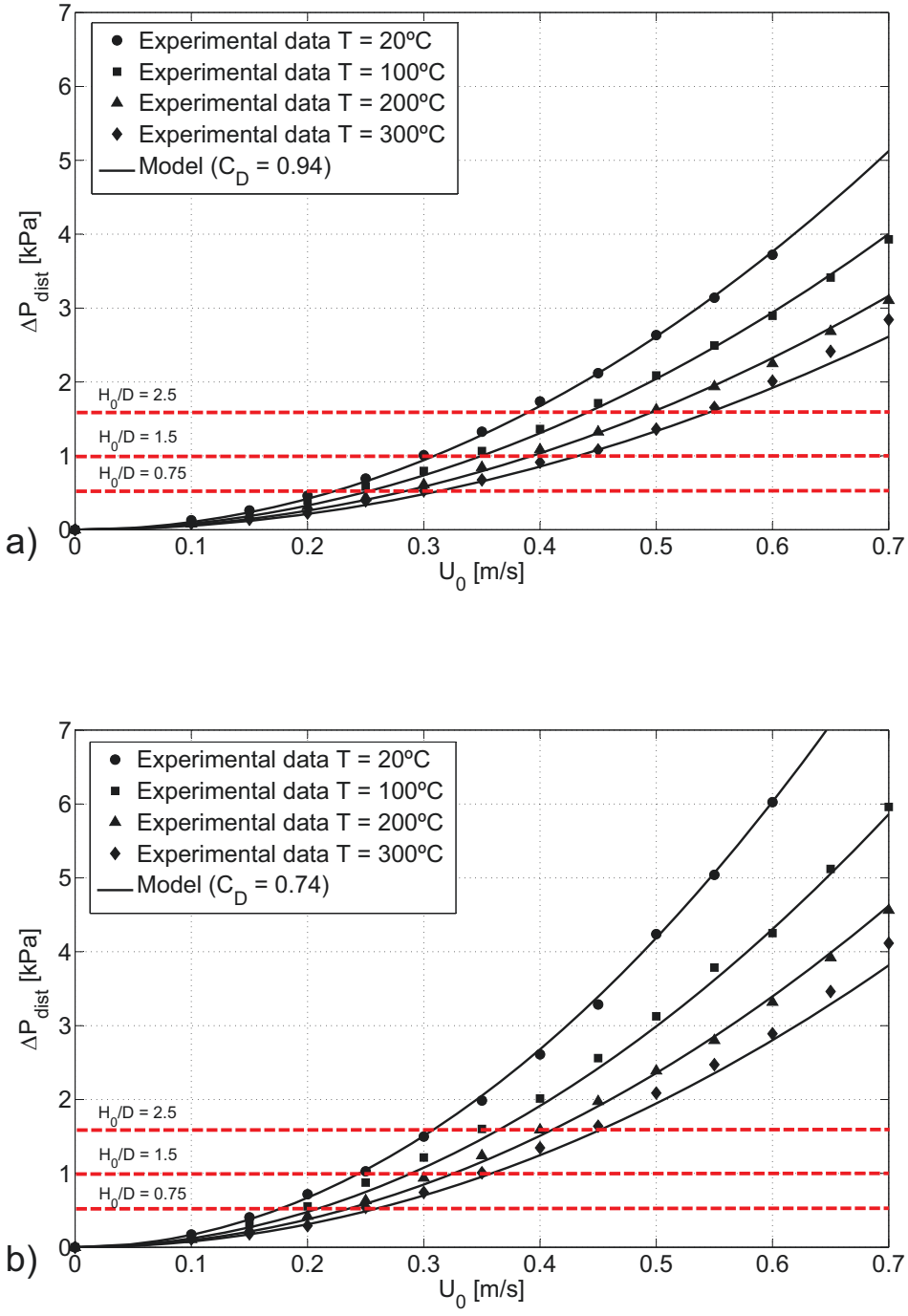

Figure 3.3: Variation of distributor pressure drop with gas superficial velocity at different temperatures: a) Multiorifice type, b) Tuyere type. Dash lines correspond to 30% of bed pressure drop for different aspect ratios (H_0/D) in a silica sand bed.

The effect of the temperature on the distributor pressure drop and therefore, on the

design value of R, is shown in Figure 3.3. To study such a temperature effect, experiments were carried out with the same values of the superficial gas velocity (corrected using Equation 3.5) and at different temperatures ranging from ambient temperature to 300°C. As stated before, the distributor pressure drop decreases when the temperature increases maintaining an equal superficial gas velocity in both distributor plates (Figure 3.4), as an effect of the gas density decrease with temperature (Equation 3.1). The orifice equation (Equation 3.6) was used to fit the distributor pressure drop curves at different temperatures, finding a good agreement with the experimental data in both cases. The determination coefficient, R^2, between experimental pressure drop data and the parabolic estimation of the model is higher than 0.99 for all the temperatures tested and both distributor plates. Therefore, the model can be said to predict the experimental data accurately. Since the bed pressure drop is fairly constant, as can be seen in Figure 3.3 the distributor pressure drop decreases significantly with the bed temperature and, as a consequence, the ratio R also decreases. It is clear that such a decrease of the distributor pressure drop with temperature has a direct effect on the distributor to bed pressure drop ratio, R. Therefore if R has to be kept above a certain value (i.e. 0.3) to avoid non-uniform gas distribution, the distributor plate should be designed at operation temperature to fulfil the process specifications.

In order to take into account the effect of the temperature on the distributor pressure drop and to facilitate the distributor design at high temperatures, a model is proposed below. The model considers the effect of temperature on the minimum fluidization velocity as well as the Qureshi and Creasy correlation (Qureshi and Creasy, 1979) to estimate the discharge coefficients for both multiorifice and tuyere type distributors.

To measure the effect of the temperature on the minimum fluidization velocity, both the minimum fluidization velocity and the minimum fluidization voidage were measured at different bed temperatures for the two bed materials, silica sand and SG36 (Sepiolite). The minimum fluidization velocity was determined experimentally using the standard deviation method (Puncochár et al., 1985) and the minimum fluidization voidage was measured by means of a differential pressure sensor. Thus, once the average pressure drop between the two sampling ports of the differential pressure sensor is measured, the minimum fluidization voidage can be obtained as follows:

$$\epsilon_{mf,T} = 1 - \frac{\Delta P}{(\rho_p - \rho_g)\, g h} \tag{3.12}$$

As reported by Flamant et al. (1991), the use of Equation 3.12 to determine the minimum fluidization voidage introduces a systematic overestimation of $\epsilon_{mf,T}$ when optical methods are not used (Formisani et al., 1998). Its use gives here an approximate

value of $\epsilon_{mf,T}$ that serves to measure the temperature effect for modelling purposes.

Previous studies (Formisani et al., 1998) showed that the variation of the minimum fluidization voidage has a linear dependence with the temperature, as expressed in equation 3.13.

$$\epsilon_{mf,T} = \epsilon_{mf,amb} + k\,(T - T_{amb}) \tag{3.13}$$

Experimental results of the minimum fluidization voidage at different temperatures are plotted in Figure 3.4 a1) and a2) for silica sand particles and SG36 respectively. A linear regression of the experimental data was performed in order to fit the data to Equation 3.13. The mean relative error between the experimental data of ϵ_{mf} and the model estimation can be found in Table 3.4. As can be observed, the variation of the minimum fluidization voidage with temperature is very small in both cases and can be neglected without significant errors. These results are in agreement with previous studies (Flamant et al., 1991; Formisani et al., 1998), which showed a small variation in the minimum fluidization voidage with temperature for type B particles.

Table 3.4: Summary of relative errors between experiments and the models used for the estimation of U_{mf} and ϵ_{mf}.

Silica Sand				Sepiolite (SG36)			
U_{mf}			ϵ_{mf}	U_{mf}			ϵ_{mf}
$E_{W\&Y}$	E_{C-K} $\epsilon_{mf} = cte$	E_{C-K} $\epsilon_{mf} = f(T)$	E	$E_{W\&Y}$	E_{C-K} $\epsilon_{mf} = cte$	E_{C-K} $\epsilon_{mf} = f(T)$	E
14.2%	4.7%	2.6%	1.75%	23%	5.7%	5.3%	2.8%

Experimental results of the minimum fluidization velocity were compared with the predictions of Wen and Yu (Wen and Yu, 1966) (Equation 3.14) correlation and Carman-Kozeny equation (Carman, 1937) (Equation 3.15). The mean relative error between the experimental data of U_{mf} and the different models tested can be found in Table 3.4.

$$U_{mf} = \left(\frac{\mu}{\rho_g d_p}\right)\left\{\left[28.7^2 + 0.0408\left(\frac{d_p^3 \rho_g\,(\rho_p - \rho_g)\,g}{\mu^2}\right)\right]^{1/2} - 33.7\right\} \tag{3.14}$$

$$U_{mf} = \frac{(\phi d_p)^2\,(\rho_p - \rho_g)\,g}{180\mu}\left(\frac{\epsilon_{mf}^3}{1 - \epsilon_{mf}}\right) \tag{3.15}$$

As can be seen in Figure 3.4 b1), the Wen and Yu model overestimates the minimum fluidization velocity of the silica sand particles and assumes a linear variation of the minimum fluidization velocity with temperature. In the case of SG36 (Figure 3.4

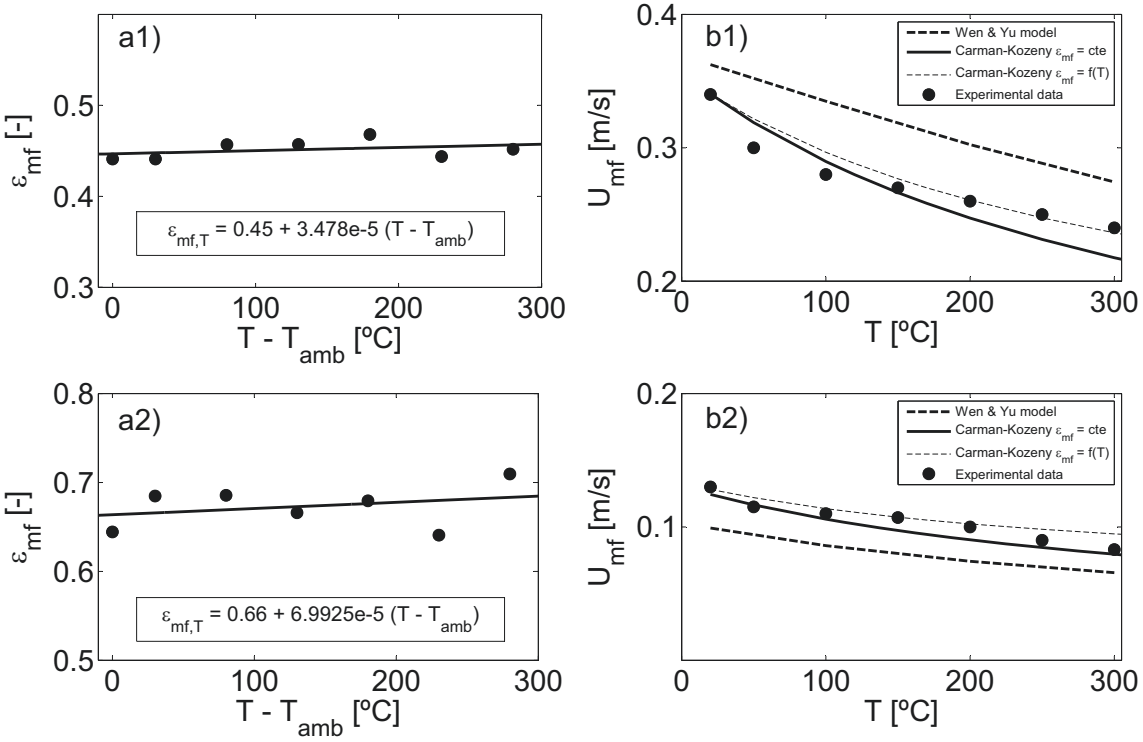

Figure 3.4: Variation of solids properties with temperature: a) Minimum fluidization voidage, b) Minimum fluidization velocity, 1) Silica sand and 2) SG36.

b2)) the Wen and Yu model underestimates the minimum fluidization velocity. The Wen and Yu correlation cannot be used to estimate the minimum fluidization velocity at high temperature probably because it does not consider the minimum fluidization voidage. In contrast, the Carman-Kozeny equation shows a good agreement with the experimental results when using a constant value of bed voidage (i.e. minimum fluidization voidage at ambient temperature). The predictions of the Carman-Kozeny equation can be improved using the empirical correlation of the minimum fluidization voidage with temperature (Figure 3.4 a)). Nevertheless, it is concluded that in these two cases (i.e. silica sand and SG36) the use of the variation of the minimum fluidization voidage with temperature does not improve appreciably the predictions and, therefore, will be neglected in the calculations for modelling purposes.

In summary, regarding the different correlation to estimate the discharge coefficient, the Quresi and Creasy correlation (Qureshi and Creasy, 1979) showed good agreement with the experimental data. Regarding the minimum fluidization voidage and velocity with temperature it was proved that the Carman-Kozeny equation (Carman, 1937)

can predict the minimum fluidization velocity at high temperature and, in case of type B particles, the variation of the minimum fluidization voidage with temperature can be neglected within the temperature range covered. Finally, from the study of the distributor pressure drop it was found that the orifice equation can predict the variation of the distributor pressure drop with the superficial gas velocity at different temperatures.

According to these findings, in order to satisfy a certain value of R at high temperatures, a model is proposed to provide the distributor open area as a function of the bed temperature. The initial hypothesis is that a minimum value for the distributor pressure drop will satisfy a given pressure drop ratio criteria for each distributor plate, each solid material, each aspect ratio and each temperature. To do so, it is assumed from a design point of view, that the pressure drop ratio must be satisfied at the minimum fluidization velocity of each temperature to avoid non-uniform gas distribution and guaranteeing the proper fluidization of the bed. It is worth to remind that higher velocities than U_{mf} would produce a value of R higher than 0.3 (Equation 3.6) ensuring a proper fluidization.

First, the minimum fluidization velocity is obtained with the Carman-Kozeny equation (Equation 3.15), neglecting the variation of the minimum fluidization voidage with temperature if type B particles are used. Then, with a given value of the aspect ratio of the bed, the bed pressure drop is calculated and therefore, taking into account the pressure drop ratio, the distributor pressure drop is also determined with the discharge coefficient obtained with the Quresi and Creasy correlation (Equation 3.8). Using Equation 3.6 the superficial gas velocity in the orifices can be calculated and assuming $U_0 = U_{mf}$ in Equation 3.7 the number of orifices per unit area is obtained. Finally, the distributor open area is calculated, defined as the ratio between orifice total area and distributor plate area.

Figure 3.5 shows the variation of the distributor open area with temperature for different bed aspect ratios and for both the multiorifice (a1) and a2)) and the tuyere type (b1) and b2)) distributor plates. The solid lines represent the results of the distributor open area estimated using experimental data (i.e. experimental variation of minimum fluidization voidage with temperature and experimental discharge coefficient) and the dash lines correspond to the data obtained following the procedure described before. A maximum relative error of 14% between experimental and model results was obtained, making the methodology described in this work a reliable, fast and useful tool that can speed up the design process of distributor plates operating at high temperature. As expected, a lower open area is needed if the process is conducted at high temperature (Figure 3.5). These curves can be obtained prior to the construction of the distributor

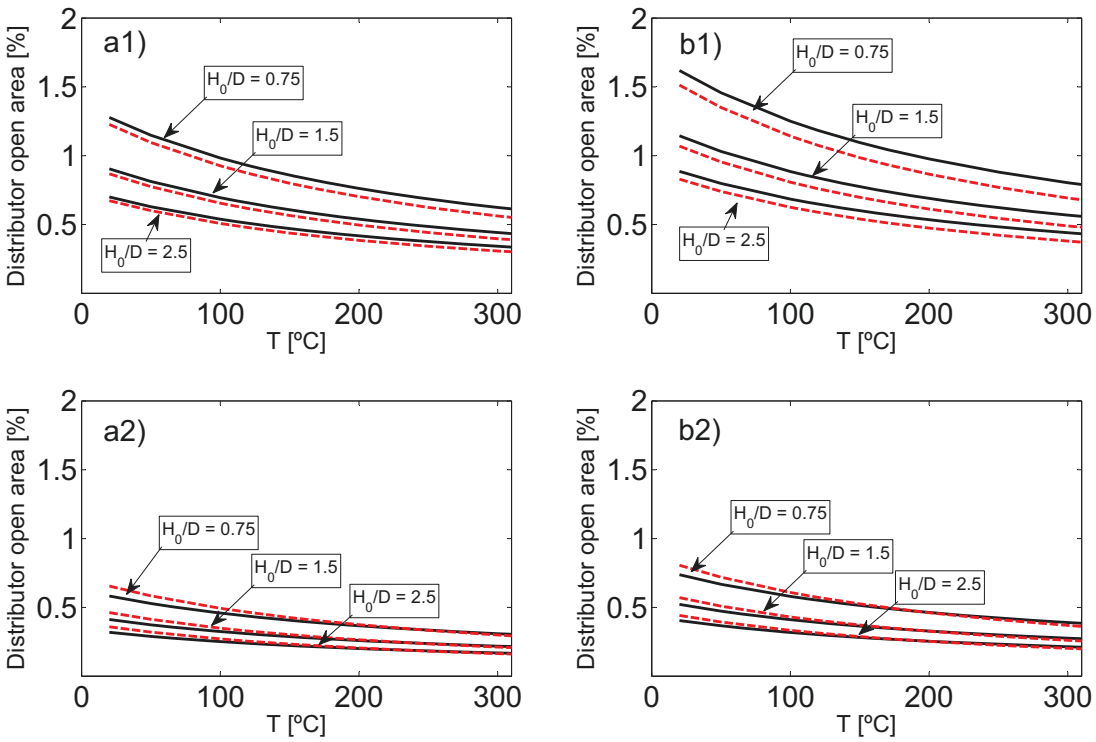

Figure 3.5: Open area of the distributor as a function of the bed temperature for different aspects ratios: a) Multiorifice type (Silica sand), b) Tuyere type (Silica sand), c) Multiorifice type (SG36), and d) Tuyere type (SG36). Comparison between experimental data (solid lines) and model data (dash lines).

plate in order to prove the feasibility of the design proposed at operating temperature. It is important to note the remarkable differences found between the minimum distributor open area required at ambient temperature and, for example, at 300°C, which should not be neglected during the design process. The bed aspect ratio has to be taken into account, since deeper beds needs higher distributor pressure drop to satisfy the pressure drop ratio required. It can be observed in Figure 3.5 that when the bed aspect ratio increases, the distributor open area should decrease in order to increase the distributor pressure drop.

Additional runs conducted to show the effect of temperature on the pressure drop ratio, R, revealed changes in the dynamic patterns of the bed due to the higher bed temperatures, which are in agreement with previous results reported in literature (Formisani et al., 1998; Botterill et al., 1982; Mathur et al., 1986; Raso et al., 1992; Lucas et al., 1986; Bena and Havlada, 1991). Thus, the superficial gas velocity was fixed to the minimum fluidization velocity (of sand particles) at ambient tempera-

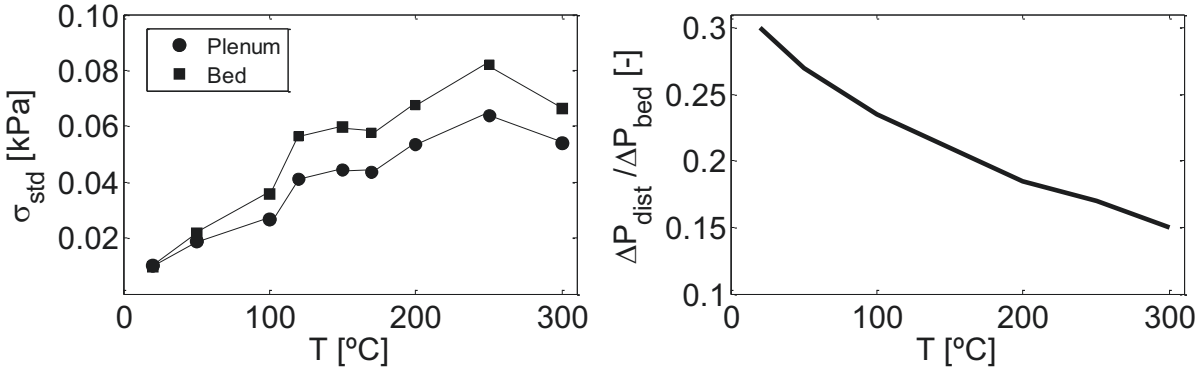

Figure 3.6: a) Standard deviation of pressure signals at $U_0 = 0.34$ m/s at different temperatures (The gas velocity correspond to minimum fluidization velocity at ambient temperature) and b) Variation of distributor to bed pressure drop ratio with temperature at $U_0 = 0.34$ m/s. (Silica sand)

ture to operate a bed of $H_0/D = 1.9$ having a pressure drop ratio R of 0.3 at ambient temperature. The standard deviation of Kistler type 5015 pressure fluctuation signals, measured at different temperatures in the plenum chamber as well as inside the bed, exhibit a fairly linear increase with temperature because of the decreasing of the minimum fluidization velocity with temperature (Figure 3.6 a)). However, the slope change observed in the standard deviation curves around 150°C, when the pressure drop ratio is close to 0.2, and beyond 250°C might indicate that there are changes in the bed hydrodynamics. Moreover, the fact that R decreases with temperature, and in this case reaching a value that is half of that at ambient temperature for a temperature of 300°C, might produce such dynamical changes. Therefore, it is clear the need of investigate these temperature effects from a dynamical point of view.

3.6 Conclusions

The effect of temperature on the distributor pressure drop in a bubbling fluidized bed was established by means of pressure drop measurement for two different distributor plates, multiorifice and tuyere, and two different bed materials. It was found that, for constant values of superficial gas velocity, the distributor pressure drop decreases with temperature as an effect of the gas density reduction with temperature. The orifice equation was used to estimate the experimental data, finding a good agreement for both reference and high temperature results.

A new methodology to design distributor plates at high temperature was developed. The aim of this model is to obtain the minimum distributor open area needed to satisfy a given pressure drop ratio, R. First, the operating temperature, the pressure drop ratio and the bed aspect ratio need to be selected. Then, if type B particles

are used, the variation of the minimum fluidization voidage with temperature can be neglected and the minimum fluidization velocity can be obtained with the Carman-Kozeny correlation. The distributor discharge coefficient can be calculated with the Qureshi and Creasy correlation and the distributor pressure drop can be estimated using the orifice theory. A gas superficial velocity has to be selected at this point. Finally, the minimum distributor open area needed to satisfy the given pressure drop ratio can be obtained. It was found that a lower distributor open area is needed if the bed is operating at high temperature, showing the importance of considering the effect of the operating temperature in the distributor plate design.

The pressure drop ratio variations with the operating temperature were evaluated under operation. The standard deviation of the pressure fluctuation signal was plotted as a function of the temperature for a constant value of the gas superficial velocity. Changes in the trend of the standard deviation were found, showing that there is an effect of the temperature on the bed hydrodynamics.

3.7 Notation

A_i	Cross sectional area of section i [m^2]
A_d	Distributor plate area [m^2]
A_h	Orifice area [m^2]
C_D	Discharge coefficient of a orifice [-]
$C_{D,h}$	Discharge coefficient of the orifice of a tuyere [-]
$C_{D,plate}$	Discharge coefficient of the orifice of a perforated plate in a tuyere type distributor [-]
D	Bed diameter [m]
D_t	Distributor plate diameter [m]
d_h	Orifice diameter [m]
d_p	Mean particle diameter [m]
d_{tuy}	Tuyere diameter [m]
E	Relative error [%]
g	Gravity [m/s^2]
H_0	Fixed bed height [m]
H_0/D	Aspect ratio [-]
h	Distance between the two sampling ports of the differential pressure sensor [m]
L_h	Distance between orifices in a distributor plate [m]
k	Slope of the variation of voidage with temperature [K^{-1}]

$\dot{m}$	Mass flow of gas [kg/s]
n	Power-law factor of the viscosity law [-]
N_h	Numer of orifices per unit area of distributor [orifices/m^2]
ΔP	Pressure drop between the two sampling ports of the differential pressure sensor [Pa]
ΔP_{bed}	Bed pressure drop [Pa]
ΔP_{dist}	Distributor pressure drop [Pa]
Q	Volumetric flow of gas [m^3/s]
R	Pressure drop ratio [-]
R^2	Determination coefficient of the fitting [-]
T	Temperature [K]
T_{amb}	Ambient temperature [K]
t_d	Distributor plate thickness [m]
U_0	Air superficial velocity [m/s]
U_h	Orifice superficial velocity [m/s]
U_M	Superficial gas velocity at which all the orifices became operative [m/s]
U_{mf}	Minimum fluidization velocity [m/s]

Greek symbols

ϵ_{mf}	Voidage at minimum fluidization conditions [-]
$\epsilon_{mf,amb}$	Voidage at minimum fluidization conditions and ambient temperature [-]
$\epsilon_{mf,T}$	Voidage at minimum fluidization conditions and temperature T [-]
μ	Air viscosity at bed temperature [kg/ms]
μ_{amb}	Air viscosity at ambient temperature [kg/ms]
ρ_g	Air density at bed temperature [kg/m^3]
$\rho_{g,amb}$	Air density at ambient temperature [kg/m^3]
ρ_p	Particle density [kg/m^3]
ϕ	Particle sphericity [-]
σ_{std}	Standard deviation of the pressure signal [Pa]
τ	Thickness parameter [-]

Abbreviattions

BFB	Bubbling fluidized bed
$BFBG$	Bubbling fluidized bed gasifier
FSS	Full-scale span

Bibliography

Bena, J., Havlada, I., 1991. The influence of particle Reynolds on voidage at fluidization. *Powder Technol.* 66, 97-99.

Botterill, J.S.M., Teoman, Y., Yuregir, K.R., 1982. The effect of temperature on fluidized bed behaviour. *Chem. Eng. Commun.* 15, 227-238.

Briens, C.L., Tyagi, A.K., Bergougnou, M.A., 1988. Pressure drop through multiorifice gas distributors in fluidized bed columns. *Can. J. Chem. Eng.* 66, 740-748.

Campoy, M., Gómez-Barea, A., Vidal, F.B., Ollero, P., 2009. Air-steam gasification of biomass in a fluidized bed: process optimization by enriched air. *Fuel Process. Technol.* 90, 677-685.

Carman, P.C., 1937. Fluid flow through granular beds, *Transactions, Institution of Chemical Engineers* 15, 150-166.

Chandrasekera, T.C., Wang, A., Holland, D.J., Marashdeh, Q., Pore, M., Wang, F., Sederman, A.J., Fan, L.S., Gladden, L.F., Dennis, J.S., 2012. A comparison of magnetic resonance imaging and electrical capacitance tomography: an air jet through a bed of particles. *Powder Technol.* 227, 86-95.

de Andrés, J.N., Narros, A., Rodríguez, M.E., 2011. Behaviour of dolomite, olivine and alumina as primary catalysts in air-steam gasification of sewage sludge. *Fuel.* 90, 521-527.

Flamant, G., Fatah, N., Steinmetz, D., Murachman, B., Luguerie, C., 1991. High-temperature velocity and porosity at minimum fluidization. Critical analysis of experimental results. *Int. Chem. Eng.* 31, 673-684.

Formisani, B., Girimonte, R., Mancuso, L., 1998. Analysis of the fluidization process of particle beds at high temperature. *Chem. Eng. Sci.* 53, 951-961.

Fotovat, F., Chaouki, J., Bergthorson, J., 2013. The effect of biomass particles on the gas distributor and dilute phase characteristics of sand-biomass mixtures fluidized in the bubbling regime. *Chem. Eng. Sci.* 102, 129-138.

Geldart, D., 1973. Types of gas fluidization. *Powder Technol.* 7, 285-292.

Geldart, D., Baeyens, J., 1985. The Design of Distributors for Gas-Fluidized Beds. *Powder Technol.* 42, 67-78.

Hiby, J.W., 1964. Critical minimum pressure drop of gas distributor plate in fluidized bed units. *Chem. Ing. Techn.* 36, 328.

Idelchik, I.E., 1994. *Handbook of hydraulic resistance*. CRC press.

Karri, S.B.R., Werther, J., 2003. Gas distributor and plenum design in fluidized beds. In: Yang, W.C. *Handbook of fluidization and fluid-particle systems*. Marcel Dekker Inc., New York, 164-179.

Kim, Y.D., Yang, C.W., Kim, B.J., Kim, K.S., Lee, J.W., Moon, J.H., Yang, W., Yu, T.U., Lee, U.D., 2013. Air-blown gasification of woody biomass in a bubbling fluidized bed gasifier. *Appl. Energ.* 112, 414-420.

Köhl, M.H., Lu, G., Third, J.R., Häberlin, M., Kasper, L., Prüssmann, K.P., Müller, C.R., 2013. Magnetic resonance imaging (MRI) study of jet formation in packed beds. *Chem. Eng. Sci.* 97, 406-412.

Kunii, D., Levenspiel, O., 1991. *Fluidization engineering*, Butterworth-Heinemann, Stoneham, UK, 2nd ed.

Lahijani, P., Zainal, Z.A., 2011. Gasification of palm empty fruit bunch in a bubbling fluidized bed: a performance and agglomeration study. *Bioresource Technol.* 102, 2068-2076.

Lucas, A., Arnaldos, J., Casal, J., Puigjaner, L., 1986. High temperature incipient fluidization in mono and polydisperse systems. *Chem. Eng. Commun.* 41, 121-132.

Mandal, D., Sharma, V.K., Pant, H.J., Sathiyamoorthy, D., Vinjamur, M., 2012. Quality of fluidization in gas-solid unary and packed fluidized beds: an experimental study using gamma ray transmission technique. *Powder Technol.* 226, 91-98.

Mathur, A., Saxena, S.C., Zhang, Z.F., 1986. Hydrodynamic Characteristics of Gas-Fluidized Beds Over a Broad Temperature Range. *Powder Technol.* 47, 247-256.

Mayerhofer, M., Mitsakis, P., Meng, X.M., de Jong, W., Spliethoff, H., Gaderer, M., 2012. Influence of pressure, temperature and steam on tar and gas in allothermal fluidized bed gasification. *Fuel.* 99, 204-209.

Mori, S., Moriyama, A., 1978. Criteria for uniform fluidization of non-aggregative particles. *Int. Chem. Eng.* 18, 245-249.

Olivares, A., Aznar, M.P., Caballero, M.A., Gil, J., Frances, E., Corella, J., 1997. Biomass Gasification: Produced gas upgrading by in-bed use of dolomite. *Ind. Eng. Chem. Res.* 36, 5220-5226.

Patel, A.K., Waje, S.S., Thorat, B.N., Mujumdar, A.S., 2008. Tomographic diagnosis of gas maldistribution in gas-solid fluidized beds. *Powder Technol.* 185, 239-250.

Pore, M., Chandrasekera, T.C., Holland, D.J., Wang, A., Wang, F., Marashdeh, Q., Mantle, M.D., Sederman, A.J., Fan, L.S., Gladden, L.F., Dennis, J.S., 2010. Magnetic resonance studies of jets in a gas-solid fluidized bed. *Particuology.* 10, 161-169.

Puncochár, M., Drahos, J., Cermák, , J., Selucký, K., 1985. Evaluation of minimum fluidization velocity in gas fluidized beds from pressure fluctuations. *Chem. Eng. Commun.* 35, 81-87.

Qureshi, A.E., Creasy, D.E., 1979. Fluidised bed distributors. *Powder Technol.* 22, 113-119.

Raso, G., DAmore, M., Formisani, B., Lignola, P.G., 1992. The influence of temperature on the properties of the particulate phase at incipient fluidization. *Powder Technol.* 72, 71-76.

Rautenbach, C., Melaaen, M.C., Halvorsen, B.M., 2013. Statistical diagnosis of a gas-solid fluidized bed using electrical capacitance tomography. *Int. J. Multiphase Flow.* 49, 70-77.

Rees, A.C., Davidson, J.F., Dennis, J.S., Fennell, P.S., Gladden, L.F., Hayhurst, A.N., Mantle, M.D., Müller, C.R., Sederman, A.J., 2006. The nature of the flow just above the perforated plate distributor of a gas-fluidised bed, as imaged using magnetic resonance. *Chem. Eng. Sci.* 61, 6002-6015.

Sathiyamoorthy, D., Sridhar Rao, C.H., 1981. The choice of distributor to bed pressure drop ratio in gas fluidised beds. *Powder Technol.* 30, 139-143.

Siegel, R., 1976. Effect of distributor plate to bed resistance ratio on onset of fluidized bed channelling. *AIChE J.* 22, 590.

Thorpe, R.B., Davidson, J.F., Downing, S.J., Dusad, A., Farthing, P., Ferdinando, G., Holden, A., Martin, A., Negyal, O., Saundry, J., 2000. On the minimum distributor pressure drop for uniform fluidization. In: *Proceedings of 3rd European Conference on Fluidization*, Toulouse 189.

Thorpe, R.B., Davidson, J.F., Pollitt, M., Smith, J., 2002. Maldistribution in fluidized beds. *Ind. Eng. Chem. Res.* 41 , 5878-5889.

Wen, CY., Yu, YH., 1966. A generalized method for predicting minimum fluidization velocity. *AIChE J.* 12, 610.

Whitehead, A.B., 1971. In Davidson, J.F., Harrison, D. (Eds.) *Fluidization.* Academic Press, London. 781.

Wilk,V., Schmid, J.C., Hofbauer, H., 2013. Influence of fuel feeding positions on gasification in dual fluidized bed gasifiers. *Biomass Bioenerg.* 54, 46-58.

Zuiderweg, F.J., 1967. In Drinkenburg, A.A.H. (Eds.) *Proc. Int. Symp. on Fluidization.* Netherlands University Press, Amsterdam. 739.

Chapter 4

Maldistribution detection in bubbling fluidized beds

Contents

4.1 Introduction

Gas maldistribution is one of the most common problems related to distributor design and has an important effect on the performance of the fluidized bed. When the gas velocity exceeds the value required for incipient fluidization, U_{mf}, gas bubbles appear in the bed; however there are zones, typically close to the distributor plate, called dead zones (Geldart and Baeyens, 1985), where the bubbles are prevented to appear. The bubbling areas and the dead zones often move with time. Thorpe et al. (2002) defined this state as the maldistribution state. These authors reported that when

the superficial gas velocity is increased above a certain value, U_M, the distribution of bubbles through the bed became uniform and the bed is termed evenly fluidized. This value of U_M has been defined as the superficial velocity at which all the orifices or tuyeres of the distributor plate become operative, which usually means they are jetting (Sathiyamoorthy and Rao, 1981; Whitehead, 1971). Sathiyamoorthy and Rao (1981) reported that the stable operation of a fluidized bed can be achieved when all the orifices or tuyeres of the distributor are operating at the same time (i.e. beyond U_M) and, additionally, when a uniform distribution of gas and solids in the bed, without any channeling, is ensured. As previously reported by Whitehead (1971), U_M depends on the gas flow rate, the bed aspect ratio, the bed material and the open area of the distributor. All these variables have been often studied in terms of the distributor to bed pressure drop ratio, R, since the onset of maldistribution seems to be directly related to this ratio, as discussed in Chapter 3.

Several authors (Briens et al., 1999; van Ommen et al., 2004a; Gómez-Hernández et al., 2014) have developed methods to detect if a fluidized bed is moving towards defluidization. The method proposed by Briens et al. (1999) is based on the attractor comparison of pressure signals. The method is capable of detecting local changes in the fluidization behavior, but the main disadvantage is the requirement of too many measurements to be applied in a large-scale fluidized bed. More recently, van Ommen et al. (2004a) reported a new method for the early defluidization detection based on the standard deviation of pressure signals. They showed that pressure fluctuations measurement is suitable for a quick detection of defluidization caused by changes in the gas feed or pressure. The authors reported that just a pressure probe is sufficient to detect the defluidization, provided that it is more or less homogeneously spread over the bed. Nevertheless, the use of several measurement positions is essential when only part of the bed is moving towards defluidization (e.g. due to problems on the gas distributor). Gómez-Hernández et al. (2014) developed a new statistical method to perform a frequency division of the power spectra of pressure fluctuations signals. The methodology was used in water-induced defluidization tests, showing its capability to detect the onset of the defluidization and when the bed is returning to the fluidization state.

In this work, the effect of the measurement position on the maldistribution detection is investigated. Thus, severe and moderate maldistribution conditions are induced in a lab scale fluidized bed by means of different orifice distributions in the distributor plate. First, the qualitative aspects regarding the effects of nonuniform gas distribution on the fluidized bed dynamics are studied by means of digital image analysis (DIA) of images of the bed surface. Complementarily, pressure fluctuation signals measured

in the plenum chamber and at several locations inside the bed were analyzed in terms of the standard deviation and the autocorrelation function to confirm that neither increasing the gas velocity nor increasing the bed aspect ratio are able to mend the severe nonuniform gas distribution induced at the bottom of the bed. To provide with a criterion for maldistribution detection in gas fluidized beds, several online monitoring methods previously used in literature to detect defluidization problems, such as the attractor comparison test (van Ommen et al., 2000), the wide band energy division method (Gómez-Hernández et al., 2014) and the statistical process control approach (Gómez-Hernández, 2015) were applied to the measured pressure fluctuation signals. To do that, the pressure fluctuation signals were compared to the uniform case (i.e. with a proper distribution of the gas in the bed). It is assumed that defluidization problems might be accompanied or generated by gas maldistribution and consequently, similar monitoring approaches, successfully used previously to detect defluidization, can be also applied to maldistribution detection. Finally, a rotating distributor plate was employed as a counteracting mechanism to overcome maldistribution.

4.2 Experimental setup

The experiments were carried out in a lab-scale cylindrical bubbling fluidized bed (BFB), sketched in Figure 4.1. The column is a transparent tube with an inner diameter of 0.192 m (D) and 1 m in height. The air flow was measured with a set of two flow meters, with ranges of 0-500 L/min and 150-3000 L/min and with an accuracy of 1% of full-scale span (FSS).

The bed material used was sepiolite (clay) particles (SG36) with a density of 1551 kg/m^3 and 450 μm mean diameter, classified as type B according to Geldart's classification (Geldart, 1973). The main physical properties of the bed material are summarized in Table 4.1, including experimental values of minimum fluidization voidage, ϵ_{mf}, and minimum fluidization velocity, U_{mf}, at ambient temperature, which were determined using pressure measurements, as described in Chapter 3. The particle sphericity, ϕ, was calculated by means of the Carman-Kozeny equation (Carman, 1937), taking into account the minimum fluidization velocity and voidage obtained experimentally (Equation 4.1).

$$U_{mf} = \frac{\left(\phi d_p\right)^2 \left(\rho_s - \rho_g\right) g}{180\mu} \left(\frac{\epsilon_{mf}^3}{1-\epsilon_{mf}}\right) \tag{4.1}$$

Black beads of 6 mm of diameter made of a low-density material (ρ_{bb} = 36.20 kg/m^3) were used to produce a high contrast in the bed surface and to facilitate the

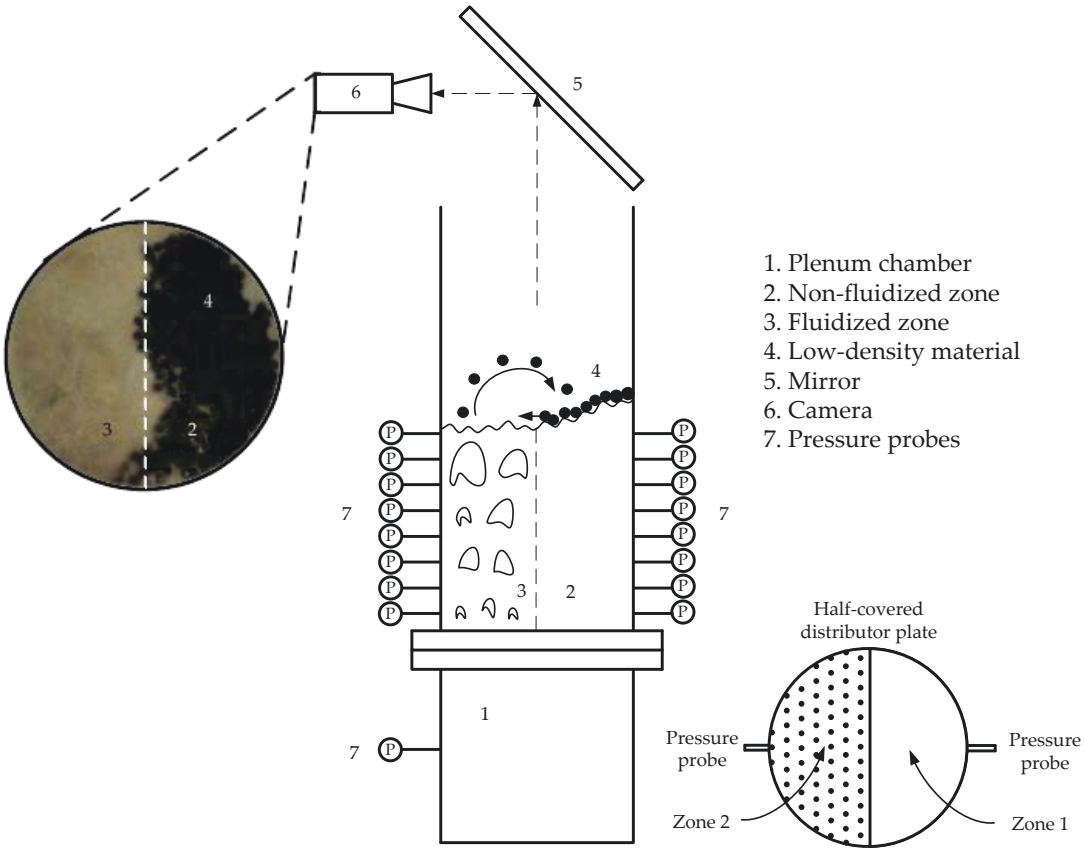

Figure 4.1: Schematic diagram of the experimental setup.

recognition of bubbles during the digital analysis of the images recorded. When a bubble explodes in the bed surface, the black beads are ejected leaving a free space of the size of the exploding bubble.

Table 4.1: Physical properties of solid particles.

	d_p [μm]	ρ_p [kg/m^3]	ϕ [-]	Geldart type	ϵ_{mf} [-]	U_{mf} [m/s]
Sepiolite (SG36)	450	1551	0.43	B	0.64	0.13

Three piezo-electric pressure transducers (*Kistler type 5015*), with an accuracy of $\pm 0.01\%$ of FSS, were used to measure the pressure fluctuations in the plenum chamber and at several locations above the distributor plate (Figure 4.1). The signals were transferred to a PC using a National Instruments data acquisition system type 9234 with 4 analog input channels, 24-bit resolution, working at a sampling frequency of 2000 Hz.

A *Casio Exilim 6.0 Mpx* digital camera was used to take images of the bed surface. The frame rate of the camera is 30 fps and the spatial resolution of the pictures is

480 x 640 pixels. A mirror was attached to the top of the bed in order to reflect the bed surface, allowing taking pictures of the bed surface with the camera located in the front part of the bed. The duration of all the videos recorded was 4 min. Since it is not usual to have optical access to fluidized bed reactor, the visual information gathered from the bed surface pictures will serve to support the information provided by the pressure fluctuations signal analysis.

The gas distributor used was a perforated plate counting on 264 orifices of 2 mm diameter arranged in a triangular configuration with 10 mm pitch. The distributor plate was designed intending to minimize the dead zones between orifices (Soria-Verdugo et al., 2011a). The distributor is equipped with a mesh to avoid the falling of particles inside the plenum chamber. Half of the total distributor orifices were covered to create an induced maldistributed region (zone 1), and a well fluidized region (zone 2); as a result the effective number of orifices of the distributor plate in the experiments is 132. The half-covered distributor plate test is considered here as an extreme case of maldistribution. Once the methodology was proven to detect the extreme case, moderate cases of maldistribution were studied.

Additional experiments were carried out opening a certain percentage of orifices of the distributor plate in zone 1, p_h, and covering the same number of orifices in zone 2, in order to obtain a similar distributor pressure drop. Therefore, the number of open orifices was always 132 with different orifices distributions. The bed aspect ratio was fixed to 1.25 in this case. The aim of these experiments is to evaluate moderate cases of maldistribution, which may be closer to maldistribution problems that can lead to defluidization in industrial fluidized beds.

For the last set of experiments, an electrical motor was connected to the distributor to allow its rotation. The objective of these experiments is to investigate the capability of the distributor rotation to suppress the maldistribution in a fluidized bed.

4.3 Results and discussion

4.3.1 Effect of bed height and gas velocity on gas maldistribution

Pressure fluctuation signals, measured at different bed heights above the distributor plate, and video images, recorded at the bed surface, were complementary taken to study the effects of the bed height and the gas velocity on bubble distribution within the bed, when the fluidized system is operating under induced maldistribution conditions.

Visual inspection of the bed surface

Videos of the bed surface were recorded for different bed aspect ratios, H_0/D, and different relative velocities, $U_r = U_0/U_{mf}$, with the half-covered distributor plate to reproduce operational situations exhibiting severe maldistribution conditions. The images were binarized, summed and rescaled with the total number of images processed, N, producing a time-averaged image that represents the fraction of time that a point of the bed surface is occupied by the black beads of low density material (Equation 4.2).

$$\widehat{C}(x,y) = \sum_{i=1}^{N} C_i(x,y)/N \tag{4.2}$$

Therefore, the fraction of time a point is occupied by bubbles is defined by Equation 4.3.

$$\widehat{B} = 1 - \widehat{C} \tag{4.3}$$

$\widehat{B}$ and $\widehat{C}$ will be, respectively, the bubble and black beads concentration on the bed surface (Hernández-Jiménez et al., 2011).

Figure 4.2 shows the bubble concentration, $\widehat{B}$, at the bed surface for all the experiments carried out under severe maldistribution conditions (with the half-covered distributor plate). The hot colours (red) correspond to low bubble concentration, whereas the cold colours (blue) correspond to high bubble concentration. As can be seen, a boundary between high and low bubble concentration can be clearly identified in all the cases, dividing the bed surface into two regions: the non-bubbling region (zone 1) where the black beads are more prone to be found and the bubbling fluidized region (zone 2) with a high probability of finding bubbles.

An increase of the relative velocity produces a reduction of the measured non-bubbling region as can be observed in Figure 4.2, suggesting that maldistribution problems can be controlled by gas velocity at the bed surface. However, from Figure 4.2 nothing can be said regarding the paths followed by the bubbles from the gas distributor. A similar effect is found when the bed aspect ratio is increased. Thus, in spite of deeper beds seem to have the ability of compensate the gas maldistribution near the bed surface, the pressure fluctuation measurements showed that even at the highest velocities tested ($U_r = 2.00$), the induced maldistribution prevails at the top of the bed. However, if the gas velocity is high enough, the maldistribution may not be detected on the bed surface.

Once the experiments with a severe maldistribution (half-covered distributor) were

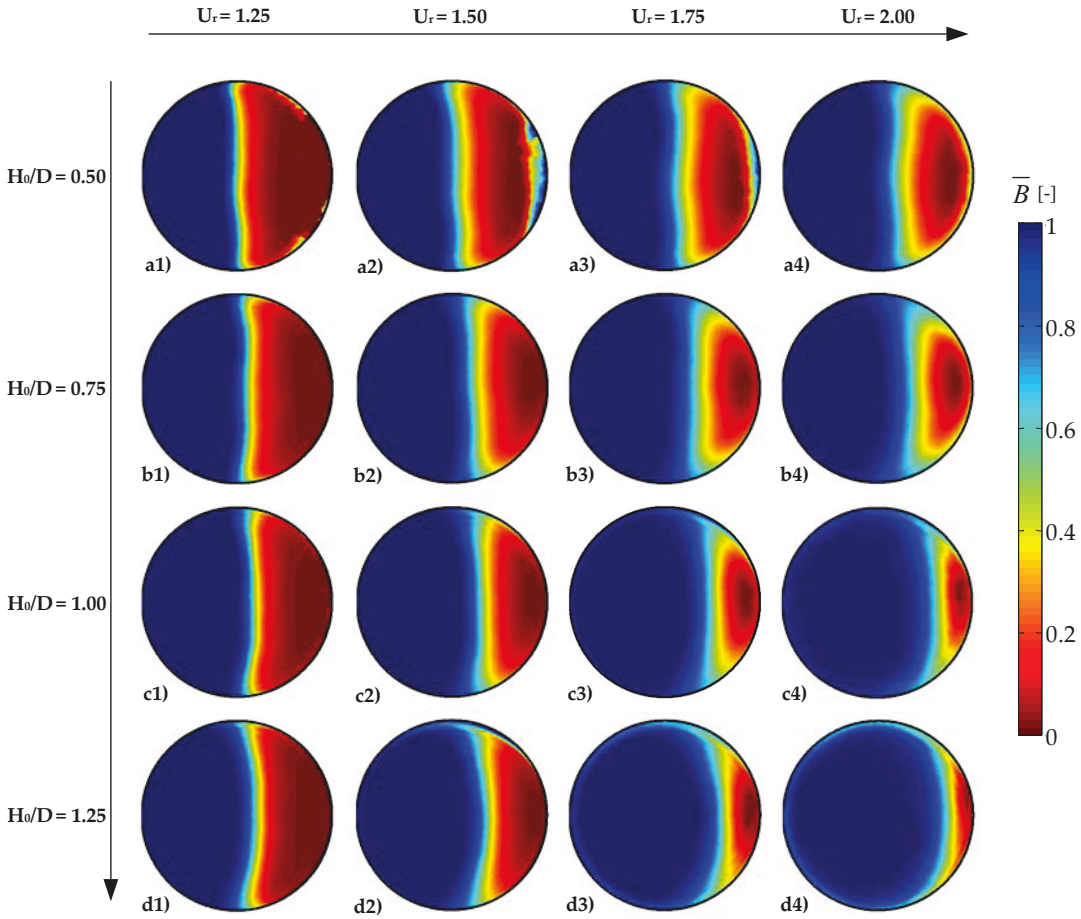

Figure 4.2: Global surface bubble concentration patterns for different values of H_0/D and U_r with the half-covered distributor plate.

analyzed, it is of interest to evaluate smooth cases of maldistribution, which may be closer to maldistribution problems that can lead to defluidization in industrial fluidized beds. A new set of experiments was carried out opening a certain percentage of orifices of the distributor plate in zone 1, p_h, and covering the same number of orifices in zone 2, in order to obtain a similar distributor pressure drop. Therefore, the number of open orifices was always the same, but the distribution of the orifices was different. The bed aspect ratio was fixed to 1.25 in this case. The measurement techniques and the post-processing was the same as for the half-covered distributor. However, in order to facilitate the information provided by the recorded images of the bed surface (Figure 4.2), polar coordinates were employed. A schematic diagram of how this change of coordinates was performed is presented in Figure 4.3.

The x and y coordinates were transformed into α and r coordinates and then the mean value of bubble concentration along the r coordinate was calculated for each value of the angle α. The results are plotted in Figure 4.4.

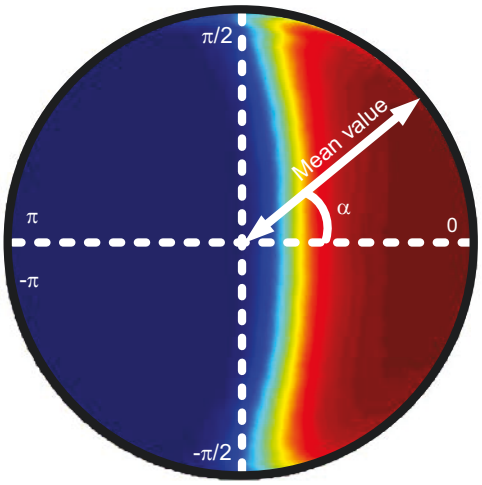

Figure 4.3: Schematic diagram of polar coordinates conversion.

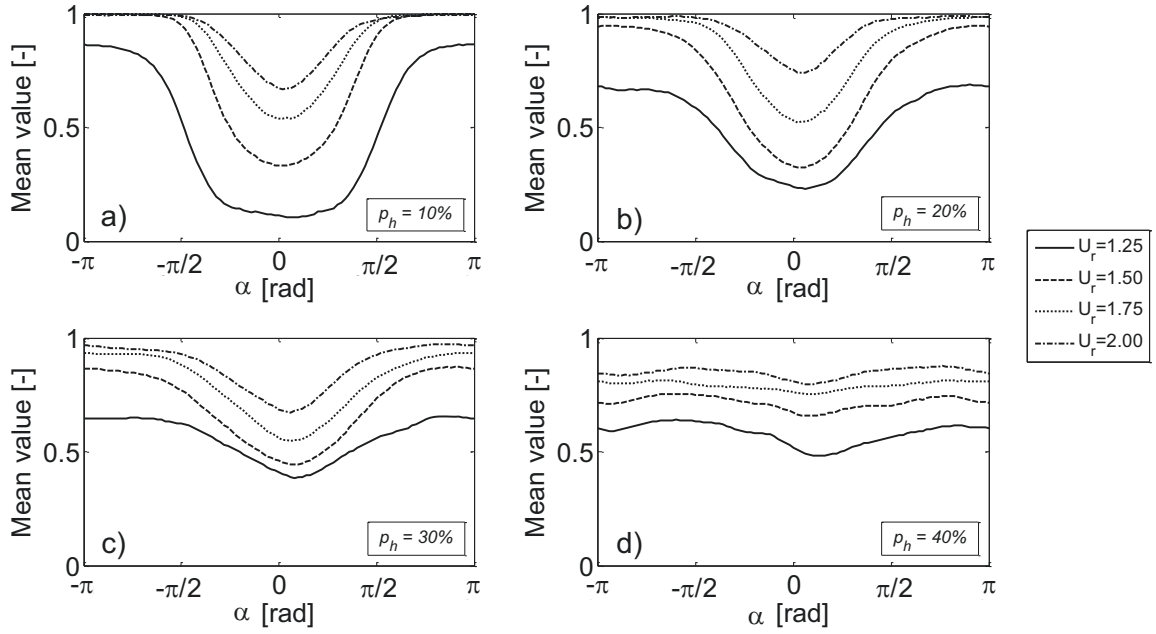

Figure 4.4: Mean values of bubble concentration represented in polar coordinates for different values of open orifices percentage and U_r.

As can be observed in Figure 4.4a, there is a dome representing a low bubble concentration over zone 1. The size of the dome decreases when the relative velocity increases, reducing the size of the non-bubbling region. As long as the percentage of open orifices increases, the size of the dome decreases drastically meanwhile the mean value of bubble concentration tends to roughly exhibit a uniform distribution. Assuming that bubbles rise only above active orifices, higher values of the gas velocity produce larger bubbles leading to a more vigorous fluidization and consequently, increasing the circulation of the black beads inside the bed, obtaining a higher mean bubble concentration

(Soria-Verdugo et al., 2011b). According to Figure 4.4d, when the percentage of open orifices is 40%, for all the gas velocities tested, the bed can be considered to be fairly well distributed at the bed surface since an almost uniform mean value for the bubble concentration is obtained.

Pressure fluctuation signals

Since the visual inspection of the bed surface does not report information about the maldistribution inside the bed, pressure fluctuation signals were analyzed to obtain information about the bubble paths inside the bed. The results of the visual inspection confirm that maldistribution problems near the bed surface can be fairly controlled by either increasing the gas velocity or the bed height. Besides, from the point of view of the maldistribution detection, it is not clear if pressure measurement location and the corresponding measured pressure fluctuation signal can be affected by gas velocity and bed height.

Considering the uniform case (i.e. $p_h = 50\%$, plotted in grey lines in Figure 4.5) as a reference, for a given bed aspect ratio and a given relative velocity, pressure fluctuation signals were subsequently recorded at different heights over both zone 1 and zone 2 (Figure 4.1). The standard deviation of the pressure fluctuation signals measured is plotted as a function of the probe height. Figure 4.5 shows the results corresponding to an aspect ratio of $H_0/D = 1.25$ and a relative fluidization velocity of $U_r = 2.00$. The standard deviation of the analogous pressure fluctuation signals measured simultaneously in the plenum chamber is also shown for comparison.

Figure 4.5a corresponds to a severe maldistribution case (half-covered distributor), whereas Figures 4.5b, c, d, e, correspond to different degrees of incipient nonuniform gas distribution cases. It can be observed that the standard deviation of pressure fluctuation signals measured along the bed height at zone 1 exhibit a lower value than the standard deviation measured in the plenum chamber for most of the unfavourable operational conditions covered (Figure 4.5a, b, c, d). However, it is worth to remark that the measured pressure signal of those pressure ports actually detects passing bubbles, and then there must be a reason why the standard deviation exhibits such lower values. To find out the origin of these fluctuation signals for the different pressure probe heights used, a cross correlation analysis between the pressure signal measured simultaneously at zone 1 and zone 2 is performed.

Figure 4.6 shows the value of the correlation coefficient between zone 1 and zone 2 as a function of percentage of open orifices. It can be observed in Figure 4.6 that the cross correlation coefficient increases at the bottom of the bed, where the local effect of the passing bubbles on the measured pressure fluctuation signals is small and

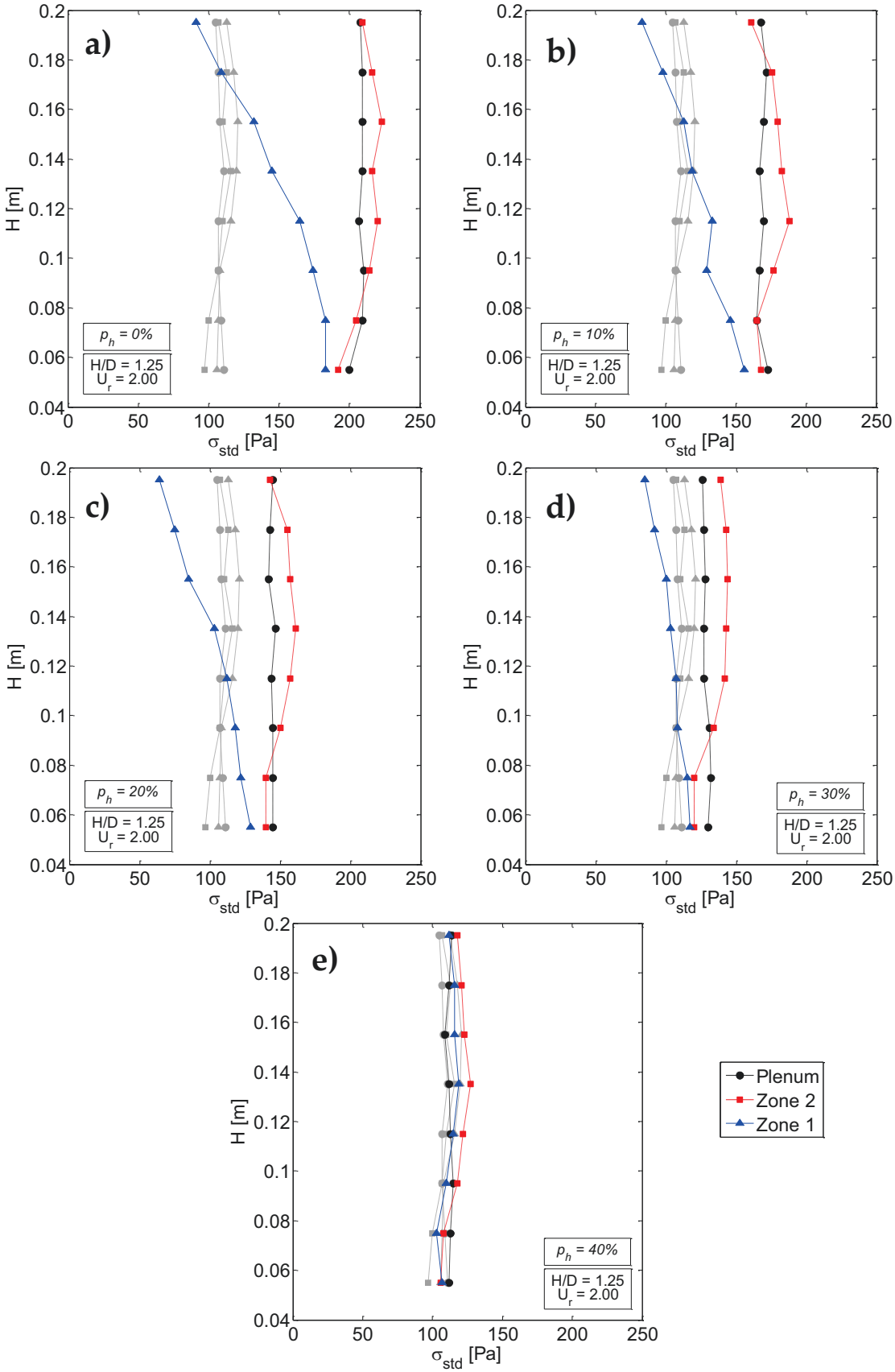

Figure 4.5: Standard deviation of pressure fluctuation signals as a function of the sensor height for different values of open orifices percentage. The nominal case ($p_h = 50\%$) is plotted in grey lines for comparison.

the measured pressure signal is mainly governed by fast-travelling waves originated by dynamical phenomena such as bed mass oscillation, bubble coalescence, bubble eruption or gas flow fluctuations (van der Schaaf et al., 2002), which are not attenuated downwards. In contrast, these fast travelling pressure waves suffer attenuation when travelling upwards, leading to a decrease of the cross correlation coefficient at the upper part of the bed. Concerning the effect of the percentage of open orifices, p_h, it can be observed in Figure 4.6 that the cross correlation coefficient decreases with p_h, approximating its value to the corresponding values of the uniform case. Therefore, it can be concluded that when the percentage of open orifices in the non bubbling region is low, the pressure fluctuation signals measured at zone 1 actually see the passing bubbles rising above zone 2.

Regarding the boundary between the even and uneven gas distribution, it can be observed in Figure 4.6, for the case of $p_h = 40\%$, that the cross correlation coefficient is almost equal to the cross correlation coefficient of the uniform case for the whole bed height. Moreover, the standard deviation values measured for both the pressure fluctuation signals collected at p_h= 40% and at uniform conditions are very similar as can be seen in Figure 4.5e. This is in agreement with the results obtained from the analysis of the images recorded at the bed surface, showed in Figure 4.4. Consequently, for the fluidized bed system investigated, the threshold for uneven gas distribution operation lies around 40% of open orifices.

Finally, from the standard deviation profiles shown in Figures 4.5a,b,c,d it is clear that even at the highest velocities tested ($U_r = 2.00$), the induced maldistribution prevails up to the top of the bed. The challenge is then the online detection of the onset of maldistribution. Furthermore, it seems clear that neither increasing the gas velocity nor increasing the bed aspect ratio can mend the severe induced nonuniform gas distribution at the bottom of the bed (Figure 4.5a).

4.3.2 Online monitoring of maldistribution

Three different monitoring methods were applied to the measured pressure fluctuation signals: the statistical process control (SPC) based on the standard deviation, the wide band energy division method and the attractor comparison method (S-test). The aim is to check the feasibility of these methods for the maldistribution detection. As stated above, it is assumed that defluidization problems might be accompanied by gas maldistribution phenomena and consequently, similar monitoring approaches, successfully used previously to detect defluidization, could be also applied to maldistribution detection.

The parameters used for the SPC of the standard deviation of pressure fluctuation

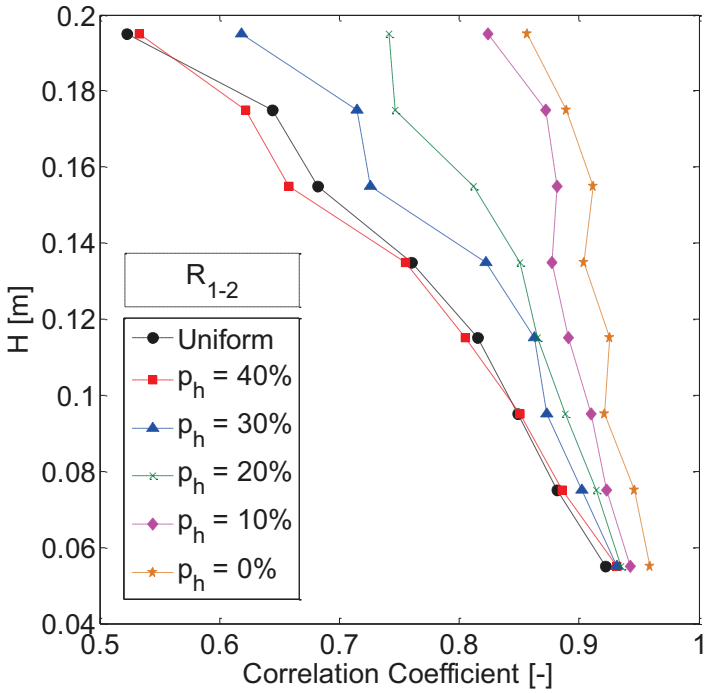

Figure 4.6: Cross correlation between zone 1 and zone 2 pressure signals as a function of the probe height for different values of open orifices percentage.

Table 4.2: Settings for SPC monitoring.

Time series length [s]	Time window [s]	Fitting	UWL	LWL
240	30	Normal distribution	$\widehat{x} + 2\sigma$	$\widehat{x} - 2\sigma$

Table 4.3: Settings for the wide band energy division method.

Time series length [s]	Time window [s]	PSD	Fitting	σ_v [-]	f_{cI} [Hz]	f_{cII} [Hz]
240	30	Welch method $N_s = 1024$	t-Student distribution	0.07	2	5

Table 4.4: Settings for the S-test method.

Time series length [s]	Time window [s]	Embedding Dimension [-]	Band Width [-]	Segment Length [s]
240	30	20	0.5	3

signals were defined by Gómez-Hernández (2015) are shown in Table 4.2. Regarding the wide band energy division method, the t-Student distribution approach developed by Gómez-Hernández et al. (2014) was applied assuming that the pressure signals follow a normal probability distribution (Table 4.3). For the attractor comparison test, the optimal parameters reported by van Ommen et al. (2000) were used to compute the S-statistic (Table 4.4).

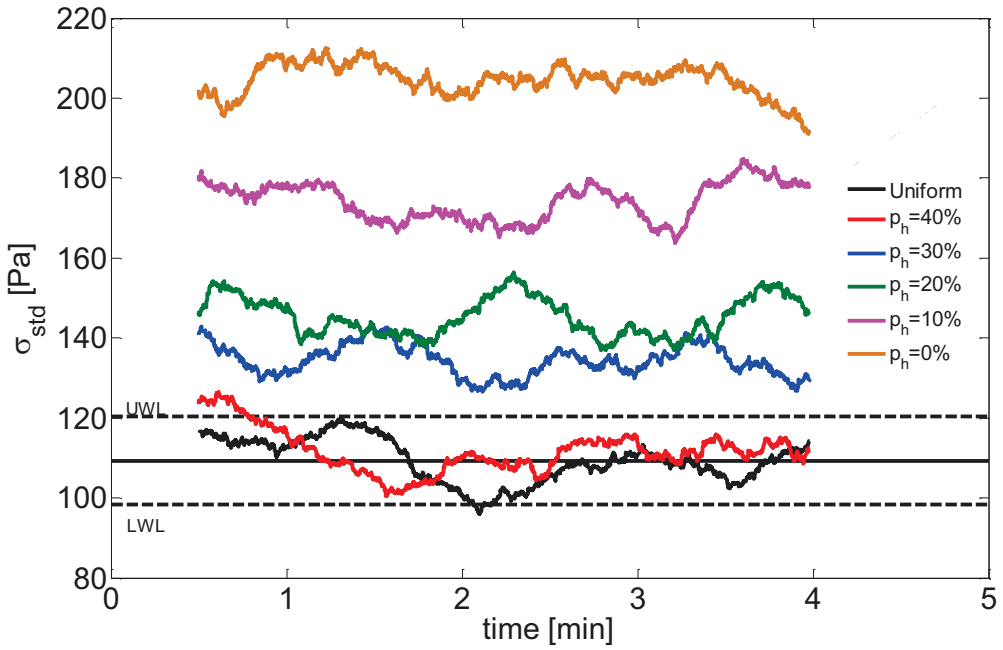

Figure 4.7: Statistical process control chart for the pressure signal measured at zone 2 (H=15.5 cm, U_r=2.00).

The pressure signal measured in zone 2 at $H = 15.5$ cm above the distributor for $U_r = 2.00$ serves to illustrate the sensitivity of the three monitoring approaches for gas maldistribution detection. Thus, Figure 4.7 shows the statistical process control chart corresponding to the standard deviation at zone 2. The pressure fluctuation signals measured for the uniform case were used for comparison and consequently the upper and lower warning limits (UWL and LWL) were established using the standard deviation data obtained during the uniform case ($p_h = 50\%$) measured at zone 2. According to that, the bed was considered to exhibit uneven gas distribution when the standard deviation of the pressure fluctuations signal falls out the warning limits. Figure 4.7 shows that the gas was evenly distributed in the bed just for the case of $p_h = 40\%$, which is in agreement with the results shown previously in Figure 4.5e and Figure 4.6. As expected from previous observation, when the percentage of open orifices was reduced the value of the corresponding standard deviation increased, falling out of the control limits. Consequently, the statistical process control of the standard deviation could be fairly applied as a monitoring tool for the online detection of gas maldistribution, which is in agreement with van Ommen et al. (2004a). The method was also tested with the pressure signal measured in the plenum chamber showing similar results.

As stated above, the unbiased method reported by Gómez-Hernández et al. (2014) for the wide band energy analysis was also applied to the pressure fluctuations signals

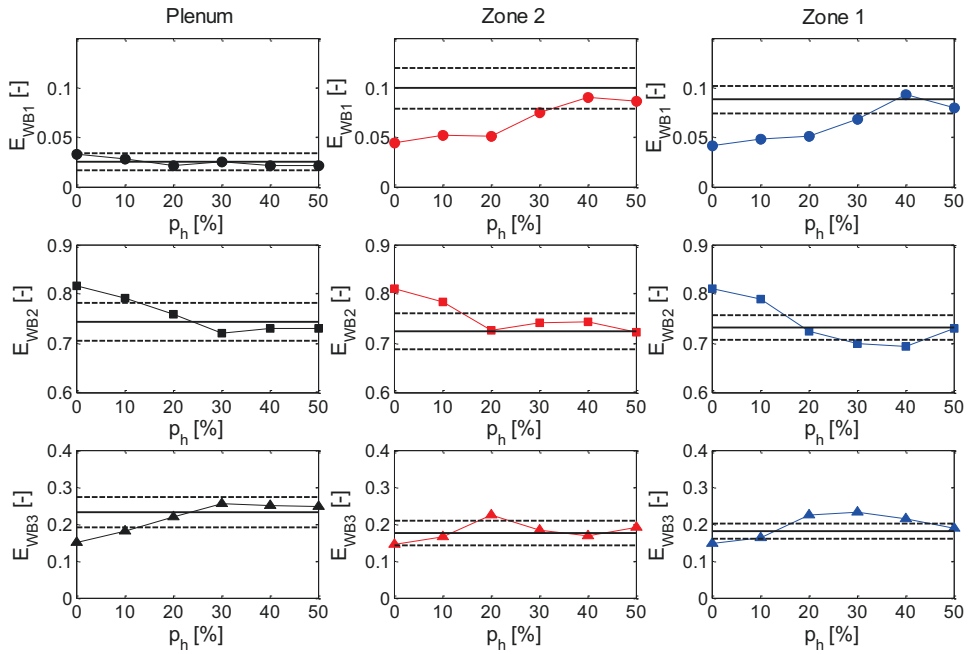

Figure 4.8: Wide band energy analysis of the pressure signal measured at the plenum chamber (left), zone 2 (centre) and zone 1 (right) (H=15.5 cm, U_r=2.00).

measured. As for the standard deviation, the pressure time series measured for the uniform case were used as reference state. Consequently, the cut-off frequencies and the limits were obtained using the uniform case. As can be seen in Figure 4.8, the energy within Region $t-I$ (E_{WB1}) is the most sensitive for maldistribution detection. In contrast, the energy within Regions $t-II$ (E_{WB2}) and $t-III$ (E_{WB3}) barely detect severe cases of maldistribution. Moreover, the different sensitivity exhibited by the wide band energy analysis when measuring at the plenum, zone 2 and zone 1 (Figure 4.8) reveals that, as for the standard deviation, the measurement position affects the results of the wide band energy analysis.

To conclude with the exploration of the monitoring methods, the attractor comparison method was tested for maldistribution detection. It is based on the S statistical test reported by Diks et al. (1996). The comparison of the S value for a pressure time series with a chosen reference time series (i.e. the uniform case) can determine whether it was measured at similar hydrodynamic conditions as the reference time series or not. A value of S larger than 3 indicates significant changes in the hydrodynamic behaviour, whereas two time series with similar hydrodynamic conditions should yield to a value of S close to zero. The S statistic was calculated in this case comparing the pressure fluctuation signals measured in zone 2 for the different values of p_h used in this study, with the pressure fluctuation signal of the uniform case also measured in zone 2.

The results of the S statistic as a function of time are shown in Figure 4.9a. It can

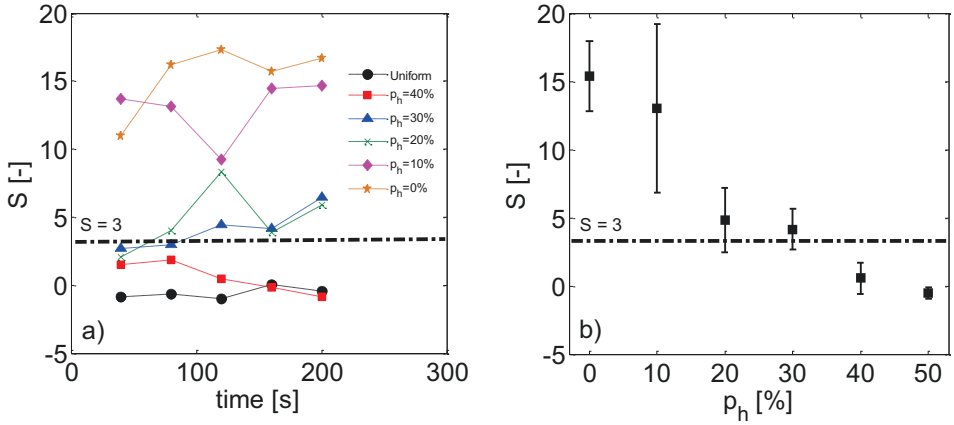

Figure 4.9: a) S statistic as a function of time for different values of open orifices percentages and b) mean S statistic as a function of open orifices percentage for the pressure signal measured at zone 2 (H=15.5 cm, U_r=2.00).

be observed that only the uniform case and the case of $p_h = 40\%$ lie below the limit of $S = 3$. As expected, the S statistic for the uniform case has a value close to zero. For a better visualization of the results, the mean value of S was plotted as a function of the percentage of open orifices in Figure 4.9b. The error bars of Figure 4.9b represent the standard deviation of S. The method seems to detect precisely severe maldistribution cases. However, this method is apparently less sensitive to detect slight maldistribution problems than the standard deviation for the signal collected at $H = 15.5$ cm.

4.3.3 Effect of pressure probe location

The different sensitivities exhibited by the different monitoring methods to the pressure measurement position makes necessary a study of the effect of pressure probe location. Figure 4.10 shows the comparison between the standard deviation and the S-test monitoring approaches as a function of the pressure measurement position, using the signals measured in zone 2. Only the softer cases of maldistribution (i.e. p_h = 30-40%) are presented in Figure 4.10 for simplicity. The wide band energy method was excluded of the discussion because of its low sensitivity for maldistribution detection.

As can be observed, the SPC method is able to distinguish between the uniform case and the $p_h = 40\%$ case at almost any position of the pressure probe. On the contrary, the S statistic method seems to be strongly influenced by the probe position and the maldistribution detection was effective just when the pressure probe was located close to the bed surface. Therefore, the statistical process control method based on the standard deviation is recommended, since it can detect cases of slight maldistribution and it is considerably easier to use than the S statistic method. Besides, according

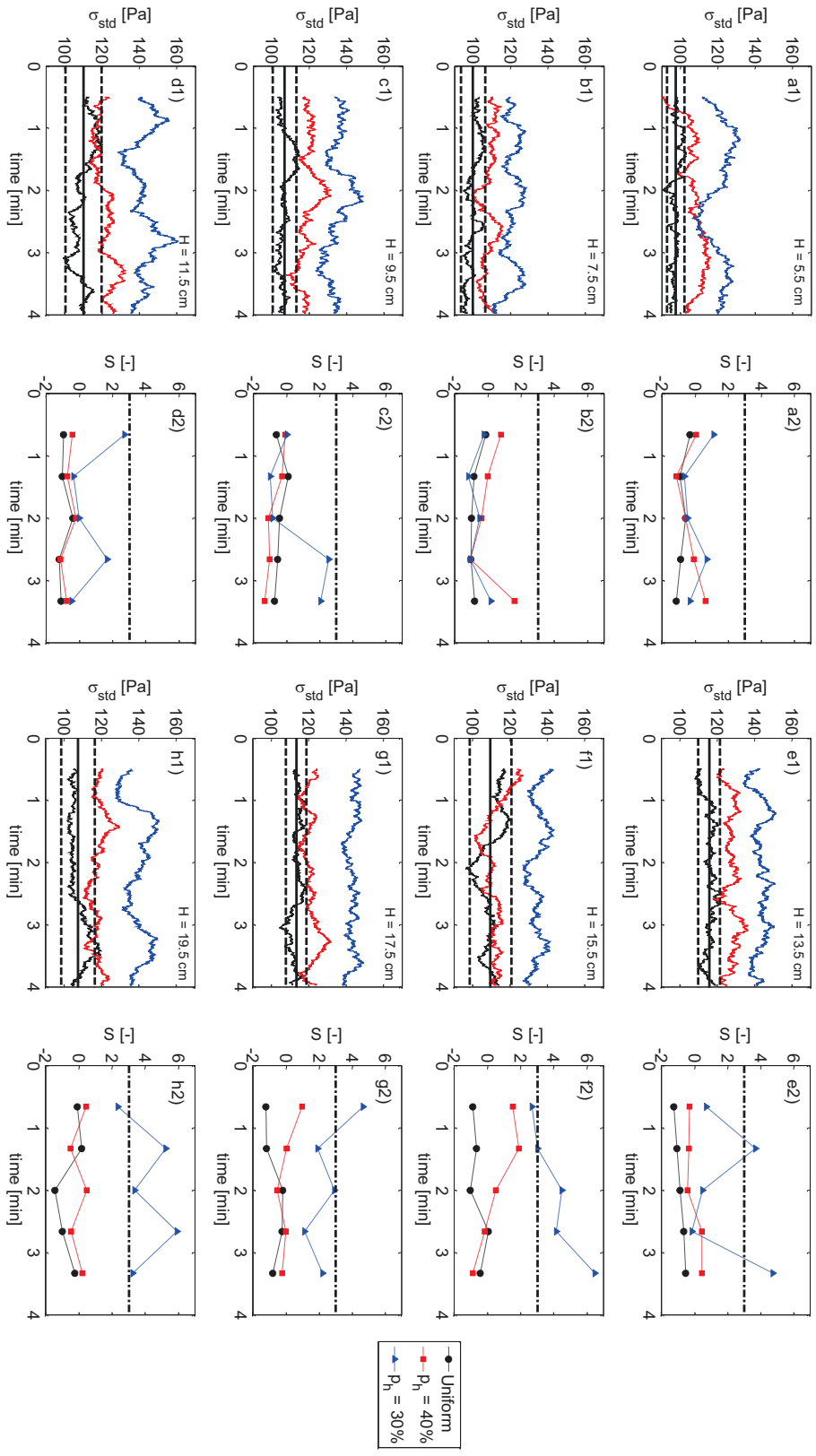

Figure 4.10: Effect of the pressure probe height on the statistical process control based on the standard deviation and on the S statistic (U_r=2.00).

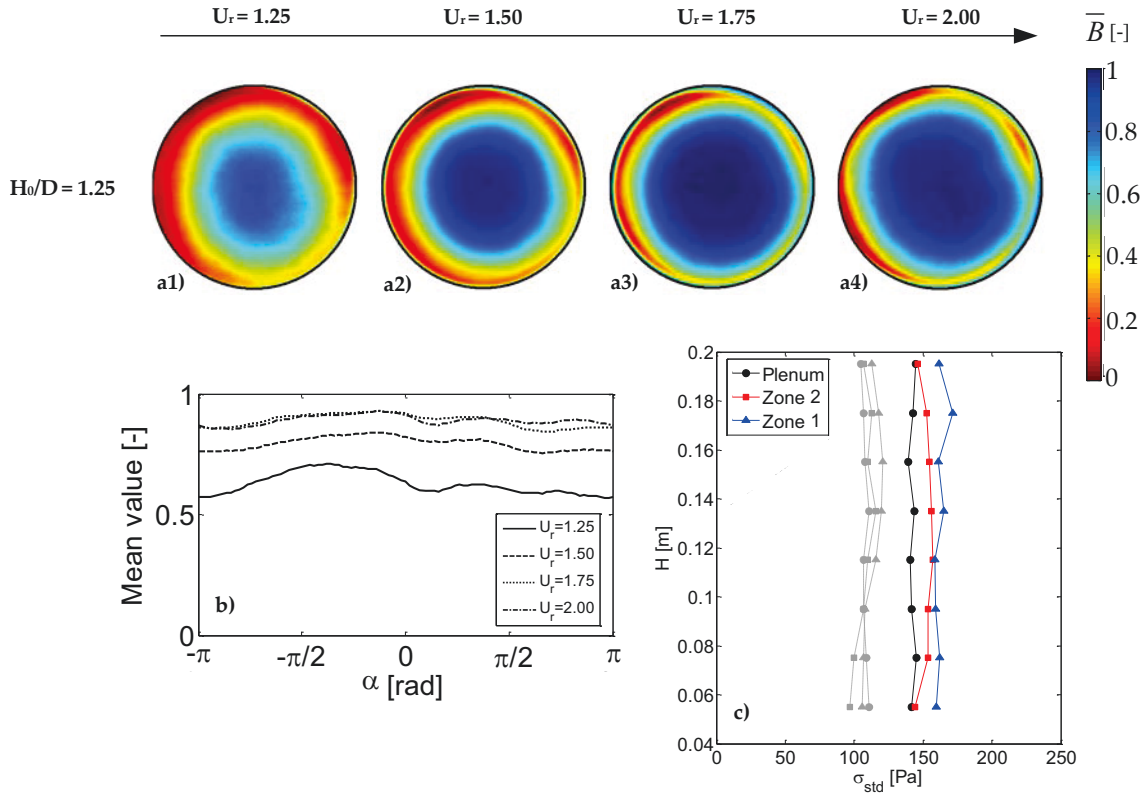

Figure 4.11: Results for the rotating distributor.

to the sensitivity exhibited by the standard deviation method (Figure 4.10), for maldistribution detection purposes, pressure probes should be located between 50-75% of the total bed height. However, due to the strong dependence of the standard deviation on the superficial gas velocity, the SPC method should be applied with caution in industrial facilities, in which the gas velocity is seldom constant (van Ommen et al., 2011).

4.3.4 Application: rotating distributor plate

Finally, a new set of experiments, where the fluidized bed was operating at different relative gas velocities, was conducted with the half-covered distributor rotating at 100 rpm. The objective of these experiments is to investigate the capability of the distributor rotation to suppress the maldistribution in a fluidized bed. To illustrate the reliability of the distributor rotation as a counteracting measure of gas maldistribution, the analysis of the images recorded at the bed surface using DIA techniques and the analysis of pressure fluctuations signals, in terms of the standard deviation profile along the bed height, are shown. The results of bubble concentration at the bed surface and the standard deviation of pressure signals are shown in Figure 4.11.

The bubble concentration patterns shown in Figure 4.11a1-a4 indicate that a uniform gas distribution is achieved at the bed surface. It can be also observed in Figure 4.11b that the mean value of the bubble concentration at the bed surface is almost uniform for all the gas velocities tested, as found before for the case of $p_h = 40\%$. The pressure fluctuation signals along the bed height were also measured at several positions above the distributor plate. The standard deviation values of the pressure fluctuation signals measured in zone 1 and 2 are very close, indicating that the bed was evenly fluidized. Moreover, assuming that bubbles rise only above active orifices, the fact that the standard deviation of the pressure signal is clearly higher than the standard deviation of the pressure signal measured in the plenum chamber guarantees the presence of passing bubbles in both zones. Therefore, it can be concluded that the rotating distributor can help to prevent or eliminate maldistribution problems, even for severe maldistribution problems such as the blocking of half of the total number of orifices of the distributor plate.

4.4 Conclusions

A fluidized bed with a half-covered distributor plate was used to study the limits of maldistribution in fluidized beds. It was shown that the non-fluidized zone created by the covered part of the distributor plate can be avoided at the bed surface provided that the bed aspect ratio or the gas velocity is high enough. In any case, there is a zone above the covered part of the distributor where motion of solids is prevented. Therefore, when the maldistribution is strong enough the effect can only be avoided at the surface of the bed.

Pressure fluctuation signals were analyzed to quantify the onset of maldistribution. The possibility of detecting maldistribution by an online monitoring tool was investigated using several methods that can be found in literature. The analysis based on the Student's t-distribution approach of the wide band energy exhibits a strong dependence on the measurement location, and shows a lower sensitivity than the SPC method. The S statistic method presents a strong influence of probe location and it can only detect maldistribution properly provided that the pressure signal is measured in the upper zone of the fluidized bed. Finally, the SPC method based on standard deviation showed a high capability of detecting moderate cases of maldistribution and it is not influenced by the probe location. However, a probe placement at 50-75% of the total bed height is recommended.

For the experimental conditions of this work, the boundary between maldistribution and stable operation corresponds to a 40% of open orifices. That value establishes the

relative size of the operational problem that can be detected by the online monitoring techniques investigated.

Therefore, it seems that only one pressure probe can be sufficient to detect hydrodynamic changes caused by maldistribution in lab-scale fluidized beds if it is properly located. However, the online monitoring methods used cannot identify the exact source of these changes. In the case of an industrial fluidized bed, whose dimensions are larger than in lab-scale fluidized beds, the optimal placement of pressure probes has to be considered. Therefore, a higher number of pressure probes should be used in an industrial facility to monitor the entire section of the bed. Finally, the rotation of the distributor was analyzed as a counteracting mechanism to maldistribution, finding that severe maldistribution can be prevented or eliminated by forcing the distributor to rotate.

4.5 Notation

$\widehat{B}$	Bubble concentration [-]
$\widehat{C}$	Black beads concentration [-]
D	Bed diameter [m]
d	Penetration ratio [-]
d_p	Mean particle diameter [m]
g	Gravity [m/s^2]
H	Height over the distributor plate [m]
H_0	Bed height [m]
H_0/D	Aspect ratio [-]
N	Number of images in each video [-]
p_h	Percentage of open orifices in zone 1 [%]
R	Pressure drop ratio [-]
r	Radial coordinate [m]
S	S statistic [-]
U_0	Air superficial velocity [m/s]
U_M	Superficial gas velocity at which all the orifices became operative [m/s]
U_{mf}	Minimum fluidization velocity [m/s]
U_r	Relative gas velocity [-]

Greek letters

α	Polar angle [rad]
ϵ_{mf}	Voidage at minimum fluidization conditions [-]

μ	Air viscosity at ambient temperature [kg/ms]
ρ_{bb}	Black beads density [kg/m^3]
ρ_g	Air density at ambient temperature [kg/m^3]
ρ_s	Particle density [kg/m^3]
ϕ	Particle sphericity [-]
σ_{std}	Standard deviation of the pressure signal [Pa]
σ_v	Standard error of shape parameter [-]

Abbreviattions

DIA	Digital image analysis.
FB	Fluidized bed.
FSS	Full-scale span.
SPC	Statistical process control.

Bibliography

Briens, C.L., Briens, L.A., Barthel, E., Le Blvec, J.M., Tedoldi, A., Margaritis, A., 1999. Detection of local fluidization characteristics using the V statistic. *Powder Technol.* 102, 95-103.

Carman, P.C., 1937. Fluid flow through granular beds. *Transactions of the Institution of Chemical Engineers* 15, 150-166.

Diks, C., van Zwet, W.R., Takens, F., DeGoede, J., 1996. Detecting differences between delay vector distributions. *Phys. Rev. E* 53, 2169-2176.

Geldart, D., 1973. Types of gas fluidization. *Powder Technol.* 7, 285-292.

Geldart, D., Baeyens, J., 1985. The design of distributors for gas-fluidized beds. *Powder Technol.* 42, 67-78.

Gómez-Hernández, J., Sánchez-Prieto, J., Briongos, J.V., Santana, D., 2014. Wide band energy analysis of fluidized bed pressure fluctuation signals using a frequency division method. *Chem. Eng. Sci.* 105, 92-103.

Gómez-Hernández, J., 2015. Paste drying control in a rotating-distributor fludized bed, PhD thesis. Universidad Carlos III de Madrid, Spain.

Hernández-Jiménez, F., Sánchez-Delgado, S., Gómez-García, A., Acosta-Iborra, A., 2011. Comparison between two-fluid model simulations and particle image analysis & velocimetry (PIV) results for a two-dimensional gas-solid fluidized bed. *Chem. Eng. Sci.* 66, 3753-3772.

Sánchez-Prieto, J., Soria-Verdugo, A., Briongos, J.V., Santana, D., 2014. The effect of temperature on the distributor design in bubbling fluidized beds. *Powder Technol.* 261, 176-184.

Sathiyamoorthy, D., Sridhar Rao, C.H., 1981. The choice of distributor to bed pressure drop ratio in gas fluidised beds. *Powder Technol.* 30, 139-143.

Soria-Verdugo, A., García-Hernando, N., Almendros-Ibáñez, J.A., Ruiz-Rivas, U., 2011a. Motion of a large object in a bubbling fluidized bed with a rotating distributor. *Chemical Engineering and Processing: Process Intensification* 50, 859-868.

Soria-Verdugo, A., García-Gutiérrez, L.M., Ruiz-Rivas, U., Santana, D., 2011b. Buoyancy effects on objects moving in a bubbling fluidized bed. *Chem. Eng. Sci.* 66, 2833-2841.

Thorpe, R.B., Davidson, J.F., Pollitt, M., Smith, J., 2002. Maldistribution in fluidized beds. *Ind. Eng. Chem. Res.* 41, 5878-5889.

van der Schaaf, J., Schouten, J.C., Johnsson, F., van den Bleek, C.M., 2002. Non-intrusive determination of bubble and slug length scales in fluidized beds by decomposition of the power spectral density of pressure time series. *International Journal of Multiphase flow* 28, 865-880.

van Ommen, J.R., de Korte, R.J., van den Bleek, C.M., 2004a. Rapid detection of defluidization using the standard deviation of pressure fluctuations. *Chem. Eng. Process.* 43, 1329-1335.

van Ommen, J.R., van der Schaaf, J., Schouten, J.C., van Wachem, B.G.M., Coppens, M.O., van den Bleek, C.M., 2004b. Optimal placement of probes for dynamic pressure measurements in large-scale fluidized beds. *Powder Technol.* 139, 264-276.

van Ommen, J.R., Coppens, M.C., van den Bleek, C.M., Schouten, J.C., 2000. Early warning of agglomeration in fluidized beds by attractor comparison. *AIChE J.* 46, 2183-2197.

van Ommen, J.R., Sasic, S., van der Schaaf, J., Gheorghiu, S., Johnsson, F., 2011. Time-series analysis of pressure fluctuations in gas-solid fluidized beds A review. *International Journal of Multiphase flow* 37, 403-428.

Whitehead, A.B., 1971. In Davidson, J.F., Harrison, D., (Eds.) *Fluidization*. Academic Press, London, 781.

Chapter 5

Experimental study of the defluidized zone of an induced maldistributed fluidized bed

Contents

5.1 Introduction

Gas maldistribution is one of the most common problems related to distributor design and has an important effect on the performance of fluidized beds. Maldistribution is industrially undesirable: for dryers, because in the dead zones the drying rate drastically decreases, for reactors, because bypassing of reactants and uneven temperature in the bed are obtained, and in general, because it affects the heat and mass transfer capabilities and it may lead to defluidization and agglomeration problems. In most of the industrial processes carried out in fluidized beds, it is of crucial importance to prevent defluidization. When a defluidization problem is not detected and solved, major

damage can be caused to bed internals, agglomeration of bed particles may occur and, as a consequence, the heat and mass transfer capabilities of the bed will be drastically reduced (van Ommen et al., 2004).

Maldistribution of gas and the design criteria to avoid it have been investigated by many researchers, such as Whitehead and Dent (1967), Fakhimi and Harrison (1970), Yue and Kolaczkowski (1982) and Thorpe et al. (2002). Thorpe et al. (2002) reviewed the existing literature concerning theoretical models used to estimate the boundary of maldistribution in fluidized beds. The authors determined U_M with bed pressure drop measurements in a 3D fluidized bed and compared the experimental results with predictions of several models: the theory of Fakhimi and Harrison (1970), the theory of Whitehead and Dent (1967) and the theory of Yue and Kolaczkowski (1982). They found the best fit with the theory of Fakhimi and Harrison (1970). They also found a good agreement with the theory of Yue and Kolaczkowski (1982), however, this theory is an attempt to improve the theory of Fakhimi and Harrison (1970) by considering the effect of bed height. The authors concluded that the theory of Fakhimi and Harrison (1970) gives the best estimation, since it is a simpler theory than that of Yue and Kolaczkowski (1982). These works were based on the study of U_M, defined as the superficial velocity at which all the orifices or tuyeres of the distributor plate become operative, which usually means they are jetting (Sathiyamoorthy and Rao, 1981; Whitehead et al., 1971). The value of U_M depends on the gas flow rate, the bed aspect ratio, the bed material and the open area of the distributor. All these variables have been studied in terms of the distributor to bed pressure drop ratio, R, since the onset of maldistribution seems to be directly related to this ratio (Sánchez-Prieto et al., 2014).

In the previous chapter it was concluded that gas maldistribution in fluidized beds can be detected using pressure signal analysis. The onset of maldistribution with Digital Image Analysis (DIA) of images of the bed surface was studied and then, several monitoring methods to quantify the boundary between stable operation and maldistribution were applied. However, nothing can be said about the internal structure of the maldistribution region generated inside the bed, since the pressure fluctuations signals were proven to detect if there is maldistribution present but could not identify the exact source of these changes in the dynamical behavior.

Visualization methods such infrared (IR) imaging are commonly used in industrial boilers and incinerators for monitoring and control purposes (Zipser et al., 2006). These methods are usually employed to obtain information about the combustion flame (Chimenti et al., 2004; Lu et al., 2005; Ballester and García-Armingol, 2010; González-Cencerrado et al., 2012), since it is directly related to the combustion performance. IR

imaging can also be used to determine temperature profiles of solid bodies such as the solid fuel particles, the reactor wall or, in case of a fluidized bed combustor, the bed material. Thus, the online monitoring of the bed surface of a fluidized bed combustor with an IR camera can help to detect dead zones caused by gas maldistribution or agglomeration.

In this chapter a new methodology is proposed to study the defluidized zone generated in an induced maldistributed pseudo-2D fluidized bed. These beds have shown to be of great importance for the understanding of fluidized beds. Two-dimensional beds typically have a transparent wall and possess a small thickness, so that optical access to the system is allowed and the behavior of the visualized particles is representative of the whole system (Hernández-Jiménez et al., 2011). The variables affecting the defluidized zone in a pseudo-2D fluidized bed were investigated to obtain a correlation for the size of this zone. The final aim of this work is the extrapolation of the 2D results to a 3D fluidized bed, in order to obtain a model capable of estimating the size of the defluidized zone in an industrial fluidized bed combustor, provided that experimental images of the bed surface are available.

5.2 Experimental setup

Two different experimental facilities were employed in this work: a pseudo-2D cold fluidized bed and a lab-scale cylindrical bubbling fluidized bed (BFB).

The dimensions of the pseudo-2D cold fluidized bed were 0.3 m x 1 m x 0.01 m (width W, height H, and thickness Z). The bed material employed was ballotini glass particles of 2500 kg/m^3 density and a mean diameter of 700 μm (600-800 μm), classified as type B according to Geldarts classification (Geldart, 1973). The air flow was measured with a set of two flow meters, with ranges of 0-200 L/min and 0-500 L/min providing an accuracy of 1% of full-scale span (FSS). The air distributor consists of a perforated plate with two rows of 30 holes of 0.001 m in diameter, arranged in a triangular configuration with 0.01 m pitch. The distributor is equipped with a mesh to avoid the falling of particles inside the plenum chamber and to ensure a proper distributor to bed pressure drop ratio, R, to avoid gas maldistribution (Karri and Werther, 2003; Sánchez-Prieto et al., 2014). The front and rear walls of the bed were made of glass and the rear wall was painted in black to increase the contrast of the images recorded at the front. A *Basler A640* digital camera was used to record images of the front wall of the fluidized bed at 100 fps. The spatial resolution of the pictures is 300 x 600 pixels. A uniform illumination of the front of the bed was guaranteed with the use of two spotlights of 650 W.

The plenum chamber was divided in two separated chambers of the same size to produce an induced maldistribution similar to that studied in Sánchez-Prieto et al. (2015), where half of the total number of orifices of the distributor plate were covered. In the experiments performed in this work, the air was only supplied to the left chamber (half of the total distributor area and orifices) and, therefore, bubbles were generated only at the left side of the bed. The right chamber, where no air was supplied, induces a defluidized zone at the right side of the bed. A schematic diagram of the pseudo-2D bed is shown in Figure 5.1 a).

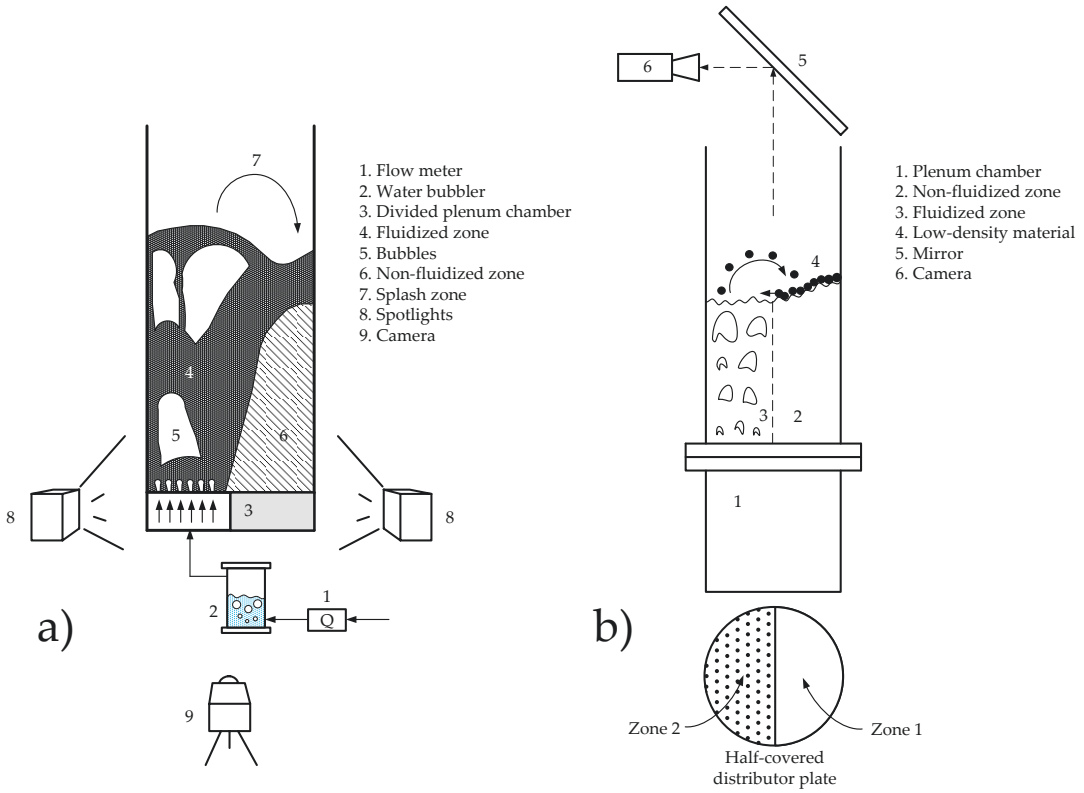

Figure 5.1: Schematic diagram of the experimental setup: 2D facility (a) and 3D facility (b).

In each experiment, the bed was filled with ballotini glass beads at the desired bed aspect ratio. The fluidizing air enters the bed across the left side of the plenum chamber with a fixed flow rate. When the bed is operating at the steady state, a handful of black painted ballotini particles were introduced from the top of the bed. These black particles have the same mean diameter, density and size as the rest of the particles used in the experiment, being the color the only difference between them. The black painted particles mix with the dense phase just in the zones where motion of particles occurs. As a result, the defluidized zone remains white, whereas the rest of the particles become a mixture of black and white (Figure 5.2), obtaining a contrast

between the defluidized zone and the rest of the bed. This methodology facilitates the recognition of the defluidized zone in the thresholded images.

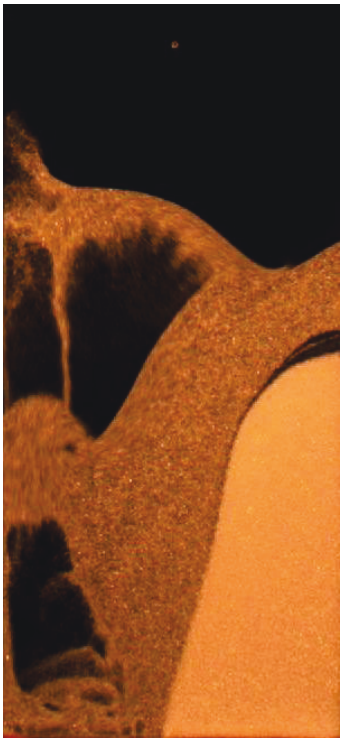

Figure 5.2: Example of an image after adding the black painted particles.

Experiments were also carried out in a lab-scale cylindrical bubbling fluidized bed (BFB), with a bed diameter of 0.192 m, previously described in Sánchez-Prieto et al. (2015). A schematic of the 3D facility is shown in Figure 5.1 b). The bed material used was sepiolite (clay) particles (SG36) with a density of 1551 kg/m^3 and 450 μm mean diameter, classified as type B according to Geldarts classification (Geldart, 1973).

Black beads of 0.006 m in diameter made of a low-density material (ρ_{bb}=36.20 kg/m^3) were used to produce a high contrast in the bed surface, which facilitate the recognition of erupting bubbles during the digital analysis of the images recorded. When a bubble explodes at the bed surface, the black beads are ejected leaving a free space proportional to the size of the exploding bubble. The bed surface was recorded to obtain an average solid concentration profile used to estimate the boundary between the fluidized and non-fluidized zones (Sánchez-Prieto et al., 2015).

The main physical properties of the bed material used in both experimental facilities are summarized in Table 5.1, including experimental values of the minimum fluidization velocity, U_{mf}, at ambient temperature. The minimum fluidization velocity of ballotini particles was measured in the 2D facility while the minimum fluidization velocity of

the sepiolite particles was measured in the lab-scale cylindrical BFB. The orifices of half the cross sectional area were covered in both experimental facilities to create an induced maldistributed region.

A summary of the experimental conditions of all the experiments carried out in this work is shown in Table 5.2. The values of $U_r = U_0/U_{mf}$ of Table 5.2 were obtained considering only the non-covered part of the distributor plate cross-section (i.e. half of the total distributor cross-sectional area).

Table 5.1: Physical properties of solid particles.

	d_p [μm]	ρ_s [kg/m^3]	Geldart Type	U_{mf} [m/s]
Ballotini glass beads	700	2500	B	0.44
Sepiolite (SG36)	450	1551	B	0.13

Table 5.2: Summary of the experimental conditions.

Facility	Aspect ratio (H_0/W;H_0/D)	Relative velocity (U_r)	Bed material
Pseudo–2D bed	0.50; 0.75; 1.00; 1.25	3.00; 4.00; 5.00; 6.00	Ballotini glass beads
Cylindrical BFB	0.50; 0.75; 1.00; 1.25	2.50; 3.00; 3.50; 4.00	Sepiolite (SG36)

5.3 Results and discussion

5.3.1 Defluidized and recirculation zones in pseudo-2D beds.

The images recorded in the 2D facility were binarized, summed and rescaled with the total number of images processed, N, producing a time–averaged image that represents the fraction of time that a point of the bed is occupied by dense phase (Equation 5.1).

$$\widehat{C}(x,y) = \sum_{i=1}^{N} C_i(x,y)/N \tag{5.1}$$

Therefore, the fraction of time a point is occupied by bubbles is defined by Equation 5.2.

$$\widehat{B} = 1 - \widehat{C} \tag{5.2}$$

$\widehat{B}$ and $\widehat{C}$ will be, respectively, the bubble and black beads concentration on the bed surface (Hernández-Jiménez et al., 2011). A similar analysis was performed for the images of the bed surface recorded in the cylindrical BFB, as will be described in Section 5.3.2.

The dense phase concentration profiles, $\widehat{C}$, are shown in Figure 5.3 a) for the case of $H_0/W = 0.75$ (the nominal case hereafter). As can be seen, as long as the relative gas velocity, U_r, is increased the high bubble concentration region (cold colour) increases. It is worth to notice that bubbles only appear in the left side of the bed, where the air is supplied. The right side, where a higher solid concentration is achieved, corresponds to the defluidized zone generated as a consequence of the blocked part of the plenum chamber.

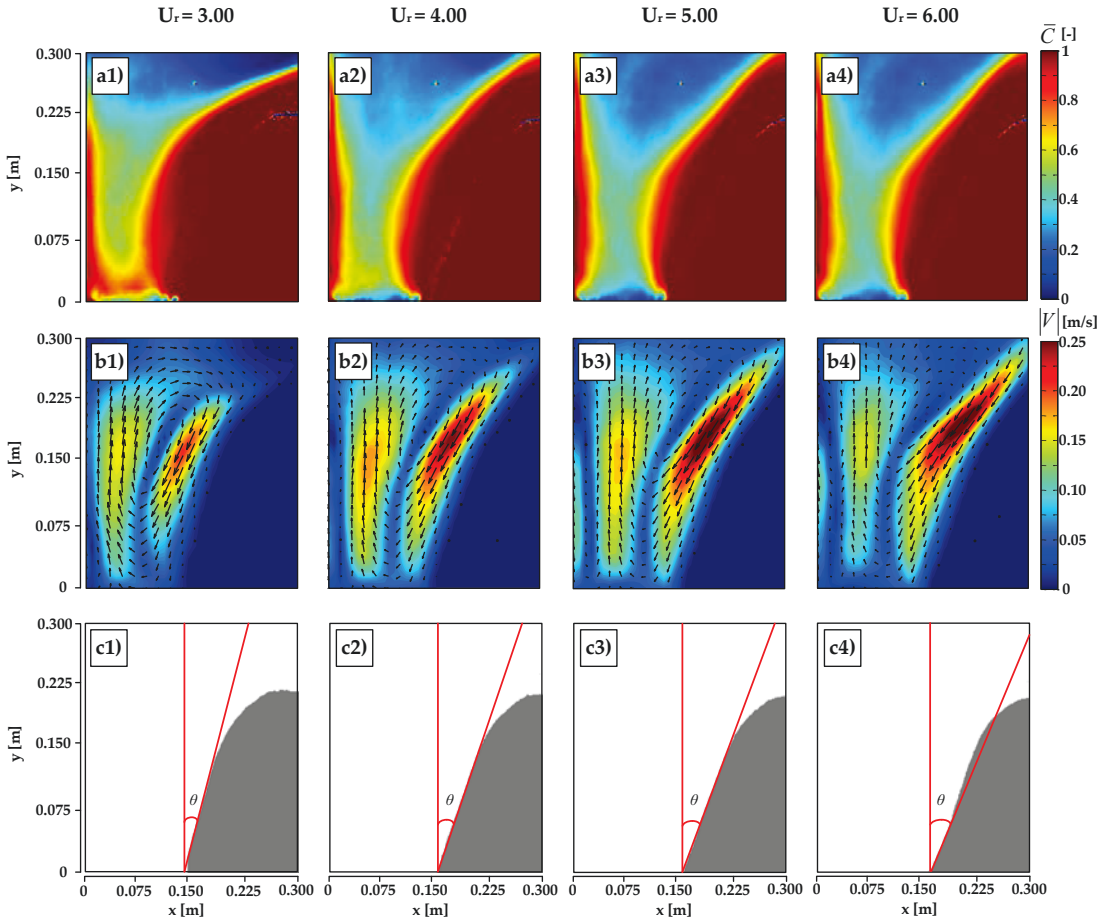

Figure 5.3: Dense phase concentration profiles (a), time-averaged dense phase velocity profiles (b) and defluidization area and penetration angle (c) for the different relative gas velocities tested. ($H_0/W = 0.75$) (Pseudo-2D bed)

The dense phase velocity profiles were also obtained by means of the multigrid PIV code MATPIV (Sveen, 1998-2008). Interrogation windows of 16 x 16 pixels with a 50% overlap were used in the PIV analysis. In Figure 5.3 b) the time-averaged dense phase velocity contours are presented together with the time-averaged dense phase velocity vectors. The time-averaged dense phase velocity was calculated averaging the instantaneous velocities obtained by PIV, as described in Laverman et al. (2008).

As can be seen, there is a vortex of solids in all cases, indicating the presence of a solids recirculation zone just above the defluidized zone. The defluidized zone can also be detected in the dense phase velocity profiles as a dark blue zone, where the time-averaged dense phase velocity is zero. Both the dense phase velocity in the recirculation zone and the size of this zone increases for higher relative gas velocities due to the more vigorous fluidization imposed by bigger bubbles (Soria-Verdugo et al., 2011). As long as the solids movement in a fluidized bed is induced by the bubbles, it seems that the size of the recirculation zone is strongly related to the bubble size. These zones were previously identified in tapered fluidized beds (Gernon et al., 2008, 2009; Gernon and Gilbertson, 2012).

A proper threshold was applied to the images to distinguish the defluidization zone. Taking into account that black painted particles are only present in the zone where the dense phase is moving, the defluidized zone is completely white (Figure 5.2). The results for the defluidized zone of the nominal case and for all the relative gas velocities tested are shown in Figure 5.3 c). As can be observed, the defluidized area decreases as long as the relative gas velocity increases because of the higher capability of greater bubbles to move dense phase. The height of the defluidization zone remains almost constant with the relative gas velocity, but the angle with the normal to the distributor increases with relative gas velocity. Additionally, the penetration angle, θ, has been plotted in Figure 5.3 c). This penetration angle is defined as the angle between the boundary of the defluidized zone and the normal to the distributor of the bed. The penetration angle is proportional to the relative gas velocity and, therefore, inversely proportional to the defluidized area.

The penetration angle measured in the pseudo-2D bed (Figure 5.3 c)) as a function of the relative gas velocity is shown in Figure 5.4 for all the bed aspect ratios tested. It was found that the variation of the penetration angle with the relative gas velocity is almost independent of the bed aspect ratio. Therefore, a correlation is proposed to estimate the penetration angle as a function of the relative gas velocity (Equation 5.3), considering that the penetration angle should be zero when the bed is operated at minimum fluidization conditions.

$$\theta = 5.5(U_r - 1) \tag{5.3}$$

The defluidized area was estimated from the time-averaged thresholded images shown in Figure 5.3 c). These values were multiplied by the bed thickness to obtain the defluidized volume and then normalized with the average volume occupied by dense phase (i.e. the average volume of the expanded bed). The normalized defluidized volume obtained is plotted in Figure 5.5 a) as a function of the relative gas velocity

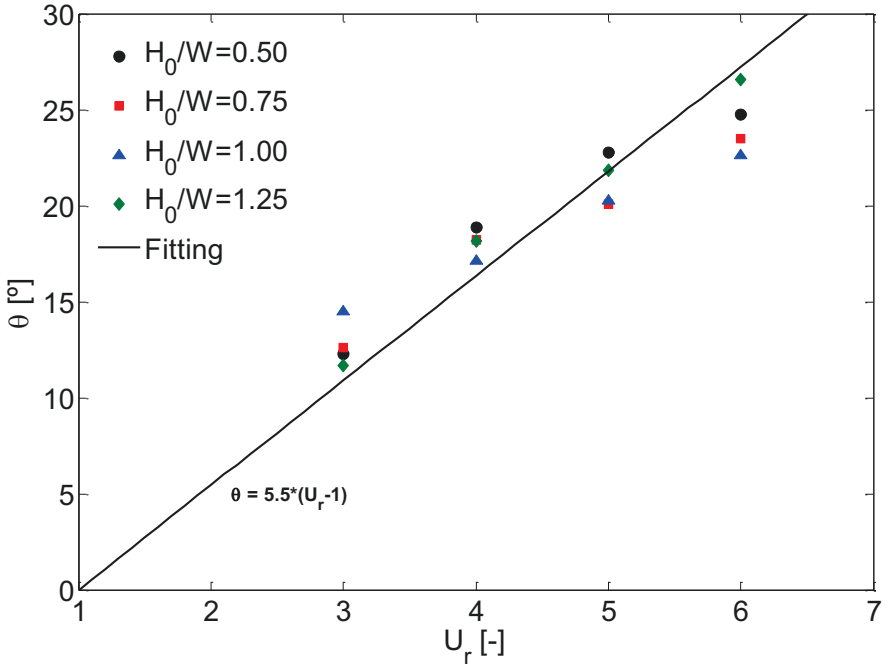

Figure 5.4: Penetration angle as a function of the different relative gas velocities tested. Solid lines correspond to the correlation proposed. (Pseudo-2D bed)

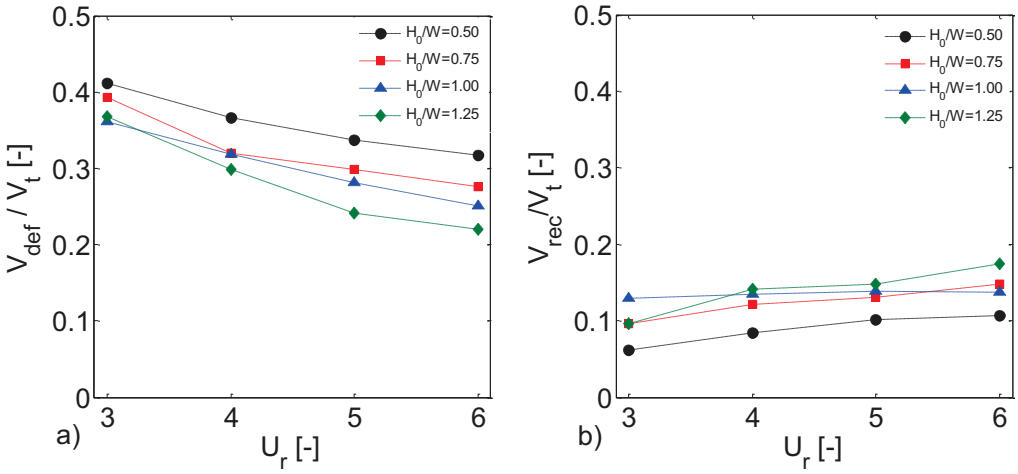

Figure 5.5: Normalized defluidized volume (a) and normalized recirculation volume (b) as a function of relative gas velocity for the different aspect ratios tested. (Pseudo-2D bed)

for the different aspect ratios investigated. As can be seen, the defluidized volume decreases with the relative gas velocity, following a similar trend for all the aspect ratios. For aspect ratios of 0.75, 1.00 and 1.25 the results of the defluidized volume are very similar, however, for an aspect ratio of 0.50 the results show a slight deviation which might be attributed to a different bubble coalescence pattern in this case, as stated by Pallarès and Johnsson (2006) who found that several bubble paths appeared

in shallow beds.

The recirculation area was defined as the high downwards velocity area located over the defluidized area (Figure 5.3 b)) and it was estimated from the time-averaged dense phase velocity contours. The results were also multiplied by the bed thickness to obtain the recirculation volume and normalized with the average expanded bed volume. The normalized recirculation volume as a function of the relative gas velocity for the aspect ratios investigated is shown in figure 5.5 b). The recirculation volume increases with the relative gas velocity, as a result of an increase in bubble size and, consequently, in solids motion. As for the defluidized volume, the results for aspect ratios of 0.75, 1.00 and 1.25 were very similar, whereas differences were observed for the case of aspect ratio of 0.50. These results suggest that both defluidized and recirculation volumes are independent of the bed aspect ratio provided that the bed aspect ratio is high enough to guarantee that a single bubble path is formed due to bubble coalescence.

In order to relate the bubble parameters with the aforementioned regions, the visible bubble flow, Q_b, was calculated in the 2D bed using Equation 5.4, as described in Sánchez-Delgado et al. (2013).

$$Q_b = \frac{1}{N} \sum_{j=1}^{N} \sum_{i=1}^{n} U_{bi} a_i \tag{5.4}$$

where a_i is the area of the i^{th} bubble cut by the horizontal section defined (i.e. at H_0), U_{bi} is the vertical bubble velocity, N is the number of images and n is the number of bubbles passing through the horizontal section at j^{th} image. The area of the i^{th} bubble cut by the horizontal section was estimated with the measured values of the bubble diameter D_b as the product of the generated arc between the bubble and the horizontal section and the bed thickness. The average bubble diameter, D_b, was obtained by means of DIA of the images recorded at the front wall of the bed and the average bubble velocity, U_b, was calculated using bubble tracking. The visible bubble flow in velocity units, U_{vis}, can be obtained dividing Q_b by the bed cross section, in this case the cross section of the active zone of the distributor plate (i.e. the half of the total cross-sectional area of the bed). The throughflow, U_{th}, was then estimated as a function of the visible bubble flow, the gas superficial velocity and the minimum fluidization velocity with Equation 5.5.

$$U_{th} = U_0 - U_{mf} - U_{vis} \tag{5.5}$$

The experimental values of U_{th} were normalized with the minimum fluidization velocity and plotted as a function of the relative gas velocity, U_r, in Figure 5.6. The

correlation proposed by Sánchez-Delgado et al. (2013) was also plotted in Figure 5.6 for comparison. The experimental results of the throughflow seem to be in agreement with the predicted values of the correlation. The differences found might be attributed to the fact that the correlation of Sánchez-Delgado et al. (2013) was developed for values of the visible bubble flow calculated at a height of $(2/3)H_0$. In view of the results showed in Figure 5.6, the variation of the throughflow with the bed aspect ratio can be neglected in pseudo-2D beds.

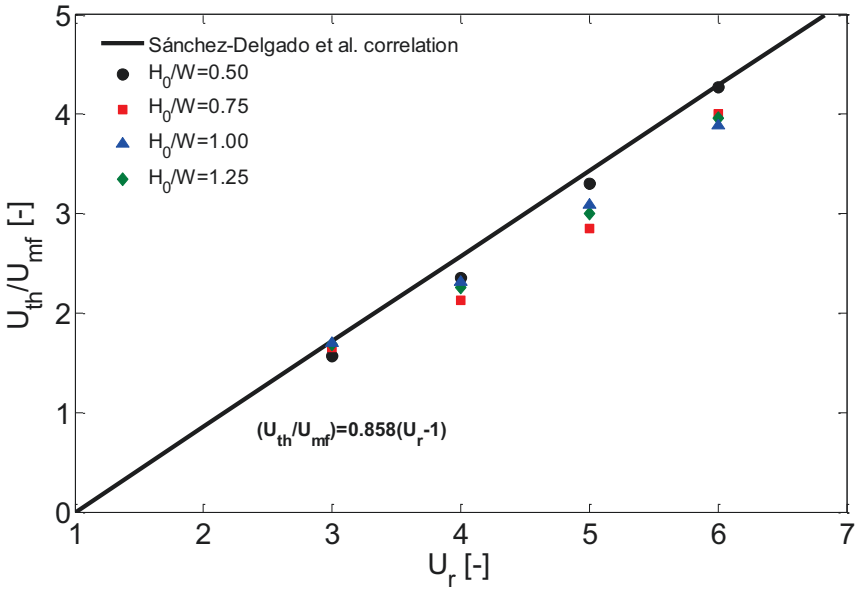

Figure 5.6: Normalized throughflow as a function of the relative gas velocity for all the aspect ratios tested.

As stated above, the defluidized region is related to the solids motion imposed by bubbles. According to that, in Figure 5.7 the experimental values of the normalized defluidized volume were related to the experimental values of the normalized visible bubble flow, U_{vis}/U_{mf}.

The normalized defluidized volume seems to follow a linear trend with the normalized visible bubble flow in the range of operation investigated. Taking into account that the relative gas velocities used in the 3D facility are similar to those used to develop the correlation, the linear fit is expected to give good predictions for the 3D facility. To extrapolate these results to a 3D bed, a relation between the normalized defluidized volume and the normalized visible bubble flow was obtained (Equation 5.6).

$$\left(\frac{V_{def}}{V_t}\right) = -0.11\left(\frac{U_{vis}}{U_{mf}}\right) + 0.41 \tag{5.6}$$

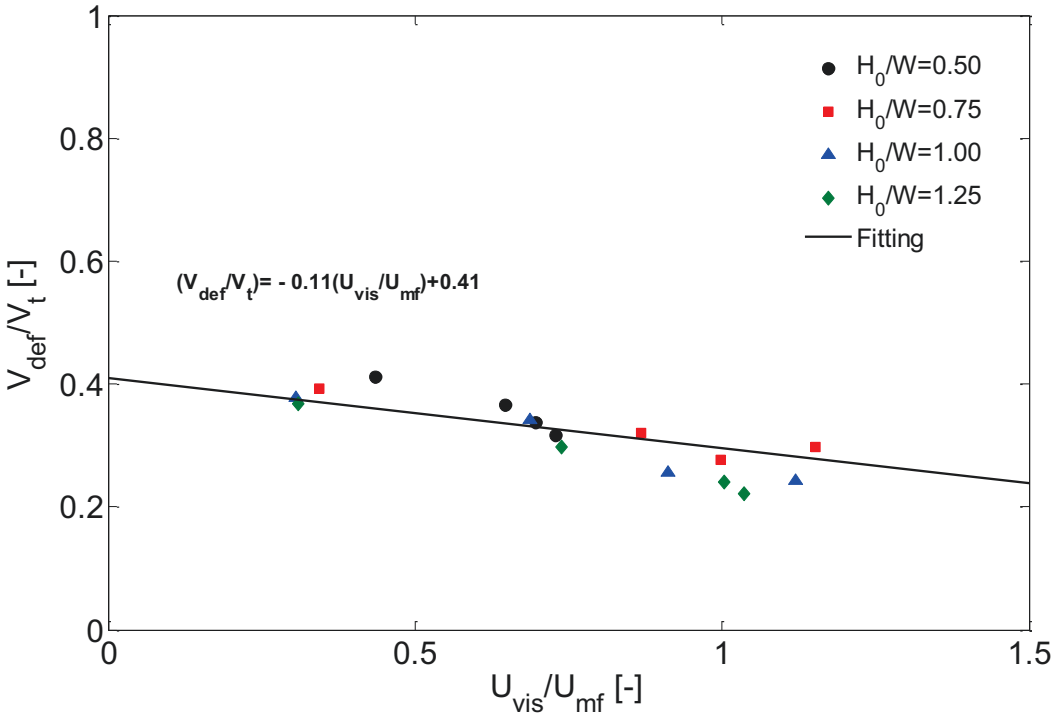

Figure 5.7: Normalized defluidized volume as a function of the normalized visible bubble flow for all the aspect ratios tested. (Pseudo-2D bed)

5.3.2 Extrapolation to 3D bed data.

The final aim is to develop a model capable of predicting the size of dead zones, caused by gas maldistribution or agglomeration, in large-scale fluidized beds using visual information of the bed surface. First, the validity of extrapolating the results of the defluidized volume obtained in the pseudo-2D bed to a lab-scale cylindrical bubbling fluidized bed (BFB) was evaluated. The extrapolation was made through a comparison of two variables: the penetration angle and the defluidized volume.

The experiments described in the experimental setup section for the 3D bed were carried out in this section. For each aspect ratio and relative gas velocity, the time-averaged black beads concentration was obtained in the bed surface by means of DIA, as shown in Figure 5.8 a).The penetration ratio, d, is defined as the distance between the bed wall and the boundary of black beads, x, divided by the bed diameter, D (Figure 5.8 b)). The penetration ratio was used to estimate the penetration angle, defined previously for the 2D bed. In the 2D bed the angle was obtained using the front images, however, in the 3D bed the penetration angle was obtained by means of the images of the bed surface, based on the penetration ratio (Figure 5.8 c)).

The penetration ratio is a function of the aspect ratio and the gas velocity, as

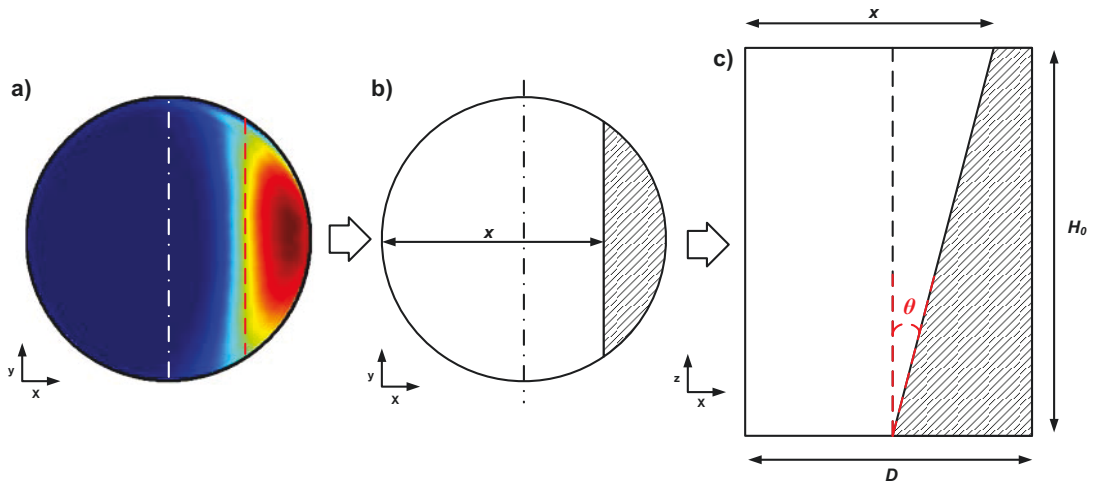

Figure 5.8: Time-averaged black beads concentration on the bed surface (top view) (a), definition of the penetration ratio (b) and definition of the penetration angle (c). (3D facility)

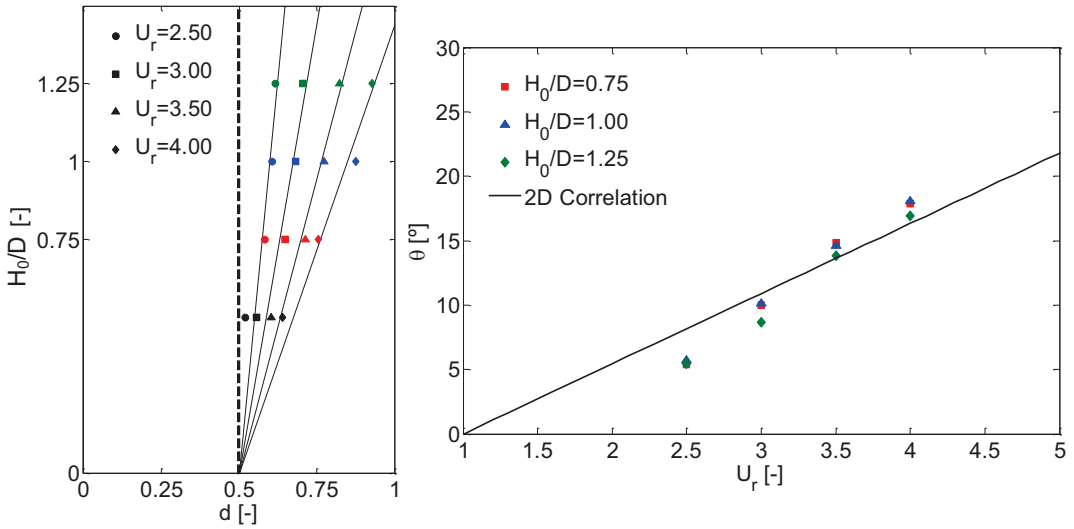

Figure 5.9: Penetration ratio (a) as a function of H_0/D for different values of U_r tested and penetration angle (b) as a function of U_r for the different values of H_0/D tested. (3D facility)

shown in Figure 5.9 a). For a constant gas velocity, the variation of the penetration ratio with the aspect ratio follows a linear trend, except for the case of $H_0/D = 0.5$. This is related to the fact that bubble coalescence is enhanced by increasing the bed aspect ratio (Darton et al., 1977; De Korte et al., 2001). As previously reported by Pallarès and Johnsson (2006), the increase of the bed aspect ratio reduces the number of preferred vertical bubble paths and, consequently, the number of vortexes in the flow structure. Taking this into account, it is expected that the case with the lowest aspect ratio ($H_0/D = 0.5$) has a different bubble flow pattern, and this could be the reason why the linear trends are not followed in Figure 5.9 a) provided that it is high enough to guarantee that a single preferred bubble path is generated. According to that, the

$H_0/D = 0.5$ data were neglected for the following calculations.

As for the results of the 2D facility, the penetration angle, θ, was found to be almost independent of the bed aspect ratio (Figure 5.9 b)). According to that, the estimations of the correlation developed for the 2D data (Equation 5.3) were compared with the experimental data of the penetration angle measured in the 3D facility. The estimations of the correlation correctly predict the trend and order of magnitude of the experimental values of penetration ratio measured in the 3D facility, as can be observed in Figure 5.9 b) and, as a result, the correlation can be used for extrapolation purposes. The proposed correlation for the penetration angle give similar results for 2D and 3D facilities, even though the experiments were performed with different bed material and the angle was estimated using different approaches.

The correlation proposed can be used then to estimate the size of the defluidized zone generated by the half-covered distributor plate and to determine whether defluidization can be detected by visual inspection at the bed surface or not. For example, for a relative gas velocity of $U_r = 6.00$ the penetration angle calculated with Equation 5.3 is $\theta = 27°$, which is high enough to obtain a penetration ratio of 1 with an aspect ratio of 1.25. This means that when a video of the bed surface is recorded with the aforementioned conditions, a uniform bubble concentration pattern is obtained at the bed surface; however a defluidized zone, whose size can be estimated using the calculated penetration angle, is present at the bottom zone of the fluidized bed. The penetration angle can be employed to determine the defluidized zone generated for any portion of covered distributor orifices produced during operation.

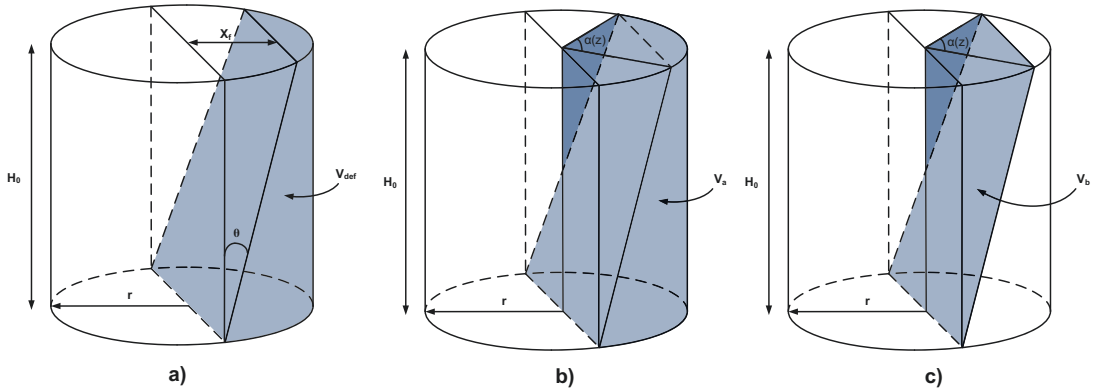

Figure 5.10: Methodology to estimate the defluidized volume of 3D cylindrical fluidized bed.

The defluidized volume in the 3D facility can be estimated by means of the experimental values of the penetration ratio, as the resulting volume of cutting the bed with a plane with an angle equal to the corresponding penetration angle. Figure 5.10 shows a schematic of the calculation of the defluidized volume. To integrate the defluidized

volume, V_{def}, (blue zone in Figure 5.10 a)) the variable x_f was defined as a function of the penetration ratio (Equation 5.7).

$$x_f = (d - 0.5)D \tag{5.7}$$

Considering the definition of x_f, the methodology to obtain the analytical expression of the defluidized volume for a 3D cylindrical fluidized bed is described. The volume V_a (Figure 5.10 b)) can be expressed as follows:

$$V_a = \int_0^{H_0} \frac{\alpha\,(z)}{2} r^2 dz \tag{5.8}$$

$$V_a = \int_{\alpha_i}^{\alpha_f} \frac{\alpha}{2} r^2 \left[-\frac{rH_0}{2rcos\,(\alpha_f/2)} sin\,(\alpha_f/2) \right] d\alpha \tag{5.9}$$

The integration limits for V_a are:

$$\alpha_f = 2cos^{-1}\,(x_f/r) \tag{5.10}$$

$$\alpha_i = \pi \tag{5.11}$$

Equation 5.9 can be rearranged to obtain an expression that can be integrated to obtain an analytical expression of the volume V_a:

$$V_a = -\frac{r^2 H_0}{2cos\,(\alpha_f/2)} \int_{\alpha_i}^{\alpha_f} \frac{\alpha}{2} sin\,(\alpha_f/2)\, d\alpha \tag{5.12}$$

$$V_a = -\frac{r^2 H_0}{2cos\,(\alpha_f/2)} \left[-\,(\alpha_f/2)\, cos\,(\alpha_f/2) + sin\,(\alpha_f/2) - 1 \right] \tag{5.13}$$

$$V_a = \frac{r^2 H_0}{(x_f/r)} \left[(x_f/r)\, cos^{-1}\,(x_f/r) - sin\left(cos^{-1}\,(x_f/r)\right) + 1 \right] \tag{5.14}$$

Following a similar methodology, the volume V_b (Figure 5.10 c)) can be expressed as follows:

$$V_b = \int_0^{H_0} \frac{r^2}{2} sin\,(\alpha\,(z))\, dz \tag{5.15}$$

$$V_b = \int_{\alpha_i}^{\alpha_f} -\frac{r^2}{2} sin\,(\alpha)\, sin\,(\alpha/2)\, \frac{rH_0}{2rcos\,(\alpha_f/2)} sin\,(\alpha/2)\, d\alpha \tag{5.16}$$

The integration limits are the same as for the integration of V_a (Equations 5.10 and 5.11). Thus, the analytical expression of the volume V_b can be obtained with the

following procedure:

$$V_b = -\frac{r^2 H_0}{4cos\left(\alpha_f/2\right)} \int_{\alpha_i}^{\alpha_f} sin\left(\alpha\right) sin^2\left(\alpha/2\right) d\alpha \tag{5.17}$$

$$V_b = \frac{r^2 H_0}{3cos\left(\alpha_f/2\right)} \left[1 - sin^3\left(\alpha_f/2\right)\right] \tag{5.18}$$

$$V_b = \frac{r^2 H_0}{3\left(x_f/r\right)} \left[1 - sin^3\left(cos^{-1}\left(x_f/r\right)\right)\right] \tag{5.19}$$

Finally, the analytical expression of the defluidized volume in a cylindrical fluidized bed (Equation 5.20) is obtained subtracting V_b (Equation 5.19) to V_a (Equation 5.14).

$$V_{def} = \frac{r^2 H_0}{\left(x_f/r\right)} \left[\left(x_f/r\right) cos^{-1}\left(x_f/r\right) - sin\left(cos^{-1}\left(x_f/r\right)\right) + sin^3\left(cos^{-1}\left(x_f/r\right)\right)/3 + 2/3\right] \tag{5.20}$$

To evaluate the extrapolation of the 2D results to 3D beds, the experimental values of defluidized volume were compared with the estimated values obtained with correlations. The correlation of Johnssoon et al. (1991) was used to estimate the visible bubble flow in a 3D bed. First, the value of f_2 is calculated with Equation 5.21 as a function of the gas velocity, and then the fraction of visible bubble flow, ψ, was estimated with Equation 5.22.

$$f_2 = \left[0.26 + 0.70exp\left(-3.3d_p\right)\right] \left[0.15 + \left(U_0 - U_{mf}\right)\right]^{-0.33} \tag{5.21}$$

$$\psi = f_2 \left(h + \sqrt{A_t/N_h}\right)^{0.4} \tag{5.22}$$

where A_t is the cross sectional area of the distributor plate, in this case half of the total distributor area, and N_h is the number of distributor orifices in that section. The height over the distributor plate at which the visible bubble flow is evaluated, h, was selected to be equal to the fixed bed height, H_0. The visible bubble flow, U_{vis}, was calculated with Equation 5.23.

$$U_{vis} = \psi \left(U_0 - U_{mf}\right) \tag{5.23}$$

The normalized visible bubble flow was related to the normalized defluidized volume in the previous section of this work (Figure 5.7). According to that, the defluidized volume in the 3D bed was estimated with Equation 5.6 using the values of visible bubble flow obtained from the correlation of Johnssoon et al. (1991). The experimental values

of normalized defluidized volume in the 3D bed, calculated with Equation 5.20, were compared with the predicted values of the correlation proposed in this work (Equation 5.6) using the Johnssoon et al. (1991) correlation for the visible bubble flow. For a better comparison, the experimental and predicted results of the normalized defluidized volume were plotted together in Figure 5.11.

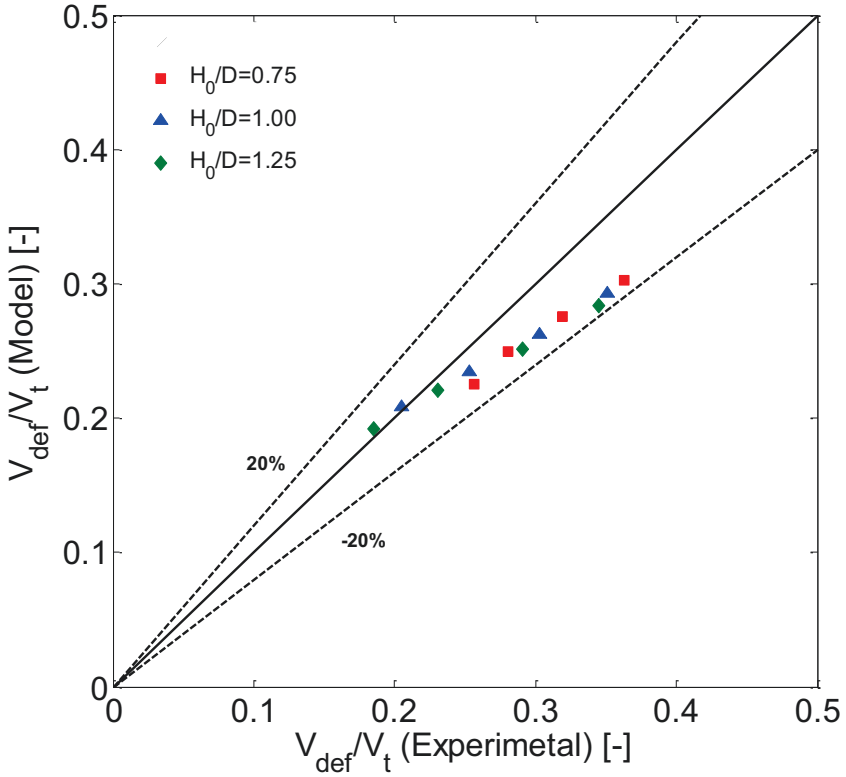

Figure 5.11: Comparison between experimental and predicted values of the normalized defluidized volume in the 3D bed.

It was found that the defluidized volume in a 3D bed can be estimated with the correlations developed for 2D beds with maximum relative errors of 20%. The maximum errors were found at low relative gas velocities whereas the model seems to predict accurately the defluidized volume for higher bed aspect ratios and higher relative gas velocities. The model developed in this work can be used then to estimate the size of dead zones in large-scale fluidized beds, assuming that the defluidized zone measured in the 3D facility can be seen as a dead zone produced by maldistribution and/or agglomeration. Visual inspection of the bed surface is needed to successfully apply the model; however, as stated above, the use of IR cameras is a common practice in industry. The concentration of CO, CO_2 and H_2O is usually measured in industry. Since reactions occur in the bubble phase, a sudden increase on the concentration of gases could be related to a maldistribution problem inside the bed.

5.4 Conclusions

The gas maldistribution in pseudo-2D beds and 3D beds was studied. The maldistribution was induced covering half of the total orifices of the distributor plate. In the pseudo-2D bed, it was found that a defluidized zone appears above the covered part of the distributor plate and a solids recirculation zone appears just above the defluidized zone. The size of the defluidized zone was obtained by means of DIA and the size of the recirculation zone was obtained by means of PIV. The experimental values of defluidized and recirculation volume were normalized with the average volume of the expanded bed. Both zones were found to be affected by the relative gas velocity and the bed aspect ratio.

The normalized defluidized volume was found to decrease with the relative gas velocity and the bed aspect ratio, while the normalized defluidized volume was found to increase with the relative gas velocity and the bed aspect ratio. The variations in the size of both zones are strongly related to the bubble phase. According to that, the visible bubble flow was obtained experimentally and a correlation was proposed to relate the normalized visible bubble flow with the normalized defluidized volume in the pseudo-2D bed.

The penetration angle, defined as the angle between the boundary of the defluidized zone and the normal to the distributor of the bed, was determined experimentally in the pseudo-2D bed. It was found that the penetration angle increases with the relative gas velocity following a fairly linear trend, but seems to be independent of the bed aspect ratio. A correlation was proposed for the estimation of the penetration angle as a function of the relative gas velocity for extrapolation purposes from the pseudo-2D bed to the 3D facility.

The extrapolation of the 2D data to a 3D bed was then investigated. Two different variables were studied: the penetration angle and the normalized defluidized volume. The experimental values of the penetration angle obtained in the 3D facility were compared to the estimations of the proposed correlation for the penetration angle in the pseudo-2D bed. The correlation gives similar results for both facilities, even though the experiments were carried out with different bed materials and the penetration angle was estimated with different methods.

The correlation of Johnssoon et al. (1991) was used to calculate the normalized visible bubble flow in the 3D facility. These estimations were then used to calculate the normalized defluidized volume in a 3D bed with the proposed correlation obtained with the 2D data. The experimental values of the normalized defluidized volume in the 3D bed, calculated by integration with the experimental values of the penetration

ratio and penetration angle, were compared with the estimations using correlations. It was found that the proposed methodology is capable of predicting the defluidized volume in a 3D bed with maximum relative errors of around 20%. The maximum errors were found at low relative gas velocities and the model seems to predict accurately the defluidized volume for higher aspect ratios and higher relative gas velocities.

It can be concluded that the model proposed can be used to estimate the size of dead zones in large-scale combustors and gasifiers, since IR cameras are usually employed in this type of industrial facility to record images during operation. A further application of the model is the relation between the estimated values of visible bubble flow and the concentration of certain gas emissions. Since reactions occur in the bubble phase, a sudden increase on the concentration of gases could be related to a maldistribution problem inside the bed.

5.5 Notation

A_t	Distributor cross-sectional area [m^2]
a_i	Area of the ith bubble cut by the horizontal section defined [m^2]
$\widehat{B}$	Bubble concentration [-]
$\widehat{C}$	Black beads concentration [-]
d	Penetration ratio [-]
D	Bed diameter [m]
D_b	Bubble diameter [m]
d_p	Mean particle diameter [μm]
f_2	Parameter of the Johnssons et al. correlation [-]
h	Height over the distributor plate [m]
H	Height of the 2D bed [m]
H_0	Fixed bed height [m]
H_0/D	Aspect ratio 3D [-]
H_0/W	Aspect ratio 2D [-]
N	Number of images in each video [-]
N_h	Number of orifices of the distributor plate [-]
Q_b	Visible bubble flow [m^3/s]
r	Bed radius [m]
R	Pressure drop ratio [-]
U_0	Air superficial velocity [m/s]
U_b	Rising bubble velocity [m/s]
U_M	Superficial gas velocity at which all the distributor orifices became

	operative [m/s]
U_{mf}	Minimum fluidization velocity [m/s]
U_r	Relative fluidization velocity [-]
U_{vis}	Visible bubble flow [m/s]
$\|V\|$	Time-averaged dense phase velocity [m/s]
V_{def}	Volume of the defluidized zone [m^3]
V_{rec}	Volume of the recirculation zone [m^3]
V_t	Total solids volume [m^3]
W	Width of the 2D bed [m]
x	Distance between the bed wall and the boundary of black beads [m]
x_f	Distance between the centre of the bed and the boundary of defluidized zone [m]
Z	Thickness of the 2D bed [m]

Greek letters

ψ	Fraction of visible bubble flow [-]
ρ_{bb}	Black beads density [kg/m^3]
ρ_s	Particle density [kg/m^3]
θ	Penetration angle [°]

Abbreviattions

BFB	Bubbling fluidized bed.
DIA	Digital image analysis.
FB	Fluidized bed.
FSS	Full-scale span.
IR	Infrared.
PIV	Particle image velocimetry.

Bibliography

Ballester, J., García-Armingol, T., 2010. Diagnostic techniques for the monitoring and control of practical flames. *Progress in Energy and Combustion Science* 36, 375-411.

Chimenti, M., Di Natali, C., Mariotti, G., Paganini, E., Pieri, G., Salvetti, O., 2004. An IR image processing approach for characterizing combustion instability. *Infrared Physics and Technology* 46, 41-47.

Darton, R.C., LaNauze, R.D., Davidson, J.F., Harrison, D., 1977. Bubble growth due to coalescence in fluidized beds. *Transactions of the Institution of Chemical Engineers* 55, 274-288.

De Korte, R.J., Schouten, J.C., Van den Bleek, C.M., 2001. Controlling bubble coalescence in a fluidized-bed model using bubble injection. *AIChE J.* 47, 851-860.

Fakhimi, S., Harrison, D., 1970. Multi-orifice distributors in fluidized beds: a guide to design. In *Chemeca 70*; Butterworth: Australia, 29.

Geldart, D., 1973. Types of gas fluidization, *Powder Technol.* 7, 285-292.

Gernon, T.M., Gilbertson, M.A., Sparks, R.S.J., Field, M., 2008. Gas-fluidisation in an experimental tapered bed: Insights into processes in diverging volcanic conduits. *Journal of Volcanology and Geothermal Research* 174, 49-56.

Gernon, T.M., Gilbertson, M.A., Sparks, R.S.J., Field, M., 2009. The role of gas-fluidisation in the formation of massive volcaniclastic kimberlite. *Lithos* 112S, 439-451.

Gernon, T.M., Gilbertson, M.A., 2012. Segregation of particles in a tapered fluidized bed. *Powder Technol.* 231, 88-101.

González-Cencerrado, A., Pea, B., Gil, A., 2012. Coal flame characterization by means of digital image processing in a semi-industrial scale PF swirl burner. *Applied Energy* 94, 375-384.

Hernández-Jiménez, F., Sánchez-Delgado, S., Gómez-García, A., Acosta-Iborra, A., 2011. Comparison between two-fluid model simulations and particle image analysis and velocimetry (PIV) results for a two-dimensional gas-solid fluidized bed. *Chem. Eng. Sci.* 66, 3753-3772.

Johnsson, F., Andersson, S., Leckner, B., 1991. Expansion of a freely bubbling fluidized bed. *Powder Technol.* 68, 117-123.

Karri, S.B.R., Werther, J., 2003. Gas distributor and plenum design in fluidized beds. In: Yang, W.C. *Handbook of fluidization and fluid-particle systems.* Marcel Dekker Inc., New York, 164-179.

Laverman, J.A., Roghair, I., van Sint Annaland, M., Kuipers, J.A.M., Investigation into the hydrodynamics of gas-solid fluidized beds using particle image velocimetry coupled with digital image analysis. *Can. J. Chem. Eng.* 86, 523-535.

Lu, G., Gilabert, G., Yan, Y., 2005. Vision based monitoring and characterization of combustion flames. *Journal of Physics: Conference Series* 15, 194-200.

Pallarès, D., Johnsson, F., 2006. A novel technique for particle tracking in cold 2-dimensional fluidized beds simulating fuel dispersion. *Chem. Eng. Sci.* 61, 2710-2720.

Sánchez-Delgado, S., Marugán-Cruz, C., Soria-Verdugo, A., Santana, D., 2013. Estimation and experimental validation of the circulation time in a 2D gas-solid fluidized bed. *Powder Technol.* 235, 669-676.

Sánchez-Prieto, J., Soria-Verdugo, A., Briongos, J.V., Santana, D., 2014. The effect of temperature on the distributor design in bubbling fluidized beds. *Powder Technol.* 261, 176-184.

Sánchez-Prieto, J., Soria-Verdugo, A., Gómez-Hernandéz, J., Briongos, J.V., Santana, D., 2015. Maldistribution detection in bubbling fluidized beds. *Chem. Eng. J.* 270, 272-281.

Sathiyamoorthy, D., Sridhar Rao, C.H., 1981. The choice of distributor to bed pressure drop ratio in gas fluidised beds. *Powder Technol.* 30, 139-143.

Soria-Verdugo, A., García-Gutiérrez, L.M., Ruiz-Rivas, U., Santana, D., 2011. Buoyancy effects on objects moving in a bubbling fluidized bed. *Chem. Eng. Sci.* 66, 2833-2841.

Sveen, J.K., 1998-2008. MATPIV. http://www.math.uio.no/jks/matpiv/.

Thorpe, R.B., Davidson, J.F., Pollitt, M., Smith, J., 2002. Maldistribution in fluidized beds. *Ind. Eng. Chem. Res.* 41, 5878-5889.

van Ommen, J.R., de Korte, R.J., van den Bleek, C.M., 2004. Rapid detection of defluidization using the standard deviation of pressure fluctuations. *Chem. Eng. Process.* 43, 1329-1335.

Whitehead, A.B., 1971. In Davidson, J.F., Harrison, D. (Eds.) *Fluidization.* Academic Press, London. 781.

Whitehead, A.B., Dent, D.C., 1967. Behaviour of multiple tuyere assemblies in large fluidized beds. In *Proceedings of the International Symposium on Fluidisation*, Enindhoven, June 6-9; Drinkenburg, A.A.H., Ed.; Netherlands University Press: Amsterdam, 802.

Yue, P.L., Kolaczkowski, J.A., 1982. Multiorifice distributor design for fluidized beds. *Trans. Inst. Chem. Eng.* 60.

Zipser, S., Gommlich, A., Matthes, J., Keller, H.B., 2006. Combustion plant monitoring and control using infrared and video cameras. *Power Plants and Power Systems Control*, Kananaskis, Canada.

Chapter 6

Conclusions

The main conclusions presented in Chapters 3, 4 and 5 are summarized in the following lines.

The design and performance of the gas distribution system is directly related to maldistribution problem in fluidized beds. Several authors have studied this issue and most of these works are focused on the distributor to bed pressure drop ratio, R. A value of R of 0.3 has been used in many works as a rule of thumb. However, as long as R is dependent on the distributor pressure drop, considering the orifice equation is also dependent of the bed temperature by means of the gas density. According to that, the effect of temperature on the distributor pressure drop was investigated using two different distributor types: multiorifice and tuyere type.

It was found that the distributor pressure drop decreases with temperature, suggesting that maldistribution problems can appear if the distributor plate has not been designed taking into account the operation temperature. A new model to design distributor plates is then proposed.

First, the temperature, the bed aspect ratio and the superficial gas velocity have to be selected. The orifice discharge coefficient can be estimated using the Qureshi and Creasy correlation if both distributor plate thickness and orifice diameter are known. Then the variation of the minimum fluidization voidage has to be taken into account in order to obtain the minimum fluidization velocity with the Carman-Kozeny equation. It was found that the variation of minimum fluidization voidage can be neglected for type B particles. Finally, using the orifice equation the number of orifices required for the distributor can be obtained. It was found that a lower distributor open area is needed if the bed is operating at high temperature.

The standard deviation of the pressure fluctuations signals inside the bed was also studied. The temperature was increased meanwhile both the bed aspect ratio and the superficial gas velocity were kept constant. Changes in the standard deviation were

observed, suggesting that the bed temperature affects the bed hydrodynamics by means of a decrease in R.

To study the maldistribution phenomena, a severe maldistribution problem was induced in a 3D fluidized bed by means of a half-covered distributor plate. It was observed that a defluidized zone appeared over the covered part of the distributor and can be detected in the bed surface. The size of this zone was found to be dependent of the gas superficial velocity and the bed aspect ratio. If the bed aspect ratio or the gas superficial velocity is high enough the maldistribution problem cannot be detected at the bed surface.

Pressure fluctuations signals were measured to evaluate the limits of maldistribution detection in fluidized beds. To do that, several cases of maldistribution generated by different orifice distribution in the distributor plate were analyzed. It was found that the standard deviation of the pressure signal is lower than the one measured in the plenum chamber if the signal is measured in the defluidized zone, while it is higher if it is measured in the fluidized zone. It was concluded that both signals measured at the same height are correlated and the signal of the defluidized zone seems to be an attenuated version of the fluidized one.

Three monitoring method used for defluidization detection found in the literature were applied for maldistribution detection. The analysis based on the Student's t-distribution approach of the wide band energy showed a strong dependence on the measurement location and a low sensitivity to the hydrodynamic changes caused by the gas maldistribution. The S statistic method was found to be useful only if the pressure signal is measured in the upper zone of the fluidized bed. Finally, the SPC method based on the standard deviation presented a high capability of detecting moderate cases of maldistribution. The boundary between maldistribution and stable operation correspond to 40% of open orifices for the experimental conditions covered.

It is concluded that a probe placement at 50-75% of the total bed height is recommended for maldistribution detection purposes. It is also concluded that a single pressure probe could be sufficient to detect the hydrodynamic changes caused by maldistribution in lab-scale fluidized bed. However, in the case of industrial fluidized beds, a higher number of pressure probes should be placed, in order to cover the whole bed cross-section.

The rotation of the distributor plate was analyzed as a counteracting mechanism to overcome maldistribution. It was found that severe maldistribution problems can be prevented or eliminated by forcing the distributor to rotate.

Finally, the internal structure of an induced maldistributed pseudo-2D bed was studied in order to develop a model to estimate the size of the stagnant regions gener-

ated by maldistribution problems. It was found that a defluidized zone appears above the covered part of the distributor plate and a solids recirculation zone appears just above the defluidized zone. Both zones were found to be affected by the realtive gas velocity and the bed aspect ratio. The normalized defluidized volume decreases with relative gas velocity and bed aspect ratio while the normalized recirculation volume increases with relative gas velocity and bed aspect ratio. These changes are related to the bubble phase and, according to that, a correlation was proposed to relate the normalized visible bubble flow with the normalized defluidized volume.

The penetration angle was found to increase with the relative gas velocity following a fairly linear trend and seems to be independent of the bed aspect ratio. Therefore, a correlation for estimating the penetration angle as a function of the relative gas velocity was proposed. The estimations of the correlation were compared with the experimental results of the penetration angle obatained in the 3D facility. It was found that the correaltion gives similar results for both 2D and 3D facilities.

The correlation of Johnssoon et al. (1991) was used to calculate the normalized visible bubble flow in the 3D facility and, coupled with the correlation proposed for the defluidized volume in the 2D bed, the normalized defluidized volume was obtained for the 3D facility. The experimental values of defluidized volume in the 3D facility obtained by integration were compared with the estimations using correlations. It was found that the proposed methodology is capable of predicting the defluidized volume in a 3D bed with maximum relative errors of 20%.

It was concluded that the model proposed can be used to estimate the size of stagnant zones in large-scale fluidized be reactors, since IR cameras are usually employed in industry to record images during operation.

Bibliography

Almendros-Ibáñez, J.A., Sobrino, C., de Vega, M., Santana, D., 2006. A new model for ejected particle velocity from erupting bubbles in 2-D fluidized beds. *Chem. Eng. Sci.* 61, 5981-5990.

Almendros-Ibáñez, J.A., Pallarès, D., Johnsson, F., Santana, D., 2010. Voidage distribution around bubbles in a fluidized bed: influence of throughflow. *Powder Technol.* 197, 73-82.

Avery, D.A., Tracey, D.H., 1968. The application of fluidised beds of activated carbon. In: *Proceedings of the I Chem E Symposium*, Montreal, Canada; I Chem E: London. 28.

Ballester, J., García-Armingol, T., 2010. Diagnostic techniques for the monitoring and control of practical flames. *Progress in Energy and Combustion Science* 36, 375-411.

Bena, J., Havlada, I., 1991. The influence of particle Reynolds on voidage at fluidization. *Powder Technol.* 66, 97-99.

Botterill, J.S.M., Teoman, Y., Yuregir, K.R., 1982. The effect of temperature on fluidized bed behaviour. *Chem. Eng. Commun.* 15, 227-238.

Briens, C.L., Tyagi, A.K., Bergougnou, M.A., 1988. Pressure drop through multiorifice gas distributors in fluidized bed columns. *Can. J. Chem. Eng.* 66, 740-748.

Briens, C.L., Briens, L.A., Barthel, E., Le Blvec, J.M., Tedoldi, A., Margaritis, A., 1999. Detection of local fluidization characteristics using the V statistic. *Powder Technol.* 102, 95-103.

Briens, L.A., Briens, C.L., 2002. Cycle detection and characterization in chemical engineering. *AIChE J.* 48, 970980.

Brown, R.C., Brue, E., 2001. Resolving dynamical features of fluidized beds from pressure fluctuations. *Powder Technol.* 119, 6880.

Busciglio, A., Vella, G., Micale, G., Rizzuti, L., 2008. Analysis of the bubbling behaviour of 2D gas solid fluidized beds: Part I. Digital image analysis technique. *Chem. Eng. J.* 140, 398-413.

Campoy, M., Gómez-Barea, A., Vidal, F.B., Ollero, P., 2009. Air-steam gasification of biomass in a fluidized bed: process optimization by enriched air. *Fuel Process. Technol.* 90, 677-685.

Carman, P.C., 1937. Fluid flow through granular beds, *Transactions, Institution of Chemical Engineers* 15, 150-166.

Chandrasekera, T.C., Wang, A., Holland, D.J., Marashdeh, Q., Pore, M., Wang, F., Sederman, A.J., Fan, L.S., Gladden, L.F., Dennis, J.S., 2012. A comparison of magnetic resonance imaging and electrical capacitance tomography: an air jet through a bed of particles. *Powder Technol.* 227, 86-95.

Chimenti, M., Di Natali, C., Mariotti, G., Paganini, E., Pieri, G., Salvetti, O., 2004. An IR image processing approach for characterizing combustion instability. *Infrared Physics and Technology* 46, 41-47.

Darton, R.C., LaNauze, R.D., Davidson, J.F., Harrison, D., 1977. Bubble growth due to coalescence in fluidized beds. *Transactions of the Institution of Chemical Engineers* 55, 274-288.

de Andrés, J.N., Narros, A., Rodríguez, M.E., 2011. Behaviour of dolomite, olivine and alumina as primary catalysts in air-steam gasification of sewage sludge. *Fuel.* 90, 521-527.

De Korte, R.J., Schouten, J.C., Van den Bleek, C.M., 2001. Controlling bubble coalescence in a fluidized-bed model using bubble injection. *AIChE J.* 47, 851-860.

de Martín, L., Villa Briongos, J., Aragón, J.M., Palancar, M.C., 2010. Can low frequency accelerometry replace pressure measurements for monitoring gassolid fluidized beds?. *Chem. Eng. Sci.* 65, 40554064

Diks, C., van Zwet, W.R., Takens, F., DeGoede, J., 1996. Detecting differences between delay vector distributions. *Phys. Rev. E* 53, 2169-2176.

Ergun, S., 1952. Fluid floe through packed column. *Chem. Eng. Prog.* 48, 89-94.

Fakhimi, S., Harrison, D., 1970. Multi-orifice distributors in fluidized beds: a guide to design. In *Chemeca 70*; Butterworth: Australia, 29.

Flamant, G., Fatah, N., Steinmetz, D., Murachman, B., Luguerie, C., 1991. High-temperature velocity and porosity at minimum fluidization. Critical analysis of experimental results. *Int. Chem. Eng.* 31, 673-684.

Formisani, B., Girimonte, R., Mancuso, L., 1998. Analysis of the fluidization process of particle beds at high temperature. *Chem. Eng. Sci.* 53, 951-961.

Fotovat, F., Chaouki, J., Bergthorson, J., 2013. The effect of biomass particles on the gas distributor and dilute phase characteristics of sand-biomass mixtures fluidized in the bubbling regime. *Chem. Eng. Sci.* 102, 129-138.

Geldart, D.,1973. Types of gas fluidization. *Powder Technol.* 7, 285-292.

Geldart, D., Baeyens, J., 1985. The design of distributors for gas-fluidized beds. *Powder Technol.* 42, 67-78.

Gernon, T.M., Gilbertson, M.A., Sparks, R.S.J., Field, M., 2008. Gas-fluidisation in an experimental tapered bed: Insights into processes in diverging volcanic conduits. *Journal of Volcanology and Geothermal Research* 174, 49-56.

Gernon, T.M., Gilbertson, M.A., Sparks, R.S.J., Field, M., 2009. The role of gas-fluidisation in the formation of massive volcaniclastic kimberlite. *Lithos* 112S, 439-451.

Gernon, T.M., Gilbertson, M.A., 2012. Segregation of particles in a tapered fluidized bed. *Powder Technol.* 231, 88-101.

Gómez-Hernández, J., Soria-Verdugo, A., Briongos, J.V., Santana, D., 2012. Fluidized bed with a rotating distributor operated under defluidization conditions. *Chem. Eng. J.* 195-196, 198-207.

Gómez-Hernández, J., Sánchez-Prieto, J., Briongos, J.V., Santana, D., 2014. Wide band energy analysis of fluidized bed pressure fluctuation signals using a frequency division method. *Chem. Eng. Sci.* 105, 92-103.

Gómez-Hernández, J., 2015. Paste drying control in a rotating-distributor fludized bed, PhD thesis. Universidad Carlos III de Madrid, Spain.

González-Cencerrado, A., Pea, B., Gil, A., 2012. Coal flame characterization by means of digital image processing in a semi-industrial scale PF swirl burner. *Applied Energy* 94, 375-384.

Hernández-Jiménez, F., Sánchez-Delgado, S., Gómez-García, A., Acosta-Iborra, A., 2011. Comparison between two-fluid model simulations and particle image analysis & velocimetry (PIV) results for a two-dimensional gas-solid fluidized bed. *Chem. Eng. Sci.* 66, 3753-3772.

Hiby, J.W., 1964. Critical minimum pressure drop of gas distributor plate in fluidized bed units. *Chem. Ing. Techn.* 36, 328.

Idelchik, I.E., 1994. *Handbook of hydraulic resistance*. CRC press.

Johnsson, F., Andersson, S., Leckner, B., 1991. Expansion of a freely bubbling fluidized bed. *Powder Technol.* 68, 117-123.

Johnsson, F., Zijerveld, R.C., Schouten, J.C., van den Bleek, C.M., Leckner, B., 2000. Characterization of fluidization regimes by time-series analysis of pressure fluctuations. *Int. J. Multiphase Flow* 26, 663-715.

Kage, H., Iwasaki, N., Yamaguchi, H., Matsuno, Y., 1991. Frequency analysis of pressure fluctuation in fluidized bed plenum. *J. Chem. Eng. Jpn.* 24, 7681.

Karri, S.B.R., Werther, J., 2003. Gas distributor and plenum design in fluidized beds. In: Yang, W.C. *Handbook of fluidization and fluid-particle systems*. Marcel Dekker Inc., New York, 164-179.

Kim, Y.D., Yang, C.W., Kim, B.J., Kim, K.S., Lee, J.W., Moon, J.H., Yang, W., Yu, T.U., Lee, U.D., 2013. Air-blown gasification of woody biomass in a bubbling fluidized bed gasifier. *Appl. Energ.* 112, 414-420.

Köhl, M.H., Lu, G., Third, J.R., Häberlin, M., Kasper, L., Prüssmann, K.P., Müller, C.R., 2013. Magnetic resonance imaging (MRI) study of jet formation in packed beds. *Chem. Eng. Sci.* 97, 406-412.

Kunii, D., Levenspiel, O., 1991. *Fluidization engineering*, Butterworth-Heinemann, Stoneham, UK, 2nd ed.

Lahijani, P., Zainal, Z.A., 2011. Gasification of palm empty fruit bunch in a bubbling fluidized bed: a performance and agglomeration study. *Bioresource Technol.* 102, 2068-2076.

Laverman, J.A., Roghair, I., van Sint Annaland, M., Kuipers, J.A.M., Investigation into the hydrodynamics of gas-solid fluidized beds using particle image velocimetry coupled with digital image analysis. *Can. J. Chem. Eng.* 86, 523-535.

Lu, G., Gilabert, G., Yan, Y., 2005. Vision based monitoring and characterization of combustion flames. *Journal of Physics: Conference Series* 15, 194-200.

Lucas, A., Arnaldos, J., Casal, J., Puigjaner, L., 1986. High temperature incipient fluidization in mono and polydisperse systems. *Chem. Eng. Commun.* 41, 121-132.

Mandal, D., Sharma, V.K., Pant, H.J., Sathiyamoorthy, D., Vinjamur, M., 2012. Quality of fluidization in gas-solid unary and packed fluidized beds: an experimental study using gamma ray transmission technique. *Powder Technol.* 226, 91-98.

Mathur, A., Saxena, S.C., Zhang, Z.F., 1986. Hydrodynamic Characteristics of Gas-Fluidized Beds Over a Broad Temperature Range. *Powder Technol.* 47, 247-256.

Mayerhofer, M., Mitsakis, P., Meng, X.M., de Jong, W., Spliethoff, H., Gaderer, M., 2012. Influence of pressure, temperature and steam on tar and gas in allothermal fluidized bed gasification. *Fuel.* 99, 204-209.

Molerus, O., 1982. Interpretation of Geldart's type A, B, C and D powders by taking into account interparticle cohesion forces. *Powder Technol.* 33, 81-87.

Mori, S., Moriyama, A., 1978. Criteria for uniform fluidization of non-aggregative particles. *Int. Chem. Eng.* 18, 245-249.

Müller, C.R., Davidson, J.F., Dennis, J.S., Hayhurst, A.N., 2007. A study of the motion and eruption of a bubble at the surface of a two-dimensional fluidized bed using particle image velocimetry (PIV). *Ind. Eng. Chem. Res.* 46, 1642-1652.

Olivares, A., Aznar,M.P., Caballero, M.A., Gil, J., Frances, E., Corella, J., 1997. Biomass Gasification: Produced gas upgrading by in-bed use of dolomite. *Ind. Eng. Chem. Res.* 36, 5220-5226.

Otsu, N., 1979. A threshold selection method from gray-level histograms, *IEEE Transactions on Systems Man and Cybernetic*s 9, 62-66.

Pallarès, D., Johnsson, F., 2006. A novel technique for particle tracking in cold 2-dimensional fluidized beds simulating fuel dispersion. *Chem. Eng. Sci.* 61, 2710-2720.

Patel, A.K., Waje, S.S., Thorat, B.N., Mujumdar, A.S., 2008. Tomographic diagnosis of gas maldistribution in gas-solid fluidized beds. *Powder Technol.* 185, 239-250.

Perry, R.H., Green, D.W., Maloney, J.O., 1997. Perry's Chemical Engineers' Handbook. McGraw-Hill: New York. 17-6.

Pore, M., Chandrasekera, T.C., Holland, D.J., Wang, A., Wang, F., Marashdeh, Q., Mantle, M.D., Sederman, A.J., Fan, L.S., Gladden, L.F., Dennis, J.S., 2010. Magnetic resonance studies of jets in a gas-solid fluidized bed. *Particuology.* 10, 161-169.

Puncochár, M., Drahos, J., Cermák, , J., Selucký, K., 1985. Evaluation of minimum fluidization velocity in gas fluidized beds from pressure fluctuations. *Chem. Eng. Commun.* 35, 81-87.

Qureshi, A.E., Creasy, D.E., 1979. Fluidised bed distributors.*Powder Technol.* 22, 113-119.

Raffel, M., Willert, C., Kompenhans, J., 2007. Particle Image Velocimetry, A Practical Guide. Springer, Berlin.

Raso, G., DAmore, M., Formisani, B., Lignola, P.G., 1992. The influence of temperature on the properties of the particulate phase at incipient fluidization. *Powder Technol.* 72, 71-76.

Rautenbach, C., Melaaen, M.C., Halvorsen, B.M., 2013. Statistical diagnosis of a gas-solid fluidized bed using electrical capacitance tomography. *Int. J. Multiphase Flow.* 49, 70-77.

Rees, A.C., Davidson, J.F., Dennis, J.S., Fennell, P.S., Gladden, L.F., Hayhurst, A.N., Mantle, M.D., Müller, C.R., Sederman, A.J., 2006. The nature of the flow just above the perforated plate distributor of a gas-fluidised bed, as imaged using magnetic resonance. *Chem. Eng. Sci.* 61, 6002-6015.

Sánchez-Delgado, S., Marugán-Cruz, C., Acosta-Iborra, A., Santana, D., 2010. Dense-phase velocity fluctuation in a 2-D fluidized bed. *Powder Technol.* 200, 37-45.

Sánchez-Delgado, S., Marugán-Cruz, C., Soria-Verdugo, A., Santana, D., 2013. Estimation and experimental validation of the circulation time in a 2D gas-solid fluidized bed. *Powder Technol.* 235, 669-676.

Sánchez-Prieto, J., Soria-Verdugo, A., Briongos, J.V., Santana, D., 2014. The effect of temperature on the distributor design in bubbling fluidized beds. *Powder Technol.* 261, 176-184.

Sánchez-Prieto, J., Soria-Verdugo, A., Gómez-Hernandéz, J., Briongos, J.V., Santana, D., 2015. Maldistribution detection in bubbling fluidized beds. *Chem. Eng. J.* 270, 272-281.

Santana, D., Nauri, S., Acosta, A., Garca, N., Macas-Machn, A., 2005. Initial particle velocity spatial distribution from 2-D erupting bubbles in fluidized beds. *Powder Technol.* 150, 1-8.

Sathiyamoorthy, D., Sridhar Rao, C.H., 1981. The choice of distributor to bed pressure drop ratio in gas fluidised beds. *Powder Technol.* 30, 139-143.

Sathiyamoorthy, D., Horio, M., 2003. On the influence of aspect ratio and distributor in gas fluidized beds. *Chem. Eng. J.* 93, 151-161.

Saxena, S.C., Chatterjee, A., Patel, R.C., 1979. Effect of distributors on gas-solid fluidization. *Powder Technol.* 22, 191-198.

Saxena, S.C., Ganzha, V.L., 1985. Heat transfer to inmersed surfaces in gas-fluidized beds of large particles and powder characterization. *Powder Technol.* 39, 199-208.

Siegel, R., 1976. Effect of distributor plate to bed resistance ratio on onset of fluidized bed channelling. *AIChE J.* 22, 590.

Sobrino, C., Sánchez-Delgado, S., García-Hernando, N., de Vega, M., 2008. Standard deviation of absolute and differential pressure fluctuations in fluidized beds of group B particles. *Chem. Eng. Res. Des.* 86, 12361242.

Soria-Verdugo, A., García-Hernando, N., Almendros-Ibáñez, J.A., Ruiz-Rivas, U., 2011. Motion of a large object in a bubbling fluidized bed with a rotating distributor. *Chemical Engineering and Processing: Process Intensification* 50, 859-868.

Soria-Verdugo, A., García-Gutiérrez, L.M., Ruiz-Rivas, U., Santana, D., 2011. Buoyancy effects on objects moving in a bubbling fluidized bed. *Chem. Eng. Sci.* 66, 2833-2841.

Sveen, J.K., 1998-2008. MATPIV. http://www.math.uio.no/jks/matpiv/.

Thorpe, R.B., Davidson, J.F., Downing, S.J., Dusad, A., Farthing, P., Ferdinando, G., Holden, A., Martin, A., Negyal, O., Saundry, J., 2000. On the minimum distributor pressure drop for uniform fluidization. In: *Proceedings of 3rd European Conference on Fluidization*, Toulouse 189.

Thorpe, R.B., Davidson, J.F., Pollitt, M., Smith, J., 2002. Maldistribution in fluidized beds. *Ind. Eng. Chem. Res.* 41 , 5878-5889.

Valverde, J.M., Castellanos, A., 2007. Types of gas fluidization of cohesive granular materials. *Phys. Rev. E* 75, 301-306.

van der Schaaf, J., Schouten, J.C., Johnsson, F., van den Bleek, C.M., 2002. Non-intrusive determination of bubble and slug length scales in fluidized beds by decomposition of the power spectral density of pressure time series. *International Journal of Multiphase flow* 28, 865-880.

van der Schaaf, J., van Ommen, J.R., Takens, F., Schouten, J.C., van den Bleek, C.M., 2004. Similarity between chaos analysis and frequency analysis of pressure fluctuations in fluidized beds. *Chem. Eng. Sci.* 59, 18291840.

van Ommen, J.R., Coppens, M.C., van den Bleek, C.M., Schouten, J.C., 2000. Early warning of agglomeration in fluidized beds by attractor comparison. *AIChE J.* 46, 2183-2197.

van Ommen, J.R., de Korte, R.J., van den Bleek, C.M., 2004a. Rapid detection of defluidization using the standard deviation of pressure fluctuations. *Chem. Eng. Process.* 43, 1329-1335.

van Ommen, J.R., van der Schaaf, J., Schouten, J.C., van Wachem, B.G.M., Coppens, M.O., van den Bleek, C.M., 2004b. Optimal placement of probes for dynamic pressure measurements in large-scale fluidized beds. *Powder Technol.* 139, 264-276.

van Ommen, J.R., Sasic, S., van der Schaaf, J., Gheorghiu, S., Johnsson, F., 2011. Time-series analysis of pressure fluctuations in gas-solid fluidized beds A review. *International Journal of Multiphase flow* 37, 403-428.

Villa Briongos, J., Aragón, J.M., Palancar, M.C., 2006. Phase space structure and multi-resolution analysis of gassolid fluidized bed hydrodynamics: part I the EMD approach. *Chem. Eng. Sci.* 61, 69636980.

Villa Briongos, J., Aragón, J.M., Palancar, M.C., 2007. Phase space structure and multi-resolution analysis of gassolid fluidized bed hydrodynamics: part II: dynamic analysis. *Chem. Eng. Sci.* 62, 28652879.

Vun, S., Naser, J., Witt, P.J., Yang, W., 2010. Measurements and numerical predictions of gas vortices formed by single bubble eruptions in the freeboard of a fluidised bed. *Chem. Eng. Sci.* 65, 5808-5820.

Wang, Y., Gu, G., Wei, F., Wu, J., 2002. Fluidization and agglomerate structure of SiO_2 nanoparticles. *Powder Technol.* 124, 152-159.

Wen, CY., Yu, YH., 1966. A generalized method for predicting minimum fluidization velocity. *AIChE J.* 12, 610.

Whitehead, A.B., Dent, D.C., 1967. Behaviour of multiple tuyere assemblies in large fluidized beds. In *Proceedings of the International Symposium on Fluidisation*, Enindhoven, June 6-9; Drinkenburg, A.A.H., Ed.; Netherlands University Press: Amsterdam, 802.

Whitehead, A.B., 1971. In Davidson, J.F., Harrison, D. (Eds.) *Fluidization*. Academic Press, London. 781.

Wilk,V., Schmid, J.C., Hofbauer, H., 2013. Influence of fuel feeding positions on gasification in dual fluidized bed gasifiers. *Biomass Bioenerg.* 54, 46-58.

Wilkinson, D., 1995. Determination of minimum fluidization velocity by pressure fluctuation measurement. *Can. J. Chem. Eng.* 73, 562-565.

Yue, P.L., Kolaczkowski, J.A., 1982. Multiorifice distributor design for fluidized beds. *Trans. Inst. Chem. Eng.* 60.

Zenz, F.A., Othmer, D.F., 1960. Fluidization and fluid particle systems. Rheinhold: New York. 260.

Zipser, S., Gommlich, A., Matthes, J., Keller, H.B., 2006. Combustion plant monitoring and control using infrared and video cameras. *Power Plants and Power Systems Control*, Kananaskis, Canada.

Zuiderweg, F.J.,1967. In Drinkenburg, A.A.H. (Eds.) *Proc. Int. Symp. on Fluidization*. Netherlands University Press, Amsterdam. 739.